NAVAL POSTGRADUATE SCHOOL

MONTEREY, CALIFORNIA

THESIS

PREDICTABILITY ASSOCIATED WITH THE DOWNSTREAM IMPACT OF THE EXTRATROPICAL TRANSITION OF TROPICAL CYCLONES

by

Justin Martin Reeves

June 2005

Thesis Advisor:	Patrick Harr
Second Reader:	Russell Elsberry

Approved for public release; distribution is unlimited

THIS PAGE INTENTIONALLY LEFT BLANK

REPORT DOCUMENTATION PAGE		Form Approved OMB No. 0704-0188

Public reporting burden for this collection of information is estimated to average 1 hour per response, including the time for reviewing instruction, searching existing data sources, gathering and maintaining the data needed, and completing and reviewing the collection of information. Send comments regarding this burden estimate or any other aspect of this collection of information, including suggestions for reducing this burden, to Washington headquarters Services, Directorate for Information Operations and Reports, 1215 Jefferson Davis Highway, Suite 1204, Arlington, VA 22202-4302, and to the Office of Management and Budget, Paperwork Reduction Project (0704-0188) Washington DC 20503.

1. AGENCY USE ONLY ***(Leave blank)***	**2. REPORT DATE** June 2005	**3. REPORT TYPE AND DATES COVERED** Master's Thesis

4. TITLE AND SUBTITLE: Predictability Associated with the Downstream Impact of the Extratropical Transition of Tropical Cyclones	**5. FUNDING NUMBERS**
6. AUTHOR(S) Justin Martin Reeves	
7. PERFORMING ORGANIZATION NAME(S) AND ADDRESS(ES) Naval Postgraduate School Monterey, CA 93943-5000	**8. PERFORMING ORGANIZATION REPORT NUMBER**
9. SPONSORING /MONITORING AGENCY NAME(S) AND ADDRESS(ES) N/A	**10. SPONSORING/MONITORING AGENCY REPORT NUMBER**

11. SUPPLEMENTARY NOTES The views expressed in this thesis are those of the author and do not reflect the official policy or position of the Department of Defense or the U.S. Government.

12a. DISTRIBUTION / AVAILABILITY STATEMENT Approved for public release; distribution is unlimited.	**12b. DISTRIBUTION CODE**

13. ABSTRACT (maximum 200 words)

Since an extratropical transition (ET) of a decaying tropical cyclone (TC) often results in a fast-moving, rapidly-developing extratropical cyclone and amplification of synoptic-scale systems far downstream, proper forecasting of ET events is critical to forecast accuracy over large ocean regions. Past studies have linked forecast accuracy to the phasing of a decaying TC with favorable midlatitudes conditions. Because ET events are sensitive to the analyzed initial conditions, this phasing is examined using 11 member ensemble predictions available four times daily from the National Centers for Environmental Prediction, which were combined into a single 44 member ensemble based on a common forecast verification time. Recurring ET patterns within the 44 member ensemble were objectively identified using a combination of EOF and cluster analysis. Ensemble spread first appears near the point where the TC moves into the midlatitudes and then propagates downstream. Although ensemble spread in the forecast fields was large at extended forecast intervals, the ensemble spread, and the number of ET patterns identified in successive EPS predictions, decreased as the ET process became better defined. Within 48 hours of the ET event, the ensemble prediction system properly identified the ET pattern with a minimum ensemble spread. Similar to Klein et al. (2002), the shifts in the initial position of the TC and the subsequent dynamical coupling can explain differences between weak and strong ET re-intensifications.

14. SUBJECT TERMS extratropical transition, ET, tropical cyclones, re-intensification, ensemble, EOF, empirical orthogonal functions, patterns, mid-latitude phasing.	**15. NUMBER OF PAGES** 115
	16. PRICE CODE

17. SECURITY CLASSIFICATION OF REPORT	**18. SECURITY CLASSIFICATION OF THIS PAGE**	**19. SECURITY CLASSIFICATION OF ABSTRACT**	**20. LIMITATION OF ABSTRACT**
Unclassified	Unclassified	Unclassified	UL

NSN 7540-01-280-5500

Standard Form 298 (Rev. 2-89)
Prescribed by ANSI Std. 239-18

THIS PAGE INTENTIONALLY LEFT BLANK

Approved for public release; distribution is unlimited

PREDICTABILITY ASSOCIATED WITH THE DOWNSTREAM IMPACT OF THE EXTRATROPICAL TRANSITION OF TROPICAL CYCLONES

Justin M. Reeves
Lieutenant Commander, United States Navy
B.S., United States Naval Academy, 1994

Submitted in partial fulfillment of the
requirements for the degree of

**MASTER OF SCIENCE IN
METEOROLOGY AND PHYSICAL OCEANOGRAPHY**

from the

**NAVAL POSTGRADUATE SCHOOL
June 2005**

Author: Justin Martin Reeves

Approved by: Patrick Harr
Thesis Advisor

Russell Elsberry
Second Reader

Philip Durkee
Chairman, Department of Meteorology

THIS PAGE INTENTIONALLY LEFT BLANK

ABSTRACT

Since an extratropical transition (ET) of a decaying tropical cyclone (TC) often results in a fast-moving, rapidly-developing extratropical cyclone and amplification of synoptic-scale systems far downstream, proper forecasting of ET events is critical to forecast accuracy over large ocean regions. Past studies have linked forecast accuracy to the phasing of a decaying TC with favorable midlatitudes conditions. Because ET events are sensitive to the analyzed initial conditions, this phasing is examined using 11 member ensemble predictions available four times daily from the National Centers for Environmental Prediction, which were combined into a single 44 member ensemble based on a common forecast verification time. Recurring ET patterns within the 44 member ensemble were objectively identified using a combination of EOF and cluster analysis. Ensemble spread first appears near the point where the TC moves into the midlatitudes and then propagates downstream. Although ensemble spread in the forecast fields was large at extended forecast intervals, the ensemble spread, and the number of ET patterns identified in successive EPS predictions, decreased as the ET process became better defined. Within 48 hours of the ET event, the ensemble prediction system properly identified the ET pattern with a minimum ensemble spread. Similar to Klein et al. (2002), the shifts in the initial position of the TC and the subsequent dynamical coupling can explain differences between weak and strong ET re-intensifications.

THIS PAGE INTENTIONALLY LEFT BLANK

TABLE OF CONTENTS

LIST OF FIGURES

ACKNOWLEDGMENTS

I would first of all like to thank my wife, Anne, for her unbelievable patience and understanding. Without her continual support, I never would have been able to reach half of my goals.

I would also like to thank Dr. Patrick Harr for his persistent guidance and support. You taught me a staggering amount of information and numerical techniques in a very compressed time-frame. Your dedication to this school and to your students is truly remarkable.

And finally, I would like to thank Dr. Elsberry for his patience on the countless number of questions I asked in and out of class and for his endless supply of green ink.

THIS PAGE INTENTIONALLY LEFT BLANK

I. INTRODUCTION

A. OBJECTIVE

Often a tropical cyclone will transition into an extratropical cyclone and track across entire ocean basins. During the extratropical transition (ET) process, a tropical cyclone may initially weaken and then re-intensify as an extratropical cyclone (Klein et al. 2000). Following re-intensification, the new extratropical cyclone may move rapidly across the ocean basin. Often, ET events that occur during the late summer/fall season produce damaging winds and seas more commonly associated with winter-time extratropical cyclones. Furthermore, these hazardous conditions often threaten vessels at sea attempting to take advantage of shorter “great circle” routes. Not surprisingly, Military Sealift Command (MSC) ships utilize great circle routes during summer months to minimize fuel costs. The MSC, in addition to other contracted vessels, provide the logistics support for forward-deployed U.S. military forces. For example, 90% of all equipment and supplies for Desert Storm were shipped by sea-going vessels (U.S. Department of Transportation (DOT) Marine Transportation System 2005). As these vessels carrying mission-critical equipment and supplies venture farther into the midlatitudes to minimize fuel costs, there is increased likelihood that they and their cargo will be damaged by the dangerous winds and seas associated with ET events. In addition to posing a threat to maritime operations, Atlantic ET events often pose a threat to Europe, and Pacific events to the northwestern portion of the United States, as they may also contain strong winds and large amounts of precipitation.

Extratropical transition of tropical cyclones impacts the distribution of synoptic-scale systems in the vicinity of the ET, downstream of the ET location, and possibly upstream of the ET location (Jones et al. 2003). Therefore, proper forecasting of the ET event is critical to accurate forecasts over near-global scales on time scales of 5 – 7 days. When a tropical cyclone transforms into an extratropical system, the numerical forecast problem is complicated due to (1) limited observations over the ocean basins where these events tend to occur, (2)

the variety of scales of motion present during the transformation stage, and (3) an incomplete understanding of the dynamics associated with ET. Because these systems, as well as downstream events, pose a serious threat to ships at sea and countries to the east of ocean basins, determining the maximum forecast interval when an operational forecast system has properly identified the ET pattern and track forecast is of interest. Therefore, the objective of this study is to examine forecasts from a global-model ensemble forecast system with respect to ET events and identify the maximum forecast interval when the ensemble forecast has properly identified the ET pattern and track forecast.

B. MOTIVATION

The ET event in which a tropical cyclone with its warm-core vortex and distinct thermodynamic structure changes into a cold-core extratropical system is a gradual process that evolves numerous processes on varying spatial and temporal scales. Accordingly, numerical model forecasts of many ET events have shown poor skill (Jones et al. 2003).

Numerical weather prediction (NWP) studies have also shown that the ET process (Rabier et al. 1996; Evans and Velden 2000; Hello and Thépaut 2000) and other active synoptic periods are extremely sensitive to the initial conditions. To examine the sensitivity of synoptic-scale forecasts to initial conditions, ensemble forecast systems (Toth and Kalnay 1997) have been developed at most operational NWP centers. The sensitivity to initial conditions typically produces a large spread in tracks of decaying tropical cyclones among the ensemble forecast members. Often, extended-range forecasts of the initial stages of the ET process exhibit the largest ensemble-based variability. However, the track spread in progressive model runs appears to decrease as the ET process evolves and becomes better defined.

One hypothesis in this study is that the ensemble spread will continue to decrease until a specific forecast interval in which the ensemble forecast has properly identified the ET pattern and track forecast. If this maximum forecast interval can be defined, then an ensemble-based forecast may provide ample

lead time to confidently route military vessels that carry mission-critical logistics away from damaging winds and seas associated with these events.

C. BACKGROUND

An extratropical transition (ET) event can be classified into two stages (Klein et al. 2000): *transformation*, in which a tropical cyclone evolves into a baroclinic system; and *re-intensification*, where the transformed storm then deepens as an extratropical cyclone. The transformation stage begins when the tropical cyclone intensity begins to decrease, which is typically associated with a rise in the central mean sea-level pressure. The tropical cyclone begins to lose its symmetric shape as it interacts with the midlatitude baroclinic environment. Remotely sensed observations provide the initial evidence that the tropical cyclone is undergoing transformation via the development of asymmetric structural changes in the cloud and precipitation. As a tropical cyclone (TC) progresses poleward, it moves into a baroclinic environment and experiences greater vertical wind shear as it becomes embedded in the midlatitudes westerlies. The increasing vertical wind shear in the midlatitude baroclinic environment drastically alters several characteristics of the transforming system. The increased vertical wind shear deforms the symmetric wind and precipitation structure found in tropical cyclones into an asymmetric structure that is more commonly found in midlatitude systems. The gale-force wind fields surrounding the transforming system expand to encompass a larger geographical area when compared to the hazardous wind region of the original tropical cyclone. Following transformation, the previously decaying TC may rapidly re-intensify as a deep, midlatitude cyclone. Broad regions of gale or even hurricane-force winds are often associated with major re-intensification scenarios.

As the transitioning storm continues to move poleward, it become further embedded in the midlatitude westerlies, which may result in a rapid increase in the storm translation speed. The faster translation speed limits the reaction time ships at sea have to avoid the damaging winds and seas produced by these storms. The maritime threat is compounded by the fact that the increased translation speed of the extratropical system can produce a significantly higher

ocean wave field than a slower moving hurricane/typhoon still in the tropics. Normally, the high energy waves that are generated by tropical cyclones propagate away from the storm center because the ocean waves have a higher group speed than the storm translation speed. Thus, the energy the wind imparts on the ocean is dispersed away from the storm in the form of long period swell. However, if the translation speed of the transforming extratropical system matches the group speed of the high energy waves, a natural resonance between the wind field and the wave field can occur, which may result in the generation of a significantly higher wave field (MacAfee et al. 2000a, b). Accordingly, these rapidly moving systems, with their rapidly expanding wind fields, pose a serious threat to the maritime industry and coastal regions. Transformation is considered complete when the cyclone no longer maintains its tropical characteristics and the center has been replaced with a baroclinic cold-core center.

Not all decaying tropical cyclones will re-intensify. Rather, re-intensification depends on complex interactions between the decaying tropical cyclone and the midlatitude environment into which it is moving (Klein et al. 2002). Klein et al. (2000) defined the start of the re-intensification stage to be the time when the mean sea-level pressure begins to decrease. Although the re-intensification stage is mostly related to the interactions between the decaying TC and the midlatitude environment, several modes of re-intensification have been identified. Thorncroft and Jones (2000) compared the re-intensification of Hurricane Felix, which was dominated by jet-streak dynamics, to that of Hurricane Iris, which was dominated by strong latent heat fluxes in the boundary layer. McTaggart-Cowan et al. (2003) classified re-intensification of decaying hurricanes over the North Atlantic as being dominated by baroclinic processes or tropical processes (i.e., latent-heat release). Harr and Elsberry (2000) classified the re-intensification process based on the position of the primary midlatitude potential-vorticity center relative to the decaying tropical cyclone. When the primary midlatitude low-pressure system is northwest of the decaying tropical

cyclone, then re-intensification is more likely to occur. Sinclair (2004) identified similar relationships with respect to ET events over the western South Pacific.

Regardless of whether a decaying TC undergoes re-intensification, the movement of the warm, moist circulation and its outflow into the midlatitudes causes a significant perturbation on the midlatitude environment (Jones et al. 2003). It is hypothesized that the source of much of the forecast variability in ensemble-based forecasts of the midlatitude flow during ET events is due to the presence of the perturbations due to the decaying TC. This ET-related variability is investigated through examination of a sequence of forecasts of Typhoon (TY) Tokage (October 2004) produced by the National Centers for Environmental Prediction (NCEP) Global Forecast System (GFS) ensemble prediction system. Furthermore, it is hypothesized that the uncertainty introduced into forecasts of midlatitude synoptic-scale features spreads downstream from the ET event. This uncertainty is also hypothesized to be larger than that due to typical synoptic-scale variability. In Chapter II, the methodology associated with the processing of the ensemble forecast data is defined. Examination of the ensemble forecasts with respect to TY Tokage is presented in Chapter III. Conclusions are listed in Chapter IV.

THIS PAGE INTENTIONALLY LEFT BLANK

II. METHODOLOGY

A. DATA

The analysis and forecast fields used for this study are from the NCEP global Ensemble Prediction System (EPS). The EPS model is a degraded version of their deterministic model and has an approximate horizontal resolution of 0.5 degree latitude by 0.5 degree longitude. The NCEP EPS is available every 6 hours, and is comprised of one control run and ten perturbations of the control field. The perturbations are generated by the breeding method based on individual ensemble integrations (Toth and Kalnay 1997).

A multivariate analysis that is based on a single ensemble system run of 11 members would not represent well the probability density function. Therefore to increase the degrees of freedom in the analysis, a 44-member combined ensemble is generated during a 24-hour period. Initially, a common verification time was established for the four ensemble runs during a 24-h period that began at 0000 UTC and ended at 1800 UTC (Fig. 1). The first 11 members originated from the 0000 UTC run. Six hours later, the next 11 members would be collected from the 0600 UTC EPS run. This process continued until all 44 members from the four EPS runs from one 24-hour period were combined into one large daily ensemble (Fig. 1).

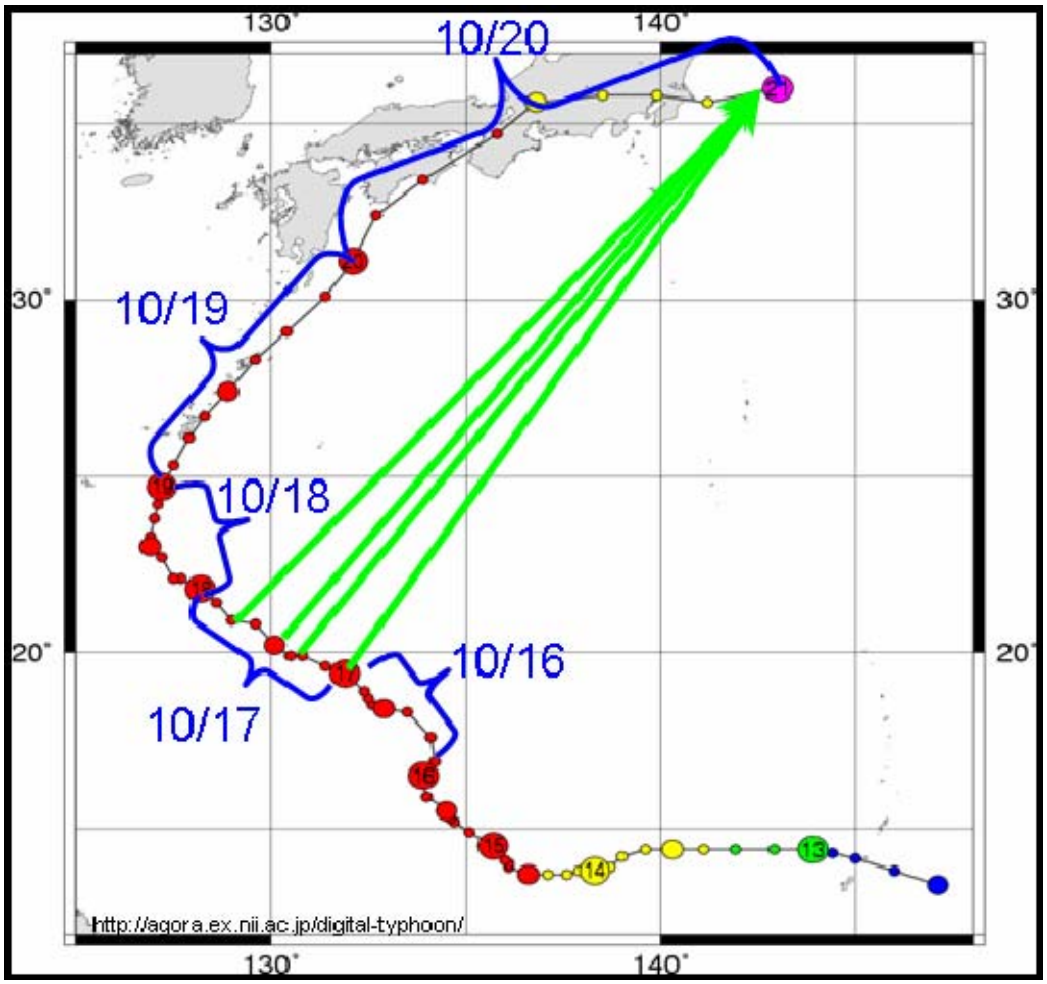

Figure 1. Analyzed best-track for TY Tokage. The temporal spacing between the dots is 3 hours. The large circles with numbers depict the dates during October 2004. Colors of the circles indicate analyzed intensity. The four green arrows indicate the four ensemble runs used to compile the 44 ensemble members (11 per run) for a common valid time of 0000 UTC 21 October 2004. Best-track graphic is from the Digital Typhoon website.

B. EMPIRICAL ORTHOGONAL FUNCTION (EOF)

Empirical Orthogonal Function analysis is a standard technique utilized to determine the underlying structure that best explains the maximum amount of variability in a multivariate data set (Richman 1986). An EOF analysis was performed on the 44 member ensemble group to determine the principle structures found in the 500 hPa height fields. Prior to computation of the EOFs, the ensemble mean was removed from each member. An area over the North Pacific from 10°N to 60°N (i.e., 50° or 21 grid points at 2.5° spacing) and from

90° E to 120° W (i.e., 150° or 61 grid points at 2.5° spacing) was the area of interest for this study. Therefore, the EOF analysis was performed over a grid that was reduced to 21 x 61 points for the 21 time steps (i.e., 00 to 120 h in 6-hour increments) where each time step was defined by a 21 x 61 matrix comprised of 1,281 data points. Each data matrix was transformed into a 1 x 1,281 data vector. Consequently, the 44 data vectors that represent each ensemble member that verifies at the target time (Fig. 1) are combined into a single matrix where the column number represents the ensemble member. Accordingly, there were 1,281 rows (i.e., data points) by 44 columns (i.e., ensemble members) in the data matrix.

The EOF analysis identifies the most common spatial structure found among the 44 members 500 hPa height field. By construction, the first mode is the most common spatial structure to all 44 members of the ensemble group. This structure explains the maximum amount of variance about the mean. Similarly, the second EOF pattern is the second most common spatial structure that maximizes the variance about the mean once the variability accounted for by the first EOF has been removed.

The principal components (PC) define the weight of each EOF mode that can be found in each ensemble member. Thus, the individual ensemble members can be decomposed into a linear summation of weighted EOF modes. The computed EOF fields for various 24-h periods during TY Tokage revealed that together the two leading modes typically explained 55% to 65% of the variance, while the third mode usually accounted for less than 10%. Therefore, the first and second EOF modes explained most of the variance of the ensemble members. Modes below this cutoff were treated as background noise and were not considered further in this study. Thus, it was reasoned that each individual ensemble member could be reasonably represented by a linear summation of the magnitude of the primary EOF structure (EOF 1) plus the magnitude of the secondary EOF structure (EOF 2).

C. CLUSTER ANALYSIS

Once the EOF analysis was complete, the first and second principal components (PCs) for all 44 ensemble members were plotted. The principal components for EOF 1 (PC1) were plotted along the abscissa and the principal components for EOF 2 (PC2) were plotted along the ordinate.

A fuzzy cluster analysis (Scott and Symons 1971; Harr and Elsberry 1995) routine was utilized in MATLAB to determine possible groupings of the ensembles members based on their PC1 and PC2 values. The clustering routine determined and assigned a relative strength to the plotted points based on the radial distance between a group center and the plotted points. To start the iterative cluster procedure, a pre-defined number of cluster centers were randomly placed in the EOF 1/EOF 2 phase space. Each ensemble member is then assigned to the closest group center. New centers are computed and each point is re-examined relative to the new cluster centers. If no points can be re-assigned because they lie closer to another center, the iterations stop. Each member is assigned a weight that identifies their relative strength of membership to their cluster. A mean strength (Fig. 2) was determined for all 44 points representing all the ensemble members. Ensemble members whose strength value fell below one standard deviation from the mean strength were not assigned to a respective group (Fig. 2). These members were then labeled as belonging to a “no cluster” group (Fig. 3).

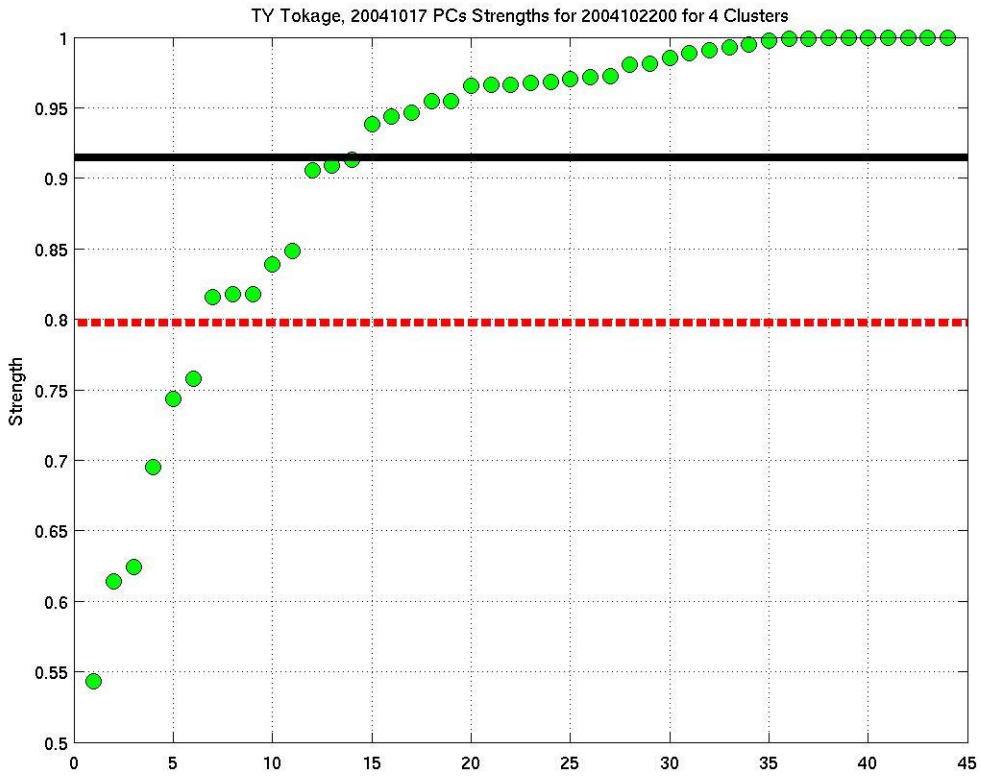

Figure 2. Strength values assigned to each ensemble member during the fuzzy cluster process for one 24-h time period. The ensemble members were sorted from lowest to highest based on their strength value. The numbers on the abscissa are a “relative” ensemble member based on the sorting technique and do not represent the true ensemble member number. The strength value is along the ordinate. The black line represents the mean strength and the red dotted line represents one standard deviation from the mean. Based on this plot, six ensemble members fell below the standard deviation threshold and were not assigned to a group.

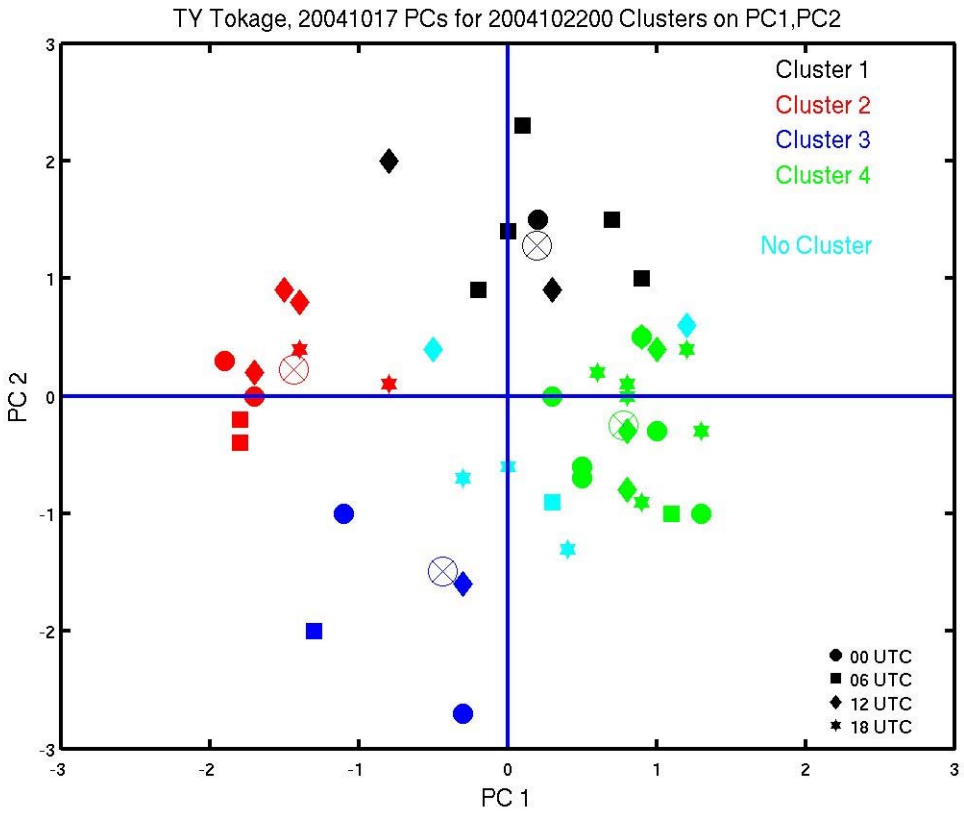

Figure 3. Cluster plot of PC values for 102-h to 120-h forecasts initiated during 17 October 2004. The common verification time is 0000 UTC 22 October. The four ensemble runs that comprise this plot are the 0000 UTC, 0600 UTC, 1200 UTC, and 1800 UTC runs on 17 October. The fuzzy logic routine has divided the plotted PCs into 4 groups. The group centers are represented by the circled 'X'.

As a first guess, the fuzzy cluster routine was used to break the PC points into two distinct groups. The groups were evaluated to ensure that no group was dominated by a majority of members from a single ensemble run (i.e., so that one group did not contain all 11 members of the 0600 UTC ensemble run). If this had been the case, this result would indicate that the grouping was a function of the ensemble run and not due to the perturbations introduced during the ensemble run (Fig. 3). It was always assumed that the clusters of PC values could be divided into more than just two groups. Progressive cluster analyses then attempted to logically break the groupings into a successively larger number of groups. When one group was sub-divided into two separate groups, the

meteorological charts (i.e., mean sea-level pressure, 500 hPa heights, etc) of the initial group and the two new groups were examined to see if two distinct weather patterns truly existed. If not, the previous grouping was considered the proper grouping of the ensemble members. At this point, the cluster analysis was terminated.

THIS PAGE INTENTIONALLY LEFT BLANK

III. ANALYSIS AND INTERPRETATION

Some tropical cyclones that undergo extratropical transition (ET) re-intensify days later as a mature midlatitude extratropical cyclone while others simply decay (Klein et al. 2000). Modes of ET have been related to the relative phasing of the tropical cyclone with respect to midlatitude synoptic systems (Klein et al. 2002). Discrete baroclinic/tropical, northwest/northeast patterns have been proposed (Harr and Elsberry 2000). Because ET events induce large amplitude perturbations in the downstream fields (Jones et al. 2003), proper forecasting of downstream systems relies heavily on the proper identification of the ET event and its phase with respect to the pre-existing midlatitude patterns.

Because both the dynamic and thermodynamic processes that occur on numerous spatial scales during an ET event are poorly understood and poorly modeled, a tropical cyclone entering the midlatitudes introduces a high degree of uncertainty into the model. To illustrate this uncertainty, Hovmoller plots of the standard deviation of 500 hPa heights on each ensemble run are constructed. The 500 hPa height standard deviation is averaged zonally between 40°N-60°N (Fig. 4). For each 120-h ensemble run in Fig. 4, the time of the last best-track position, which is taken as the ET time, is defined by the horizontal line and tropical cyclone symbol. As the ET time of TY Tokage first appears at 120 h of the 0000 UTC 16 October ensemble forecast, increased standard deviations appear at the 96-h time of 0000 UTC 20 October (Fig. 4a). As the ET time moves to 108 h (Fig. 4b), a rapid increase in standard deviation occurs downstream of the ET location. This trend continues over the ensuing six ensemble runs that proceed from 0000 UTC 17 October (Fig. 4c) – 1200 UTC 19 October (Fig. 4h). During this period, the ET time moves from 96 h to 36 h in the forecast sequence. Also, the region of increased standard deviation spreads downstream to eventually encompass nearly 180° of longitude.

Therefore, the pattern of increased variability in the EPS 500 hPa height pattern spreads immediately downstream of the forecast ET location, but then

decreases as the ET time is forecast to occur within 36 hours (Figs. 4i-j). The spatial pattern of variability associated with the downstream propagation in ensemble height standard deviation is investigated with the EOF analysis.

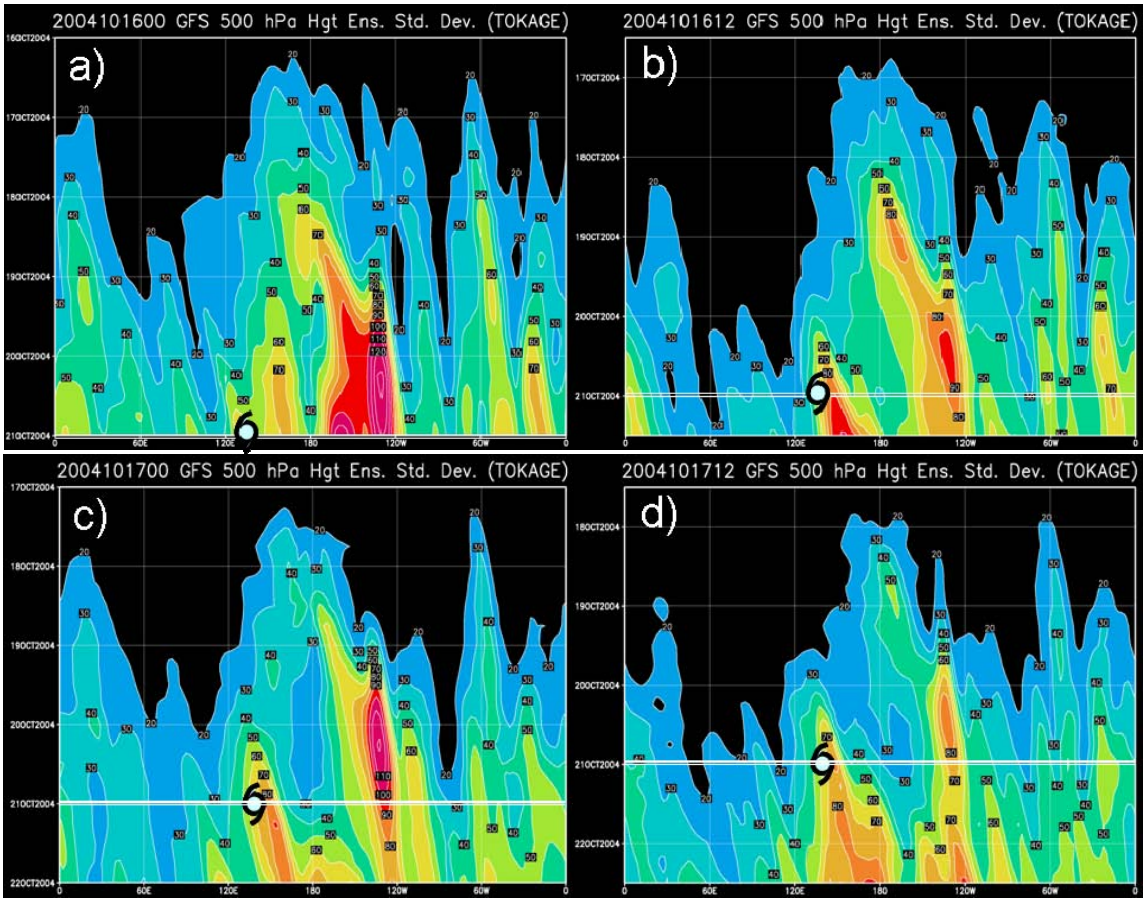

Figure 4. Hovmoller plots of the standard deviation (m) of the eleven 500 hPa height ensemble members comprising each operational run. Figures 4a–j depict the evolution of the model uncertainty associated with the ET event. Only the 0000 UTC and 1200 UTC runs were examined. The longitude is plotted along the horizontal axis and the ensemble forecast valid time is plotted in the vertical. To capture the variations in the midlatitude height field, the standard deviation was averaged across 40° – 60° N. The tropical cyclone symbol (and the horizontal line) depicts the end of the best-track for TY Tokage and the beginning of the transformation stage.

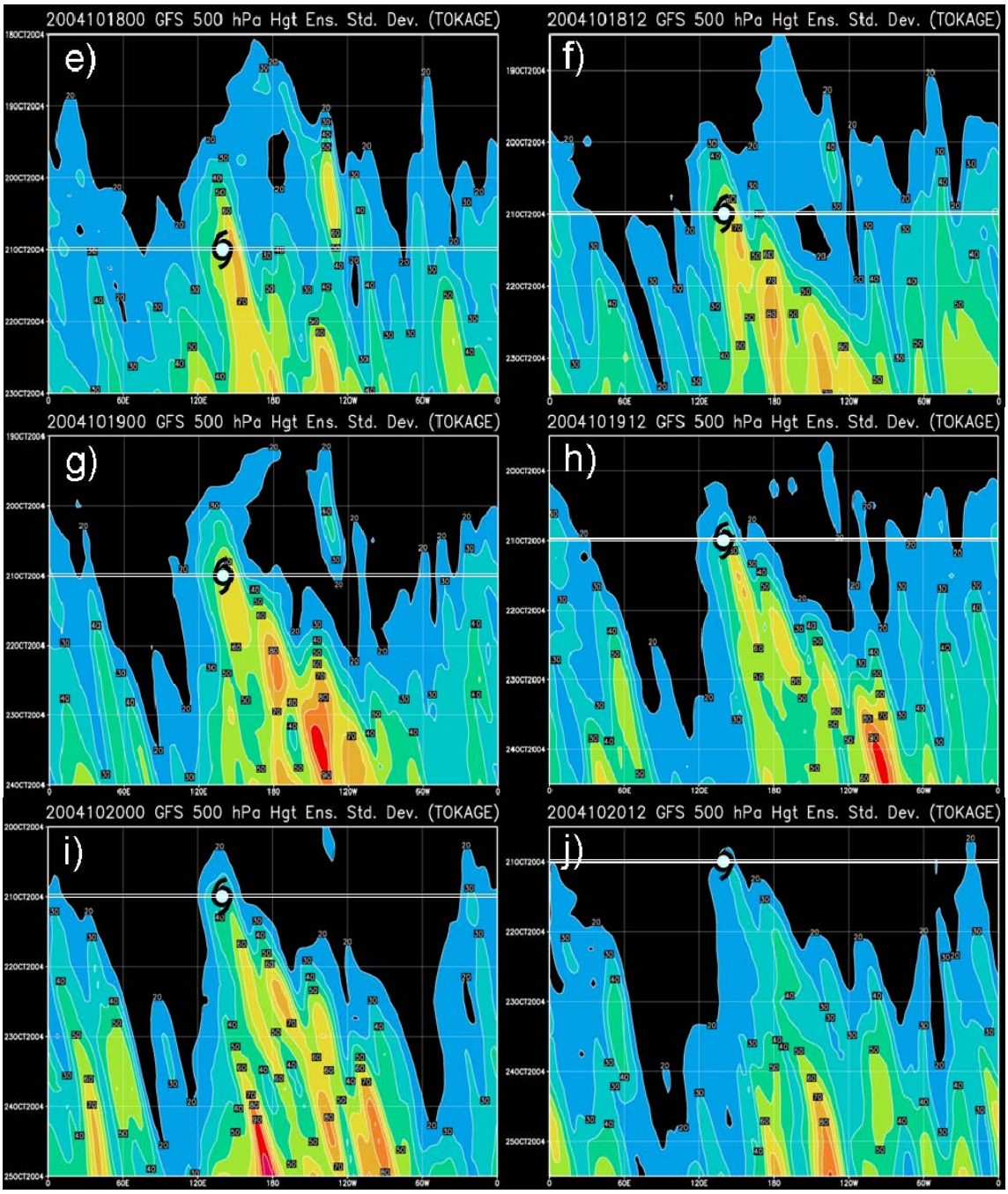

Figure 4. (continued)

A. EMPIRICAL ORTHOGONAL FUNCTIONS

The mean height field, which was calculated across all 44 ensemble members (Figs. 5a, 6a, 7a, 8a, and 9a) was removed prior to the EOF analysis to produce a 500 hPa height anomaly chart. The raw EOF structures were then calculated and the PCs were normalized. Finally, the normalized PCs, in concert

with the raw EOF structures, were then projected back onto the height anomaly field to define the EOF pattern in heights. The final EOF charts are contour plots that indicate the height variation from the mean of all 44 ensemble members (Figs. 5b-c). The first EOF (EOF 1) pattern represents the statistically most common structure of the 500 hPa height field that is recurrent to all 44 ensemble members. Furthermore, the second EOF (EOF 2) pattern represents the next most common structure of the 500 hPa height deviations once the first EOF pattern has been removed. Since the first two EOF patterns explained 55 – 65% of the variance, only EOF 1 and EOF 2 are considered in further analyses. To ensure that TY Tokage had completed its transformation from a tropical cyclone into an extratropical system within each EPS run, a common forecast valid time was established 24 hours after the Joint Typhoon Warning Center (JTWC) had classified it as extratropical. This date is 0000 UTC 22 October. All plots and figures were generated with the assumption that TY Tokage had completed its transformation into an extratropical system by the common forecast valid time.

1. Structural Analysis: 17 October (102-h to 120-h forecasts)

The primary EOF pattern, which explains 37% of the variability (Fig. 5b), indicates that the ET of TY Tokage would cause significant modifications to the downstream height fields. Depending on the sign and weight of the principal component (PC1), the ET may intensify the downstream ridge over the southern tip of the Kamchatka Peninsula (Figs. 5a and b) (i.e., a high positive PC value), or it may cause the height fields to fall (i.e., a high negative PC value). Enhanced ridging would be related to advection of Tokage's upper-level warm core, as well as the downstream advection of low potential-vorticity air associated with Tokage's outflow. Additionally, warm-air advection ahead of the low-level vortex is aiding to build the downstream ridge. Downstream height deviations of greater than 120 meters that result from the ET of TY Tokage are to be noted. This large variability near Kamchatka represents widely varying solutions among the 44 members in this location. In so-called "spaghetti diagrams" often used to display ensemble solutions, the chosen isoheight would have widely spread values in this area. Conversely, there is virtually no variability evident in the upstream 500

hPa height fields, so that in a spaghetti diagram, the 44 isolines would be closely packed here. Large amplitude 500 hPa height variations continue downstream of the Kamchatka Peninsula. A rising (lowering) of the 500 hPa height fields over the Kamchatka Peninsula will be associated with a lowering (rising) of the adjacent downstream fields over the central Pacific. Likewise, the falling (rising) height fields in the central Pacific would then be associated with a rising (falling) response over the west coast of the United States. This high amplitude variability in the longwave pattern downstream of the ET will impact the development and track of midlatitude baroclinic systems across the entire width of the ocean basin.

The EOF 2 pattern explained an additional 13% of the variability (Fig. 5c). The second EOF pattern contained a similar spatial pattern of variability as in the primary EOF, but on a smaller horizontal scale. The EOF pattern suggests the variability of the height field among the 44 ensemble members associated with the ET of TY Tokage, but the immediate downstream amplitude variation in the longwave pattern is not as drastic (roughly 50% less than EOF 1). As with EOF 1, an alternating structure of positive height changes followed by negative height changes is predicted by the ensemble members. Whereas, the height variability in the two EOF patterns is nearly in phase over the Kamchatka Peninsula and the west coast of the United States, the height patterns are out of phase in the central Pacific and Gulf of Alaska. As with EOF 1, the upstream flow patterns associated with EOF 2, do not appear to have significant variability initiated by the ET event.

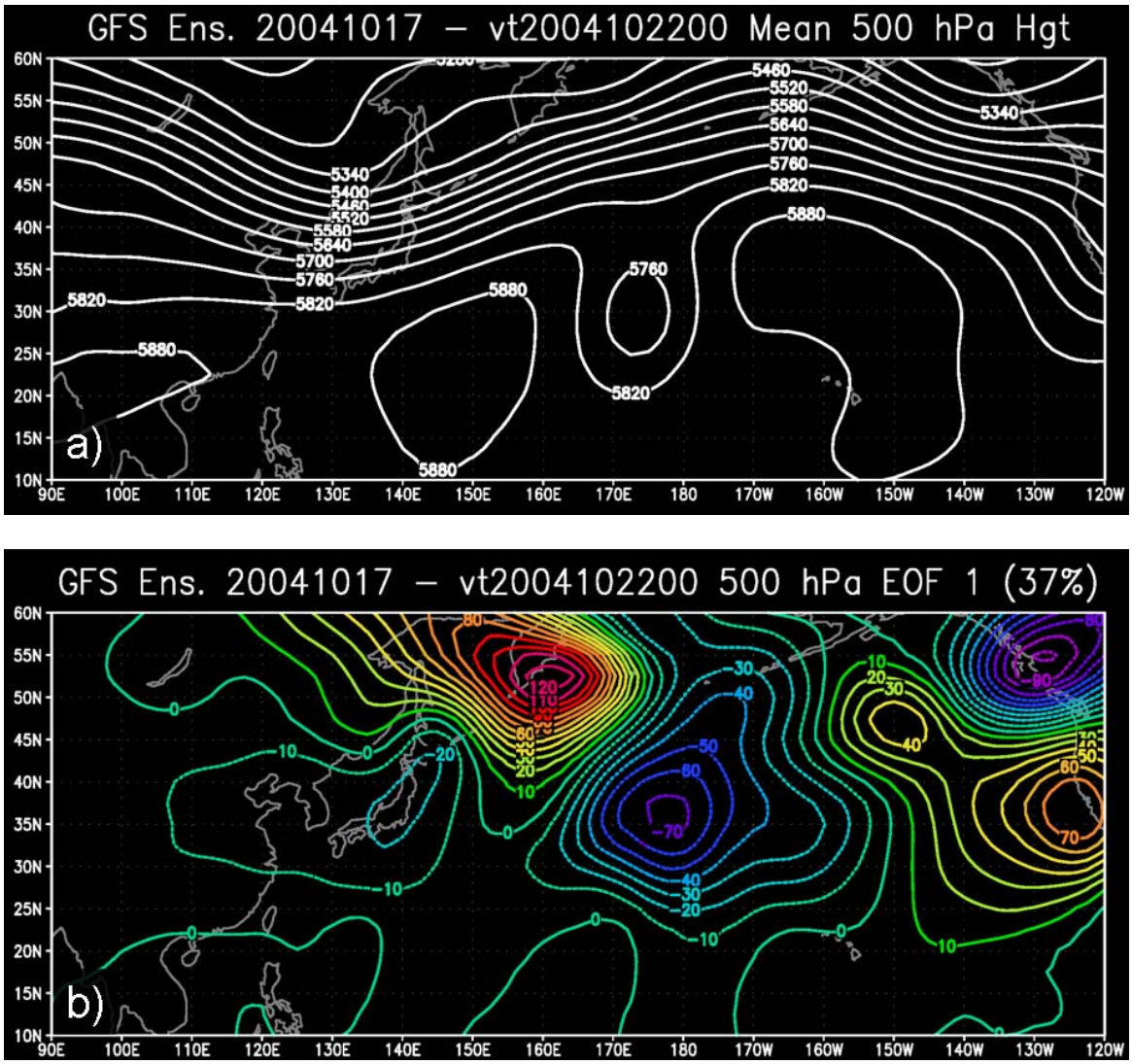

Figure 5. a) The mean 500 hPa height field for all 44 ensemble members for the 102-h to 120-h forecasts from four EPS runs that verify at 0000 UTC 22 October using all four EPS runs produced on 17 October. The 44 ensemble members come from the 0000 UTC, 0600 UTC, 1200 UTC and 1800 UTC EPS forecasts (11 per run) during 17 October. b) The primary 500 hPa EOF structure identified for the 102-h to 120-h forecasts from four EPS runs that verify at 0000 UTC 22 October using all four EPS runs produced on 17 October. The contours indicate the height deviation (in meters) from the mean height field, which is a mean of all 44 ensemble members. c) As in (b), except for the secondary 500 hPa EOF structure.

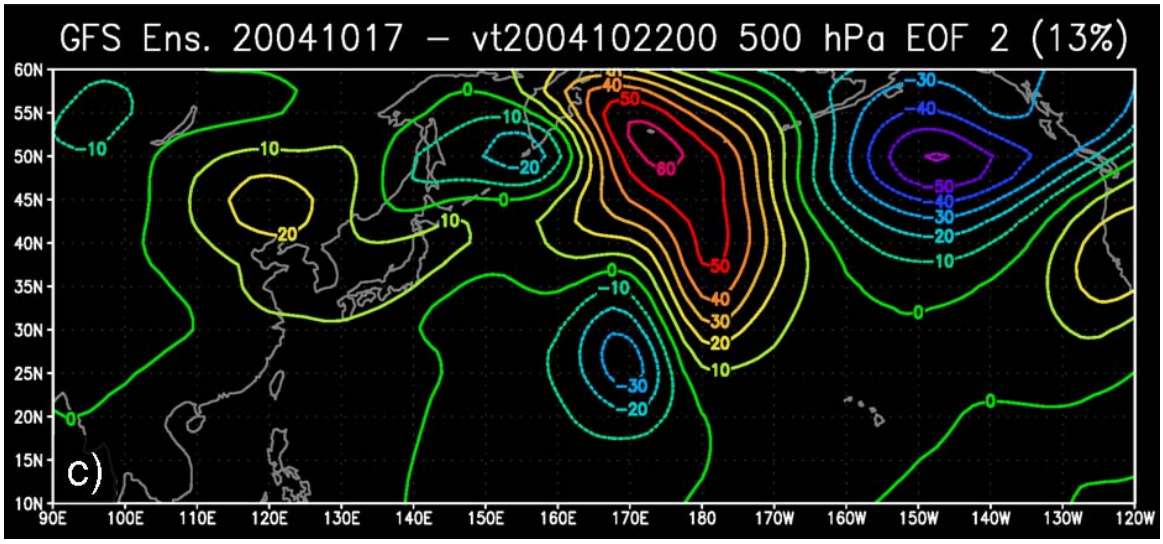

Figure 5. (continued)

2. Structural Analysis: 18 October (78-h to 96-h forecasts)

The leading EOF (Fig. 6b), which explains 36% of the variability, continues to indicate considerable variability in the 44 ensemble member height fields immediately downstream of the ET event. However, this new numerical guidance indicates that the downstream disparity will not be of the same magnitude as was forecast 24 hours previously (compare with Fig. 5b). The EOF analysis of these 96-h forecast fields continues to indicate that the majority of the ensemble members contain centers of high amplitude variability over the central Pacific. It is also of note that the largest variability in the height field is concentrated in the central and western portions of the Pacific basin, and less variability among the 44 members in the eastern Pacific. To the west of the ET location, the height field variability is relatively unaffected by the ET event, which again means that height isolines in the spaghetti diagram would be tightly clustered in this area.

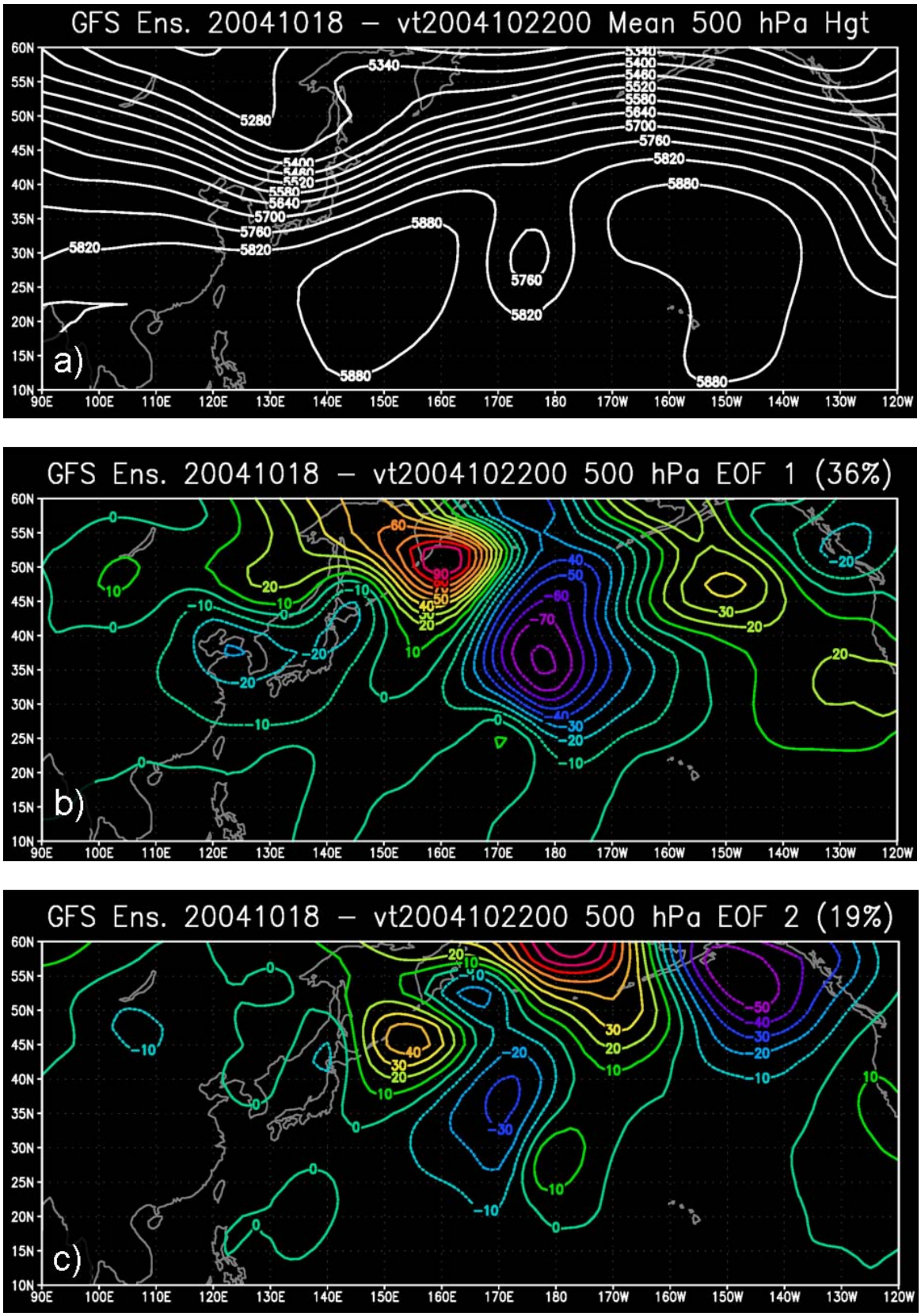

Figure 6. Same as Fig. 5, except for 18 October.

The second EOF pattern (Fig. 6c), which explains 19% of the variability, has centers of fairly large variability over the central North Pacific and poleward of the centers in EOF 1. As in the previous 24-h period, this variability associated with EOF 2 has smaller magnitudes and smaller horizontal scales.

Both the primary and secondary EOFs have identified significant variations about the ensemble mean as expected over the Kamchatka Peninsula, central Pacific, and the Gulf of Alaska (Fig. 6b and 6c). However, the ensemble members are predicting strong agreement in the height fields upstream of the ET event and in the extreme eastern portions of the ocean basin.

3. Structural Analysis: 19 October (54-h to 72-h forecast)

The leading EOF, which explains 42% of the variability, continues to identify a center of variability over southern Kamchatka (Fig. 7b). Similar to the previous set of ensemble forecasts from 18 October, a slight decrease is predicted in the magnitude of the downstream variability among the 44 ensemble members. The height field variability continues to be concentrated over the western and central North Pacific. The secondary EOF (Fig. 7c), which explains 16% of the variability, is identifying centers of variability that are slightly shifted ahead of the variability centers in EOF 1 (i.e., 90° out of phase with EOF 1). The upstream height fields continue to contain less variability in the 44 member ensemble than what occurs across the North Pacific. At this time, the EOF patterns are clearly representative of a downstream wave-like response to the ET event.

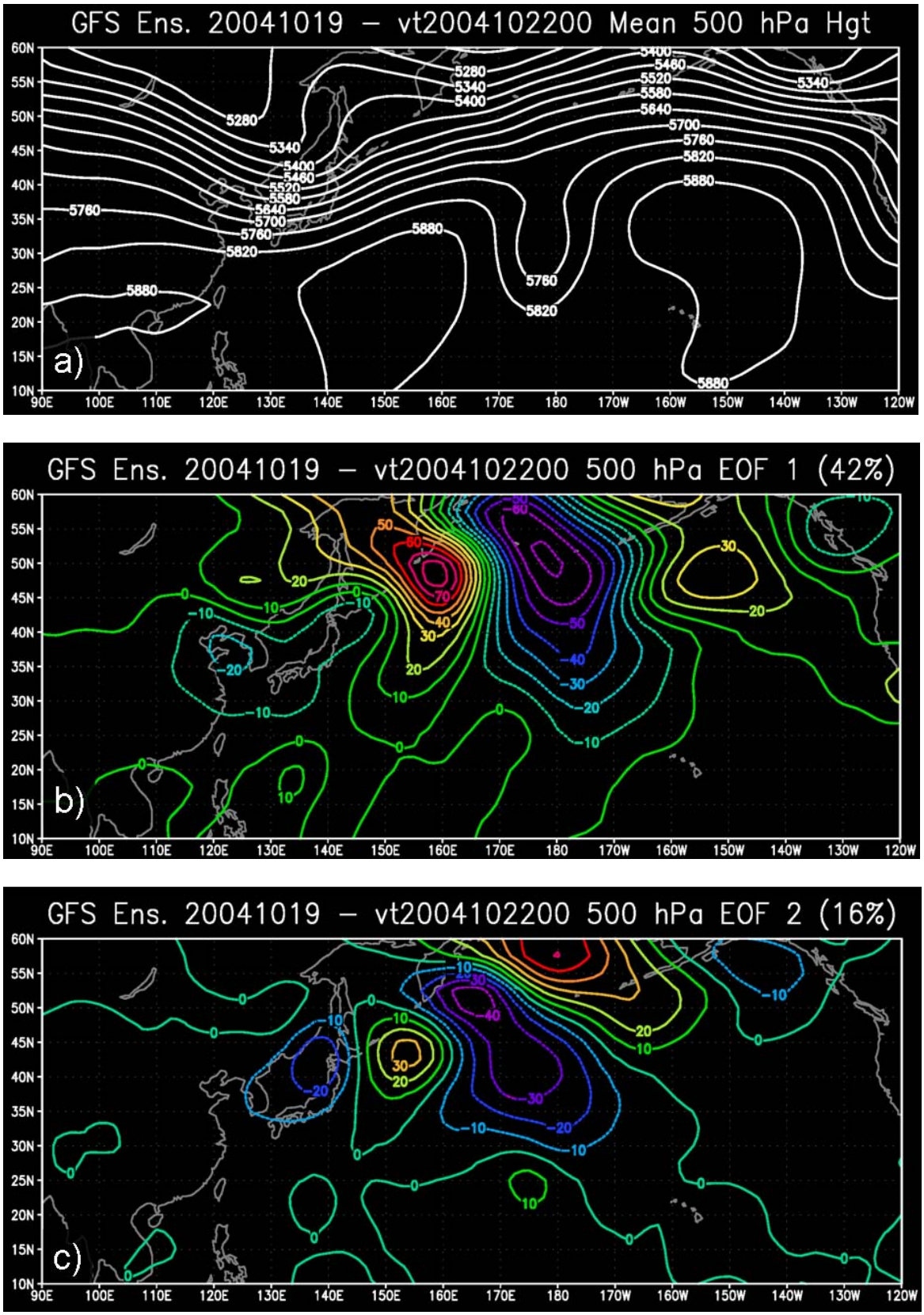

Figure 7. Same as Fig. 5, except for 19 October.

4. Structural Analysis: 20 October (30-h to 48-h forecasts)

The amplitudes of individual centers of variability in EOF 1 (Fig. 8b) for the ensemble predictions from 20 October continue to decrease in magnitude relative to the amplitudes of EOF 1 patterns from previous ensemble runs. Furthermore, the amount of total variability explained by EOF 1 (44%) remains consistent with previous EOF 1 structures. The wave-like pattern to the centers of variability is consistent with the EOF pattern from 19 October. In combination with the decreasing magnitude of the variability (i.e., spread in the ensembles), this suggests that the solution is converging toward the ensemble mean.

Whereas the EOF 2 (Fig. 8c) from previous ensemble runs had also defined a wave-like pattern, it was often poleward of the EOF 1 pattern. However, the EOF 2 pattern from the ensemble predictions from 20 October has begun to shift such that a dipole of variability exists over the central North Pacific centered near 30°N. Therefore, as 20 October is within 24-48 hours of the ET event a shift in relative influence may be occurring such that the ET event is becoming less of a factor in the variability over the North Pacific as defined by EOF 2.

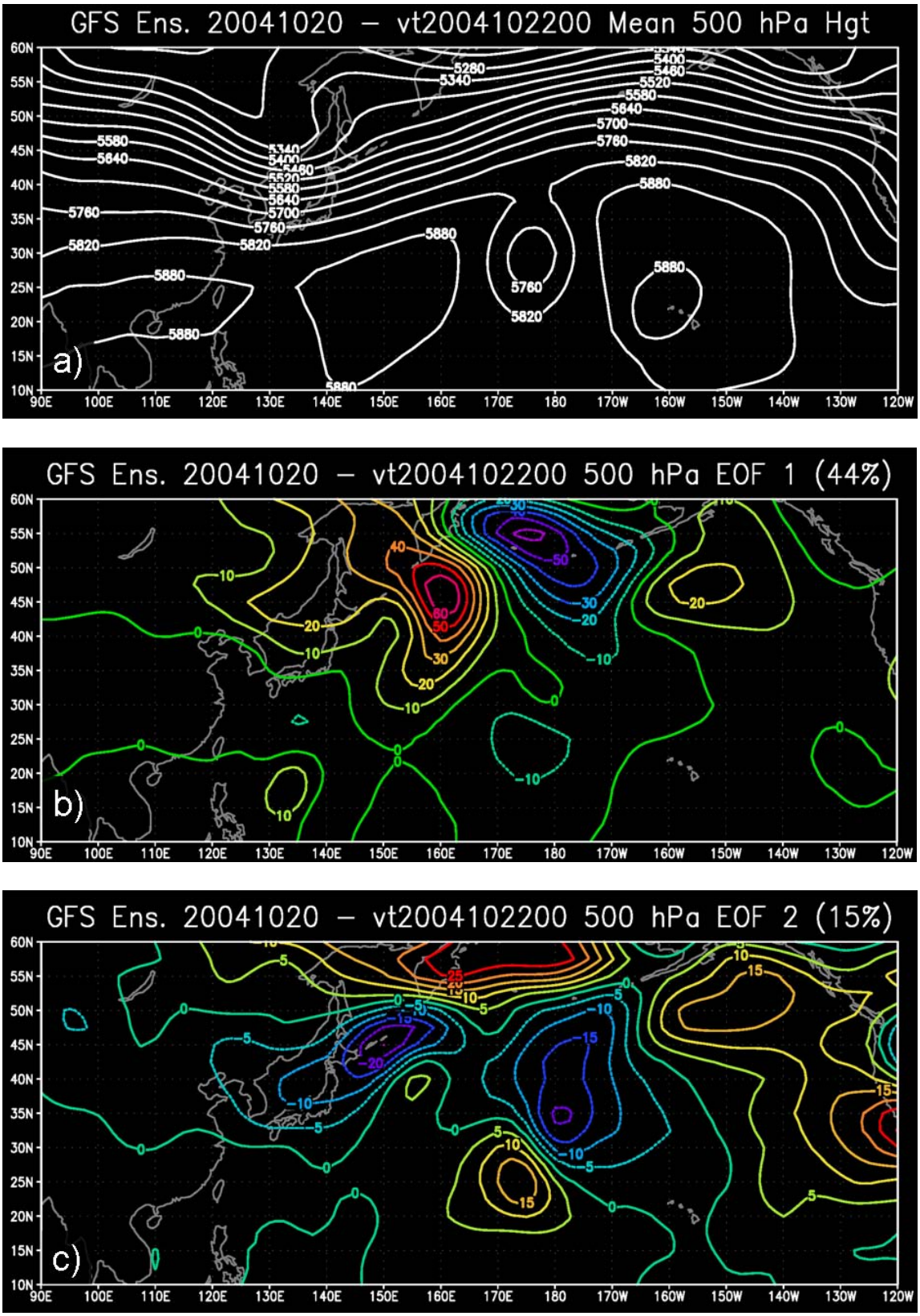

Figure 8. Same as Fig. 5, except for 20 October. Note that the contour interval shifted from 10 meters (previous figure) to 5 meters.

5. Structural Analysis: 21 October (06-h to 24-h forecast)

Although the EOF 1 pattern (Fig. 9b) continues to define a wave-like structure of variability, the amplitudes of the individual centers are smaller than previous times. The largest variability in the height field continues to be over the central and western North Pacific as defined for the 20 October EOF 1 pattern (Fig. 8b). The shift in variability away from the region of the ET to the central North Pacific has continued in the EOF 2 pattern of 21 October (Fig. 9c).

In summary, the primary EOF patterns analyzed in successive ensemble model runs define a persistent characteristic of ET events; namely, that the height perturbations induced by the ET of TY Tokage generate a large amplitude response to the downstream wave pattern. Furthermore, the magnitude of individual centers of variability decreased as the ET event becomes part of shorter-range forecasts. Eventually, when the ET event was within the 48-h forecast interval, EOF 2 began to evolve such that the variability shifted away from the ET toward the central North Pacific, which was related to a deep midlatitude trough that extended into subtropical latitudes. In other words, as the ET event becomes better defined in successive ensemble runs, the uncertainty associated with the ET event will decrease, and the ET event will no longer be the primary source of variability in the ensemble forecast as the variability centers shift toward the next active region that is producing the largest spread in the ensemble forecast. Accordingly, the EOF 2 pattern from 21 October (Fig. 9c) is identifying a “new” variability center in the ensemble 500 hPa forecast associated with a midlatitude trough over the central North Pacific.

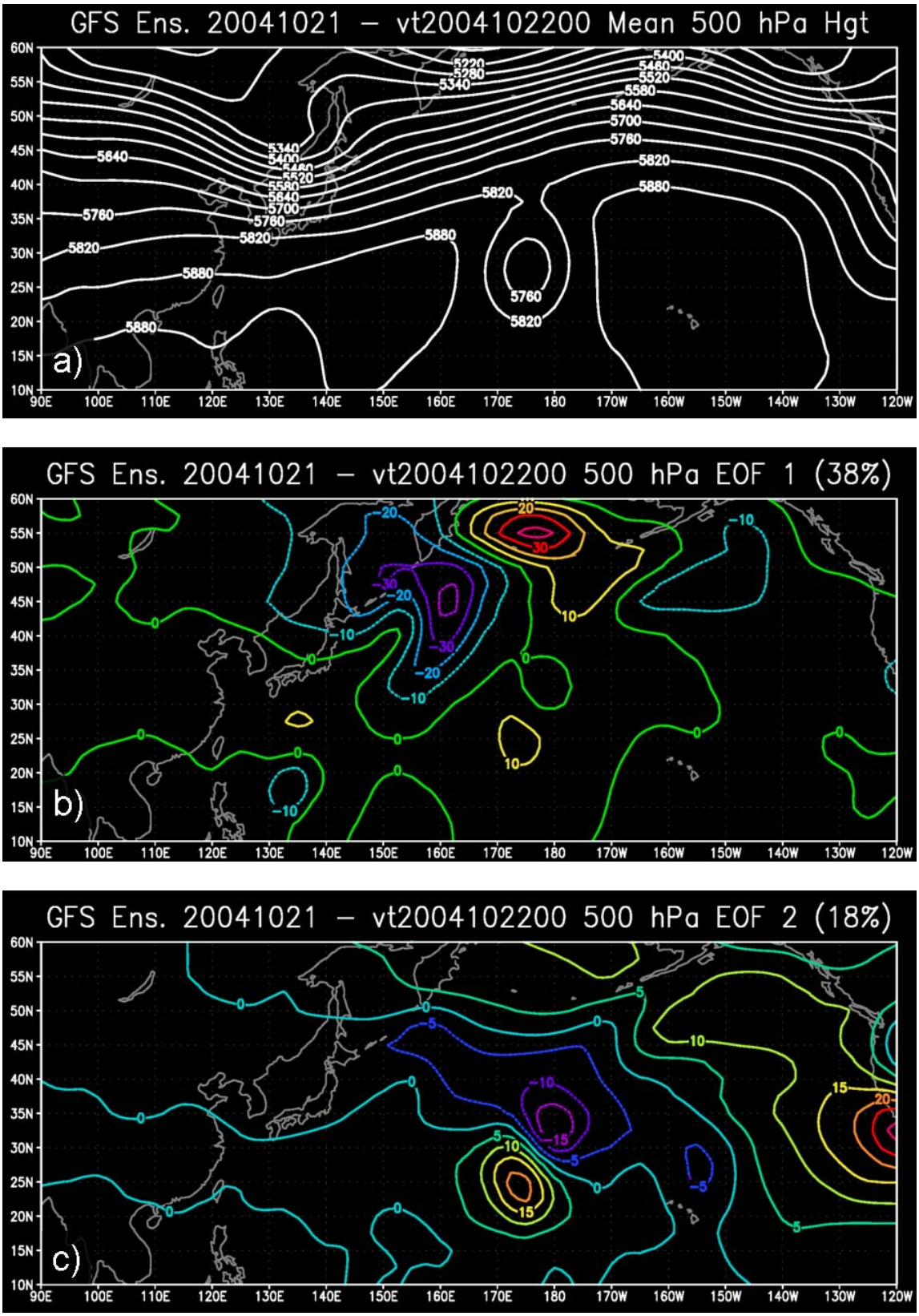

Figure 9. Same as Fig. 5, except for 21 October. Note that the contour interval of 5 meters.

B. IDENTIFICATION OF EXTRATROPICAL TRANSITION PATTERNS USING FUZZY CLUSTER ANALYSIS OF THE PRINCIPAL COMPONENTS (PC)

As stated earlier, the contribution of each EOF structure to the total field in an individual ensemble member is weighted by the sign and magnitude of their respective principal components (PCs). Accordingly, PC1 specifies how much of the first EOF structure (EOF 1) is contained in each ensemble member. Similarly, the second principal component (PC2) identifies how much of the second EOF structure (EOF 2) is found within each ensemble member. For example, if the PC1 value for the second ensemble member from the forecasts initiated on 17 October (Fig. 10) is very small (~0), very little EOF 1 structure characteristic is predicted in the second ensemble member. In this case, the second ensemble member has a relatively high negative PC2 value, which indicates a strong (negative) presence of the second EOF structure (EOF 2) such that it would be the inverse of the EOF 2 pattern of 17 October (Fig. 5b). Accordingly, the second ensemble member would have a stronger ridge just south of the Kamchatka Peninsula and the downstream trough centered over the central north Pacific would be deeper than the ensemble mean height field (Figs. 5b and 10).

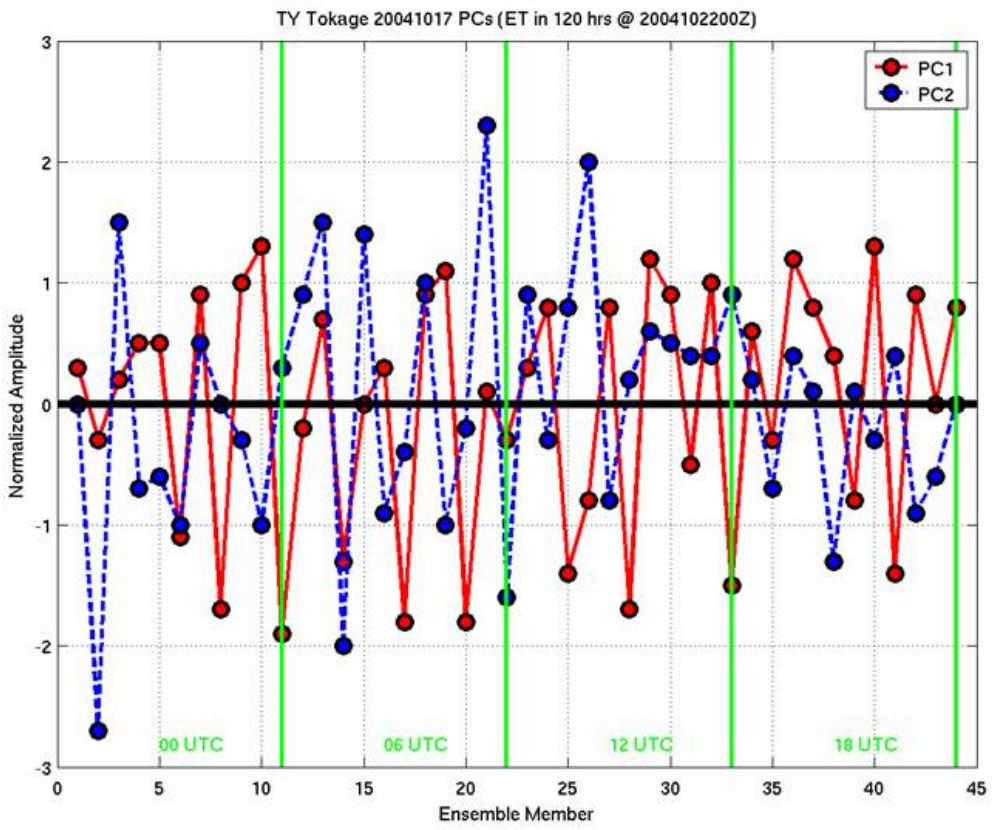

Figure 10. First (PC1, solid line) and second (PC2, dashed line) principal components from the EOF analysis of the four 17 October ensemble runs. The horizontal axis specifies the 44 ensemble members and the vertical axis is the normalized amplitude (i.e., weight). The green lines define the separation between the consecutive model runs. Note that there are 11 members per operational ensemble run.

To aid in the identification of ensemble forecasts that contain similar characteristics, the principal components for EOF 1 were plotted against the principal components for EOF 2 (Fig. 11). A fuzzy k-means cluster routine in MATLAB was utilized to objectively identify a pre-specified number of groups. The initial group centers were randomly picked at the beginning of the clustering routine. The sensitivity to the initial location of the randomly chosen starting cluster positions was examined by performing the analysis ten times with varying starting locations to check for instabilities in the solutions. When an instability was noted, the most frequent pattern was assumed to be the correct grouping solution.

As stated earlier, it is hypothesized that when the ET event is first realized by the model at extended forecast intervals the initial number of groups into which the ensembles members can be separated should be large due to the high uncertainty associated with this event. It is the objective of this study to show that progressive ensemble runs reduce the number of groups (i.e., number of forecast scenarios) as the extratropical transition process becomes better defined in the model. The following subsections examine the evolution of the cluster definitions for the ensemble runs of each day leading to the ET event.

1. 17 October (102-h to 120-h forecasts)

a. Cluster Analysis

At this time, the EPS runs first identified the ET event at the extended forecast range (102-120 hours). In the first trial, three cluster centers were randomly chosen as initial conditions to the fuzzy cluster analysis (Fig. 11a). For identification purposes, clusters will be labeled by two numbers. The first number defines the total number of clusters and the second number defines the cluster number within the total number. For example, cluster (3-2) is the second cluster in the three-cluster solution.

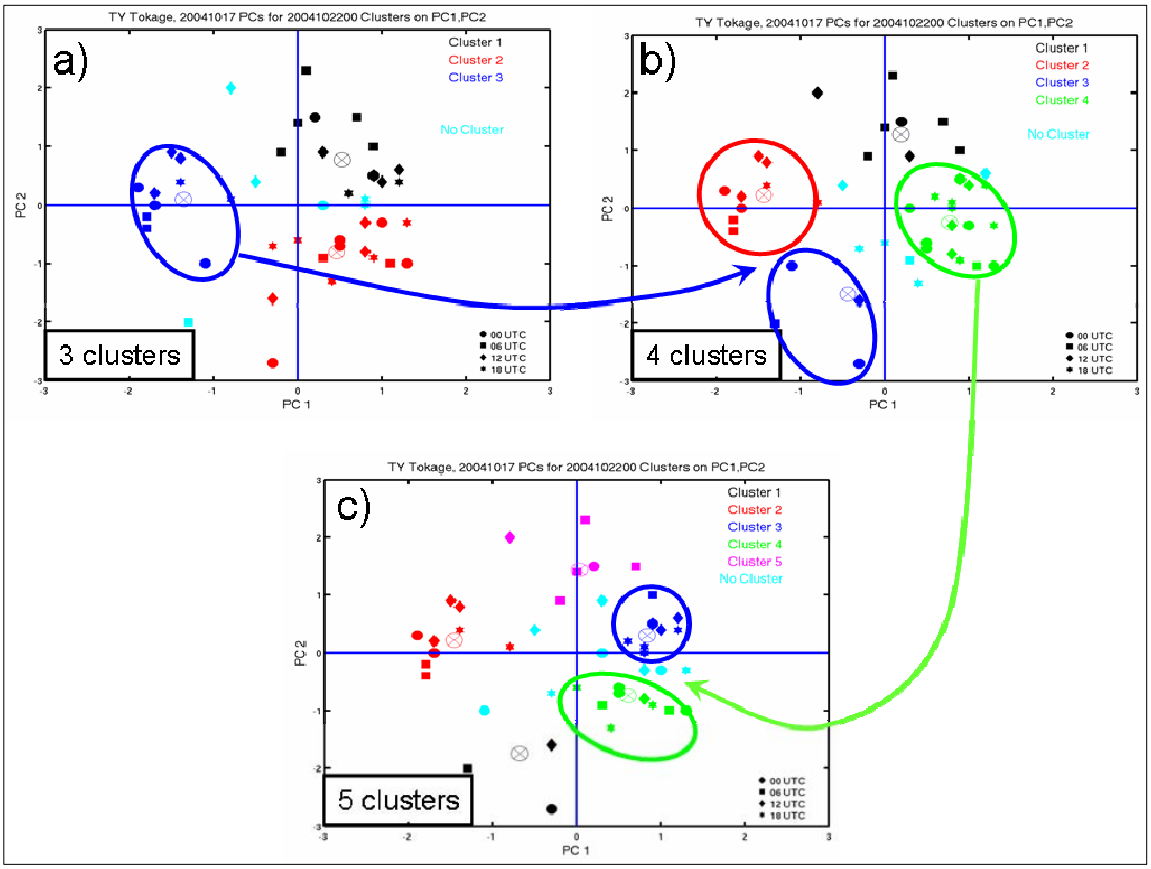

Figure 11. a) The three cluster solution for 17 October. The blue circle highlights cluster (3-3) that was subdivided into clusters (4-2) and (4-3) (red and blue circles in Fig. 11b). b) Analyzed four cluster solution. The green circle defines cluster (4-4) while the green arrow points to the split of cluster (4-4) into cluster (5-3) and (5-4) (blue and green circles in Fig. 11c). c) The five cluster solution in which the blue and green circle depicts the subdivision of cluster (4-4).

Whereas clusters (3-1) and (3-2) (Fig. 11a) lie on the positive part of the PC1 axis, they are separated by the zero line of the PC2 axis. However, cluster (3-3), which is circled in Fig. 11a, represents the negative PC1 group but this cluster straddles the zero line of PC2. Therefore, the EOF 2 structure contributes in a positive and negative sense to clusters (3-1) and (3-2), but has only a small (value near zero) contribution in cluster (3-3). However, another solution may exist that splits group (3-3) into two clusters about the PC2 axis. Therefore, a four-cluster solution (Fig. 11b) was sought to test whether or not cluster (3-3) could be sub-divided into two unique clusters.

Grouping the 17 October PCs into four clusters (Fig. 11b) did not split cluster (3-3) into positive and negative PC2 values. Rather, an outlier near (-1, -1) was removed from (3-3) and put in a new cluster (4-3). These new clusters reduced the variability in cluster (3-2) in Fig. 11a. The four-cluster solution now resulted in cluster (4-1) that straddled the PC1 axis, and two clusters that straddled the PC2 axis, clusters (4-2) and (4-4) respectively. A five-cluster solution (Fig. 11c) was then examined. Cluster (4-4) was divided into two smaller groups (5-3) and (5-4) on either side of the PC2 axis. Also, the size of cluster (4-3) was reduced to only three members. Cluster (4-1) remained intact with its cluster center located on the PC2 axis (Fig. 11c).

To examine the physical representation of these cluster solutions, representative 500 hPa and mean sea-level pressure (MSLP) fields were generated for each cluster by averaging the ensemble members that belonged to each cluster. When a cluster group was divided into two new clusters as in Fig. 11, the representative fields were examined to ensure that the division did in fact identify two distinct synoptic patterns that were previously tied together.

Examination of the MSLP fields during the subdivision of cluster (3-3) into clusters (4-2) and (4-3) reveals two distinct ET transformation modes of TY Tokage (Fig. 12a). Whereas cluster (4-2) defines a split of cluster (3-3) such that Tokage re-intensifies as a strong midlatitude extratropical cyclone, cluster (4-3) has identified a weak transformation of TY Tokage. Both scenarios have the position of the former typhoon east of the Kamchatka Peninsula. However, cluster (4-3) has also identified a broad baroclinic region of low pressure centered over Hokkaido Island associated with a weak short wave propagating through the midlatitudes (Fig. 12b).

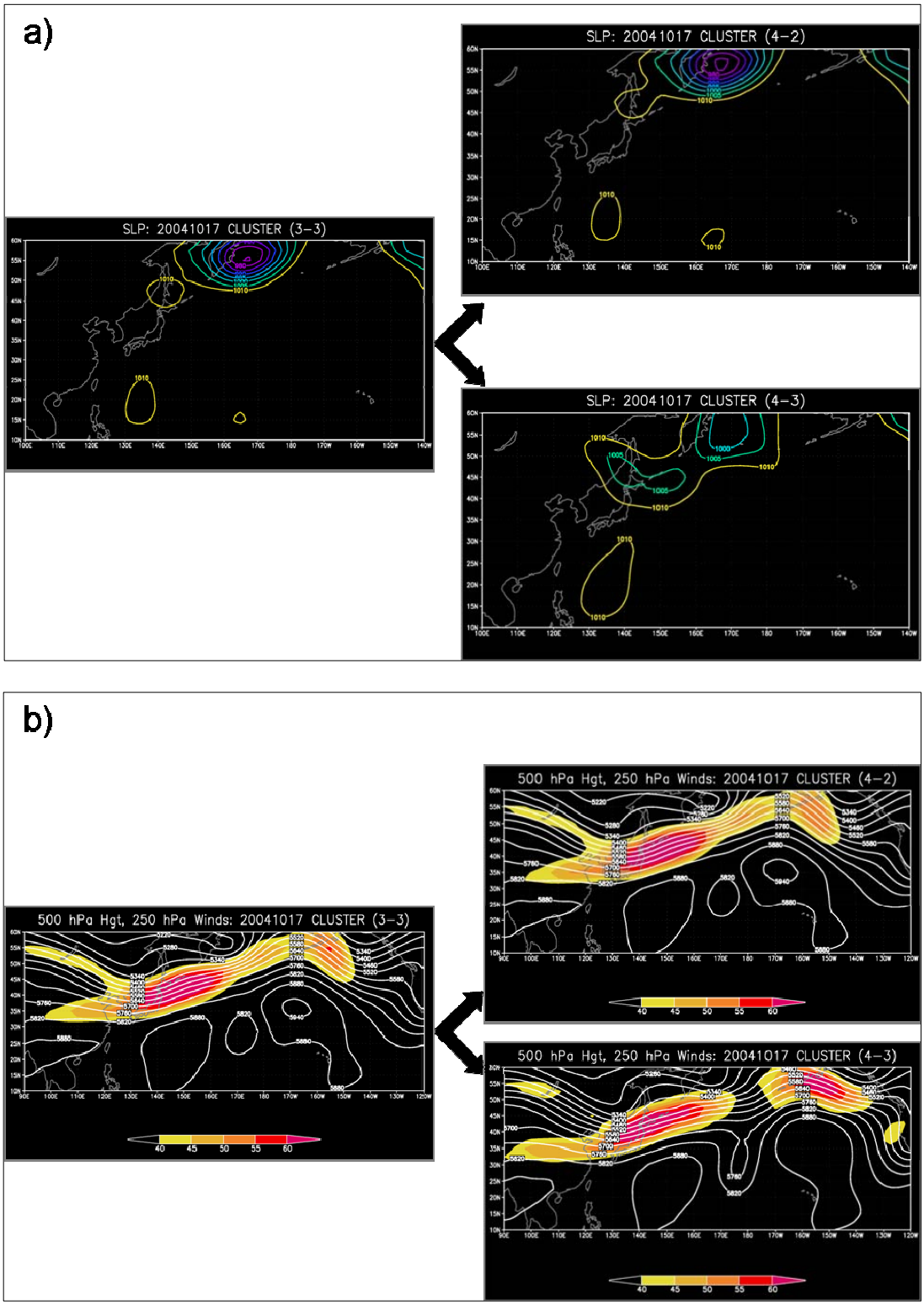

Figure 12. a) Mean sea-level pressure (MSLP) charts (hPa, only values below 1010 shown) for clusters (3-3) on the left side, and (4-2) and (4-3) on the right side. Subdividing cluster (3-3) clearly reveals two distinct ET modes in the EPS forecast. b) As in (a), except for 500 hPa heights (m) with 250 hPa winds (shaded, m s^{-1}).

The further subdivision of cluster (4-4) in Fig. 11b into two new clusters was also examined. The separation was deemed unnecessary as there was no noticeable intensity or location change for the ET event (Fig. 13). It was determined that four clusters were the proper grouping for the 44 ensemble members produced on 17 October.

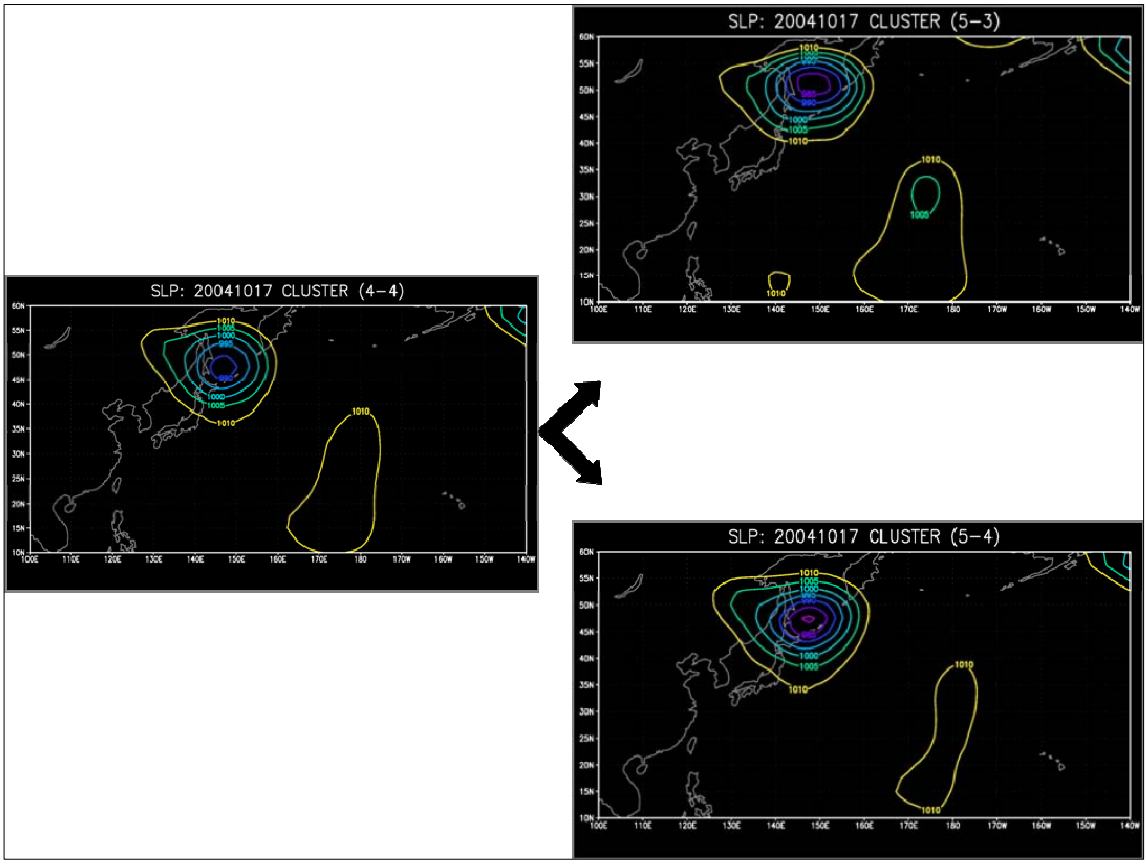

Figure 13. Same as Fig. 12a, except depicting the division of cluster (4-4) on the left side into cluster (5-3) and (5-4) on the right side.

By subdividing the 44 members into four clusters, four distinct ET scenarios could be discerned from the ensemble solution:

- Cluster (4-1) identified a moderate ET event (Fig. 14a and 14e)
- Cluster (4-2) revealed a major re-intensification of TY Tokage after it completed its transformation. (Fig. 14b and 14f)

- Cluster (4-3) implied that the ET result would be a weak extratropical cyclone (Fig. 14c and 14g)
- Cluster (4-4) also suggested a moderate ET event. However, the storm motion was significantly slower than the ET event identified in cluster (4-1) (Fig. 14d and 14g).

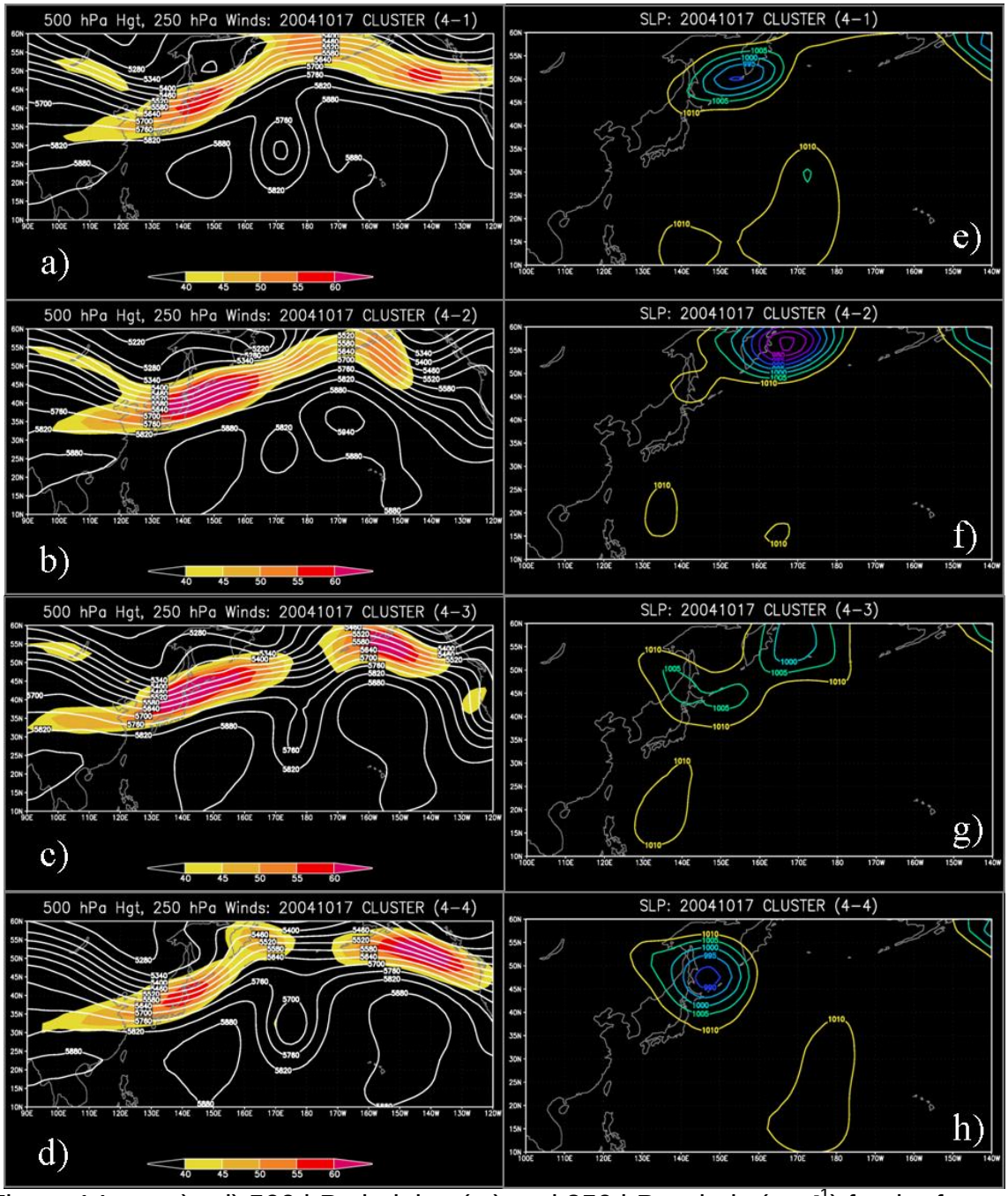

Figure 14. a) - d) 500 hPa heights (m) and 250 hPa winds (m s^{-1}) for the four clusters identified via fuzzy k-means clustering of the ensemble forecast from 17 October. e) - h) Corresponding MSLP (hPa, only values less than 1010 shown) patterns for the four clusters.

b. Variations in the Analysis for Each Set of Ensemble Cluster Forecasts

The cluster analysis technique has reduced the number of meteorological scenarios from 44 to four. These four solutions represent four different atmospheric responses to slightly different initial conditions. Therefore, variations in the forecast analysis of 500 hPa heights and 250 hPa winds averaged for those ensemble members in each of these four clusters were examined to correlate the model response (i.e., Fig. 14) to varying modeled analysis fields (Fig. 15). This was examined by constructing an average analysis field for each cluster that was then subtracted from the 44 member analysis average. For example, the 500 hPa height analysis anomaly for cluster (4-3) (Fig. 15c) has a deeper trough (by 70 m) northeast of Japan compared to the 44 ensemble average. The most striking feature of Fig. 15 is the amplitude of the midlatitude anomalies in these ensemble members. Whereas the initial condition perturbations in an ensemble forecast are supposed to represent observational uncertainty, typical perturbation amplitudes over data-sparse areas (i.e., the oceans) are expected to be on the order of approximately 30 meters (National Centers for Environmental Prediction, April 2005). Clearly the midlatitude anomaly values for 17 October appear to be too large.

Clusters (4-2) and (4-3), which propagate the system quickly into the midlatitudes (Fig. 15b and 15c), had Tokage in the initial conditions slightly ahead or centered over the best-track position. Clusters (4-1) and (4-4) (Fig. 15a and 15d) had Tokage well behind the best-track position. Therefore, the speed at which the decaying Tokage moved through the ET process and into the midlatitudes varied consistently with the placement of the tropical cyclone with respect to the best-track position. However, the re-intensification scenario of the ET process did not depend on the TC position relative to the best-track. That is, ET scenarios that were fast were weak (4-3) and strong (4-2) and the ET scenarios that were slow were both moderate ((4-1) and (4-4)). Therefore, it is inferred that the phasing of Tokage into the midlatitudes is the critical factor in determining the translation speed during ET, but not the re-intensification

scenario. The re-intensification scenario of the ET is more related to the intensity anomaly (Fig. 15). For the strong and moderate re-intensifications, the perturbed tropical cyclone is deeper than the mean. For the weak ET of cluster (4-3), the amplitude of the tropical cyclone was not changed from the 44 member mean.

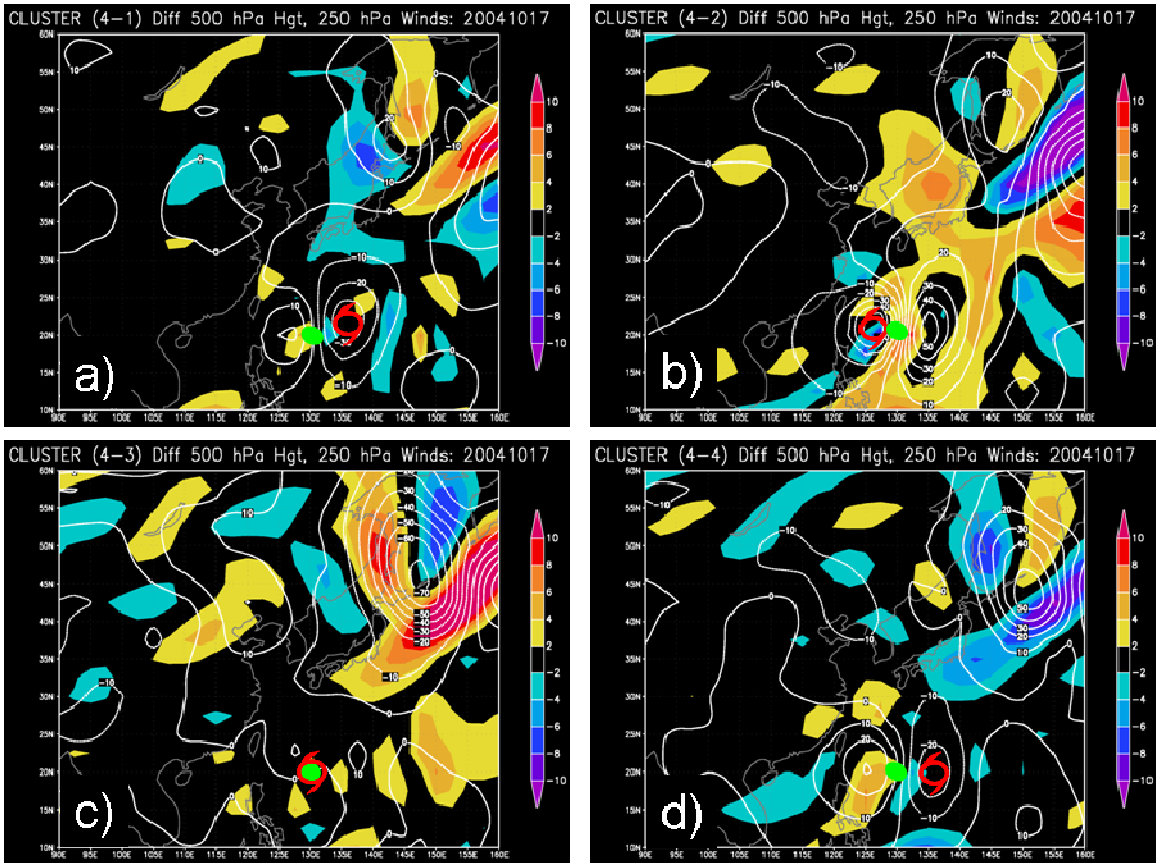

Figure 15. Analyzed 500 hPa height and 250 hPa wind anomalies for the four clusters resolved using the four daily EPS runs from 17 October. The height anomaly (solid lines) contours are spaced every 10 meters and the wind anomalies (color filled contours) have a contour interval of 2 m s^{-1}. The red tropical cyclone symbols depict where Tokage was located in the analysis. The green filled oval depicts Tokage's best-track position during 17 October. a) Cluster (4-1): Weak to Moderate re-intensification stage. b) Cluster (4-2): Strong re-intensification that propagates quickly across the northwestern Pacific. c) Cluster (4-3) Weak re-intensification that propagates quickly in the midlatitudes. d) Weak to Moderate re-intensification stage that moves slowly in the westerlies.

To examine the phasing between the tropical cyclone and the midlatitudes in each cluster, 250 hPa divergence was calculated for each cluster

(Fig. 16). Because strong, upper-level divergence acts to deepen a surface vortex, only positive values were plotted, which are identified in Fig. 16 with a filled circle, and the color of the circle identifies the cluster group. These local divergence maxima were overlaid on the mean sea-level pressure chart (Fig. 17) to aid in the identification of coupling between the tropical cyclone and the midlatitude flow. The local maxima in upper-level divergence will be examined with respect to the evolution of each cluster from the analysis time through the 120-h forecast (Fig. 18).

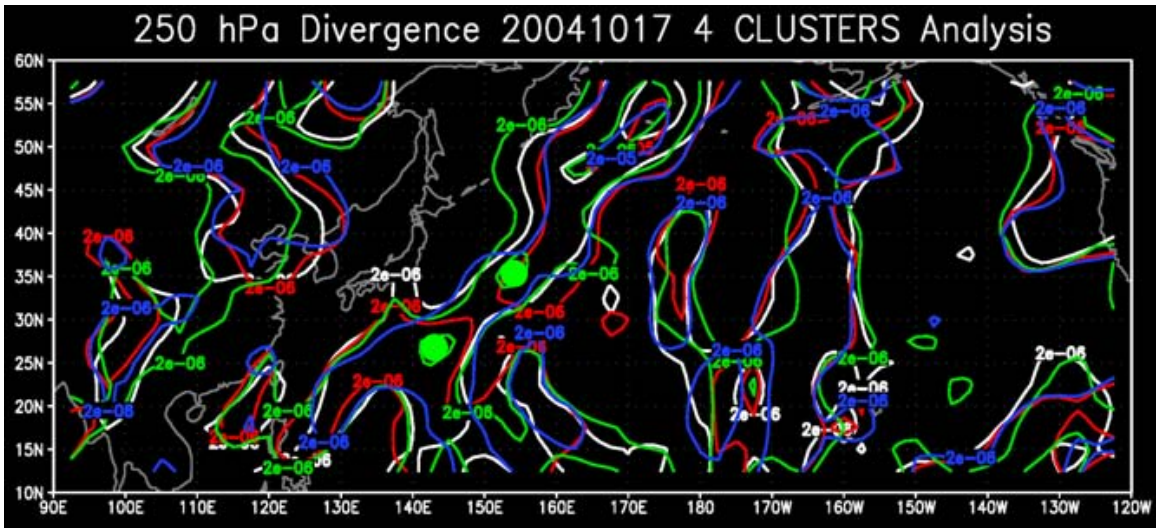

Figure 16. Divergence at 250 hPa based the cluster analysis of the 17 October ensemble run. Only positive contours were plotted at intervals of 2 x 10^{-6} s^{-1} and 2 x 10^{-5} s^{-1}. White (4-1), red (4-2), green (4-3) and blue (4-4) represent the four cluster groups. Two local divergence maxima (>2 x 10^{-5} s^{-1}) have been identified at 35°N, 154°E and 27°N 143°E in Cluster (4-3) (green circles).

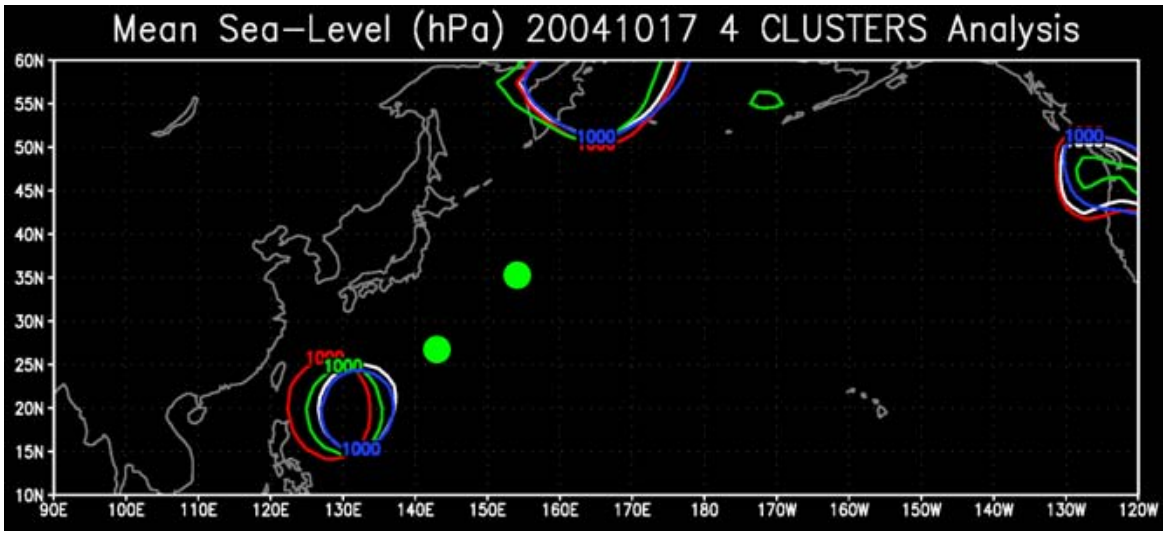

Figure 17. MSLP chart based on the 17 October analysis. Only the 1000 hPa isobar was plotted. The divergence maxima (filled circles) identified in Fig. 16, have been overlaid. Cluster definitions are as defined in Fig. 16.

At the analysis time, it is clearly evident that TY Tokage in cluster (4-2) (Fig. 18a and b) is ahead of the other three cluster positions. The divergence maxima in cluster (4-3) (green) indicate that some of Tokage's outflow is flowing into the mid-latitude trough south of Kamchatka (Fig. 18a and b). By the 12-h forecast (Fig. 18c and d), the outflow from cluster (4-3) into the midlatitudes has stopped and all divergence maxima are found directly above the tropical system, which indicates that all four clusters are isolated from the midlatitudes. By the 24-h forecast (Fig. 18e and f), outflow from cluster (4-2) (red) is extending ahead of the decaying tropical cyclone and into the mid-latitudes. Over the next 24-36 hours (Figs. 18g and h, 18i and j), a divergence maximum remains ahead of cluster (4-2) and appears to contribute to its rapid re-intensification as a midlatitude cyclone. The decaying tropical cyclone in the other three clusters (4-1, 4-3 and 4-4) did not become coupled with the midlatitude jet until the 48-h forecast (Fig. 18i and j). At this time, a divergence maximum was ahead of each low-level vortex. Because these three clusters remained uncoupled with the mid-latitude jet for a longer period of time, they failed to re-intensify as a strong baroclinic cyclone. The examination of the upper-level divergence relative to the location of the low-level vortex center helps to

clarify the apparent sensitivity of the ensemble forecast to the phasing of Tokage with the midlatitudes.

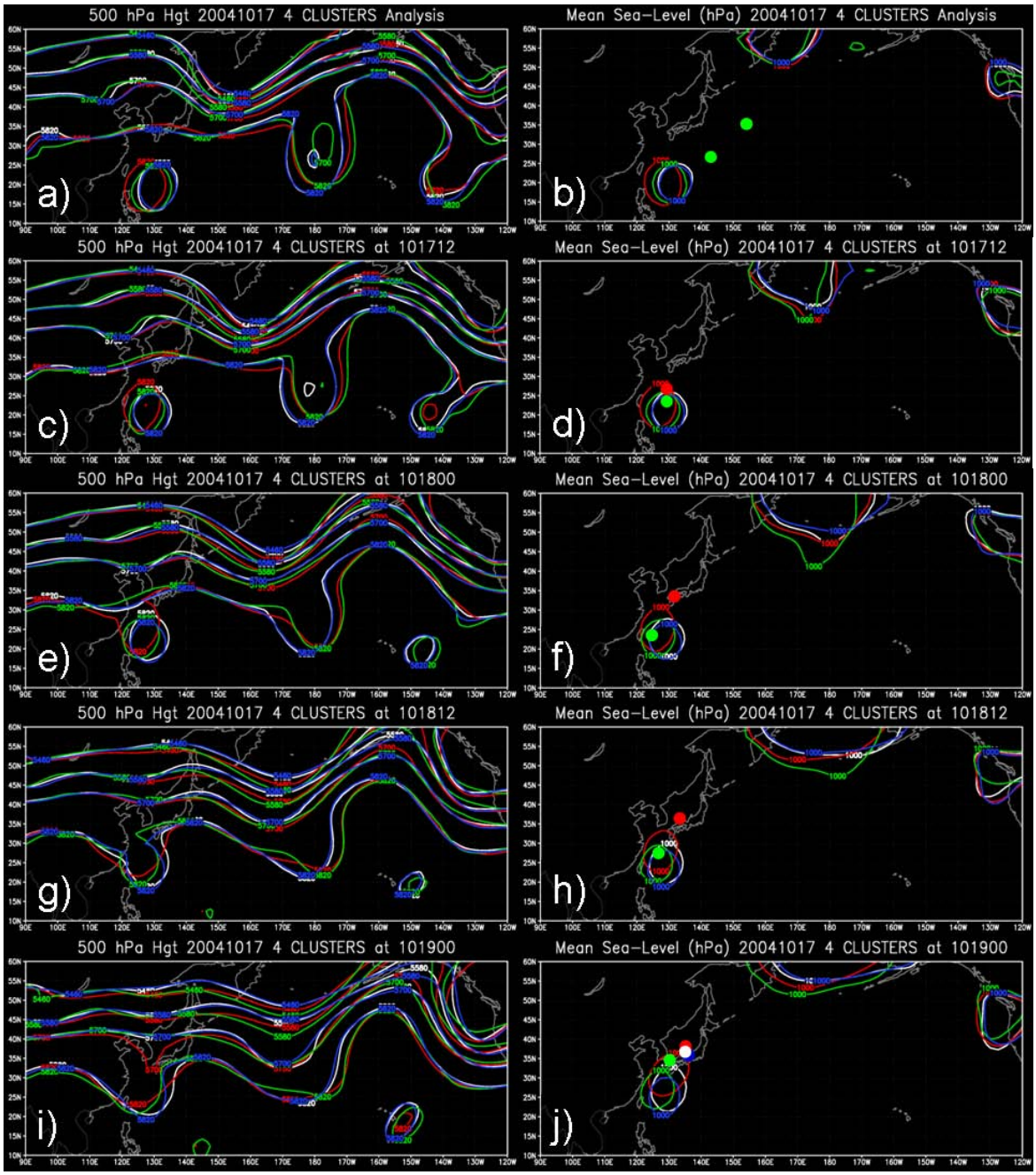

Figure 18. The five day forecast for clusters (4-1) (white), cluster (4-2) (red), cluster (4-3) (green), and cluster (4-4) (blue) starting at 0000 UTC 17 October. The forecast interval is every 12 hours. The plots on the left side are the 500 hPa height fields for all four clusters. The figures on the right are the MSLP charts with the 1000 hPa isobars plotted (colored contour lines). The color-filled circles on the MSL charts identify 250 hPa divergence maxima (> 2×10^{-5} s^{-1}).

As Tokage continues to move into the midlatitudes, its influence on the midlatitude long-wave pattern is better examined by combining Fig. 4c and similar charts as on left side of Fig. 18. Starting with the 48-h forecast for 17 October, which is where Fig. 18i and 18j left off, differences in the phasing of Tokage into the midlatitudes is apparent. Clusters (4-2) and (4-3) have propagated the system ahead of the other two clusters as indicated in Fig. 19a by the troughing over the East China Sea. The different phasing of Tokage by each cluster is already introducing a spread among the ensemble members (shaded regions, Fig. 19a). Over the next 12 h (Fig. 19b), clusters (4-2) and (4-3) accelerate in the westerlies while clusters (4-1) and (4-4) lag behind. The troughing associated with the ET process initiated by cluster (4-2) is already over the Sea of Japan, while the troughs associated with the other three clusters are farther west. By the 72-h forecast for 17 October (Fig. 19c), the trough associated with cluster (4-2), by now firmly embedded in the westerlies, continues to move rapidly to the east and is now over Japan. Conversely, cluster (4-4) has kept Tokage isolated from the midlatitude flow as indicated by the relative zonal orientation of the 500 hPa height contours north of 40°N. The differences in phasing of Tokage into the midlatitudes are forcing a rapidly increasing spatial separation between the disturbances initiated by ET process for each cluster. As the spatial separation continues to increase through the 84-h (Fig. 19d) and 96-h (Fig. 19e) forecasts, the standard deviation (i.e., ensemble spread) also increases. That is, leading up to the forecast interval when Tokage was classified as extratropical, phasing differences introduced in the 17 October analysis are producing a rapidly increasing ensemble spread across the four clusters. Also, note that as the ET process evolves in Figs. 19a – 19e, the uncertainty perturbations introduced in the 500 hPa height fields by the phasing of Tokage into the midlatitudes is limited to the downstream flow. Even by the 96-h forecast (Fig. 19d), the 500 hPa height contours indicate little variability between the four clusters upstream of the ET event (i.e., over mainland China). Thus, the ET process does not appear to perturb the upstream atmosphere.

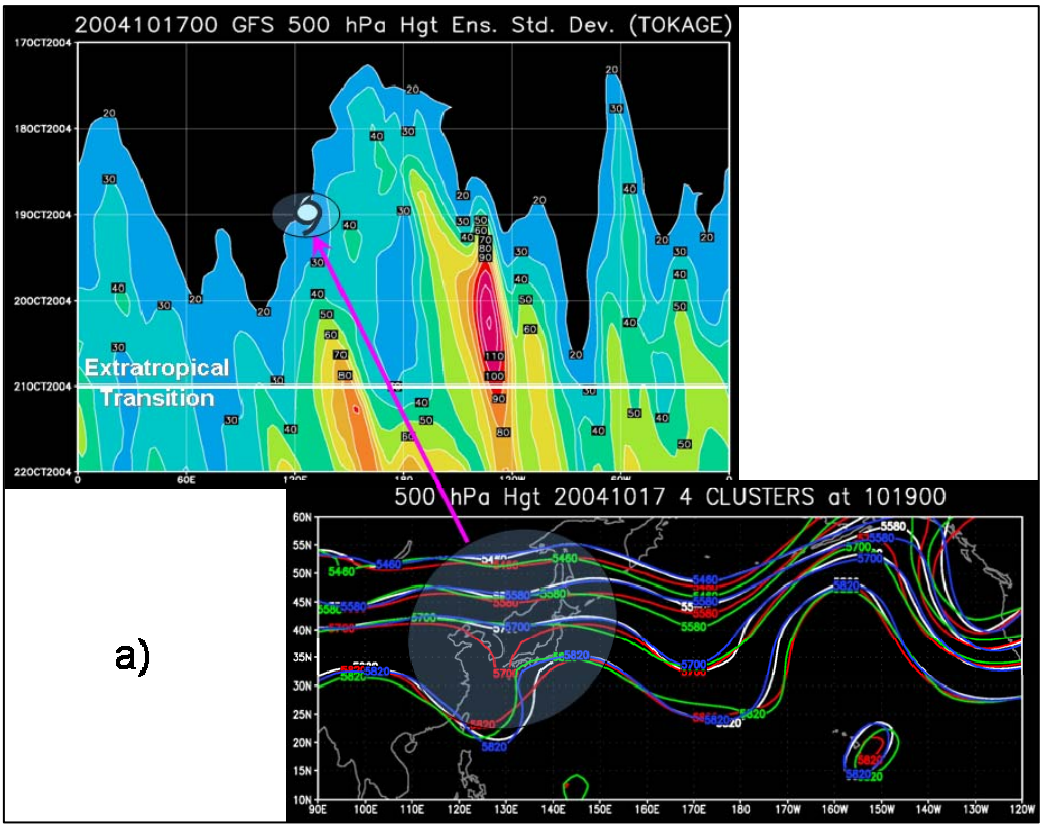

Figure 19. a) - e): A combination of Hovmoller plots of the 500 hPa ensemble standard deviation and the 500 hPa cluster analysis for 17 October. On the Hovmoller charts, the horizontal white line indicates when Tokage was classified as extratropical by JTWC. The tropical cyclone symbol indicates the appropriate longitude of Tokage. The shaded areas indicate corresponding spatial regions between the two plots. In the 500 hPa height charts, clusters (4-1), (4-2), (4-3), and (4-4) are represented by the white, red, green, and blue lines, respectively. a) 48-h forecast when Tokage was classified as ET. Largest ensemble spread has been shaded. Note that the lower right figure in Fig. 19a is identical to Fig. 18i. b) – e) Phasing differences of Tokage into the midlatitudes lead to a large ensemble spread that propagates to the east. Also note that the figure in the lower right depicting the spread between the cluster-averaged 500 hPa height contours are often referred to as “spaghetti diagrams.”

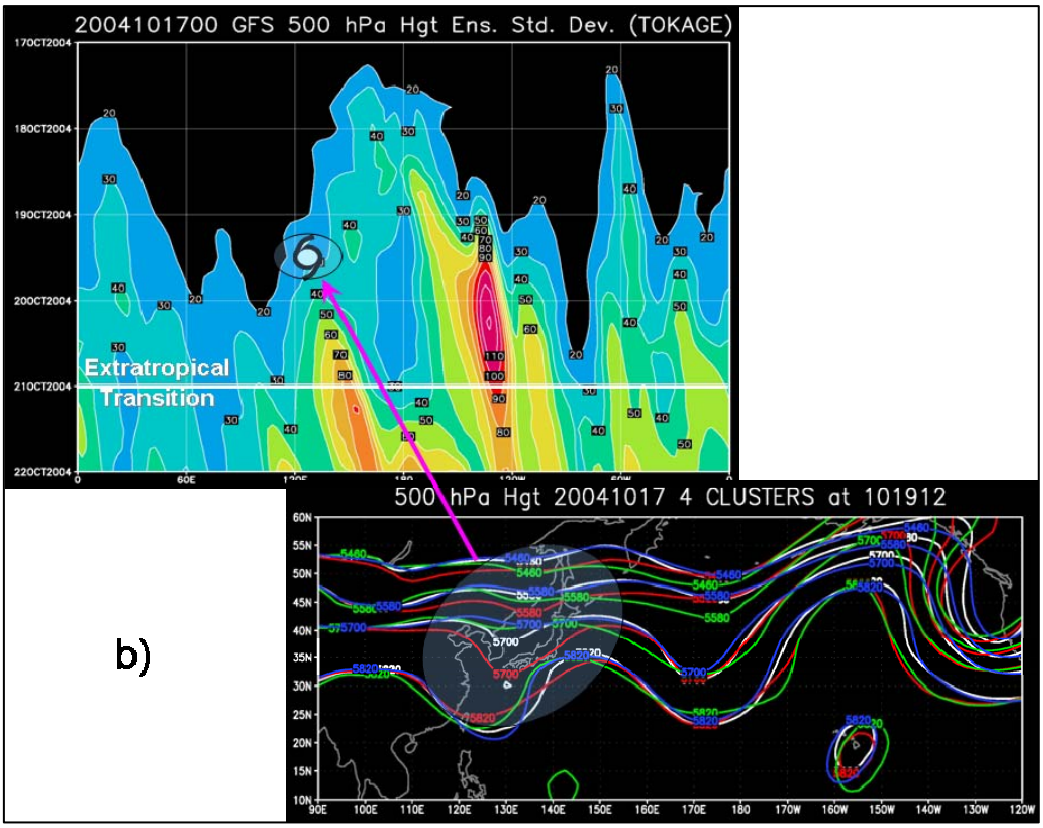

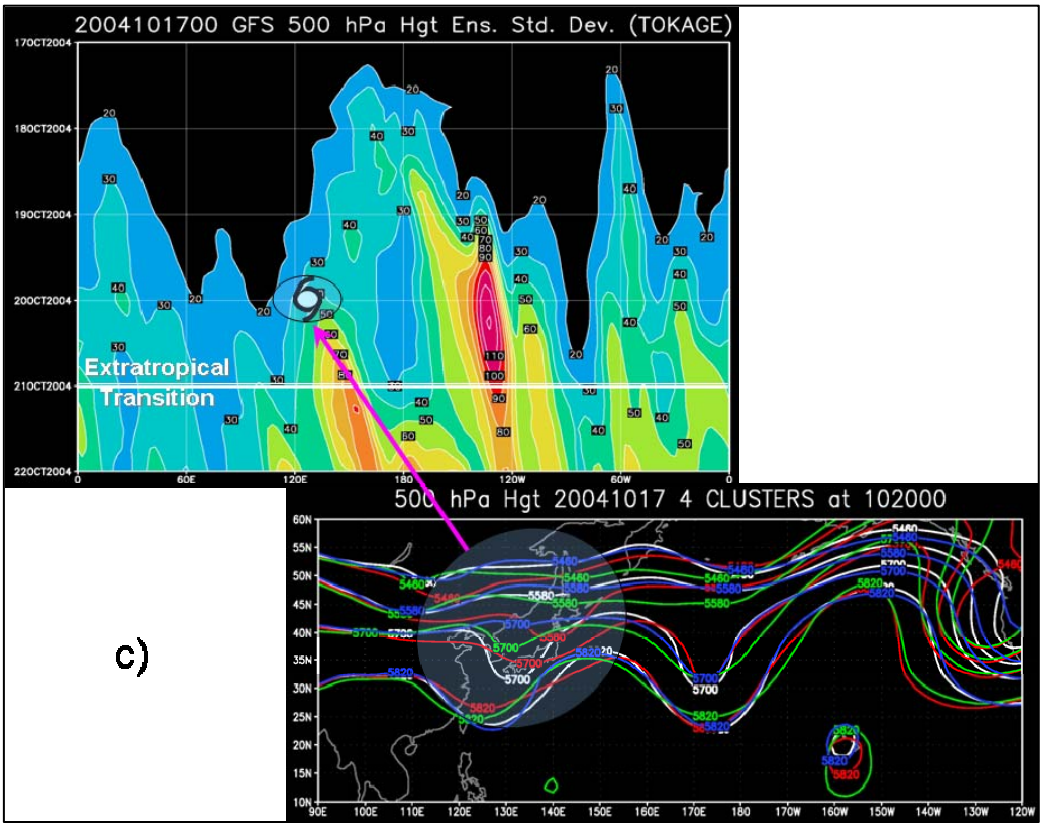

Figure 19. (continued)

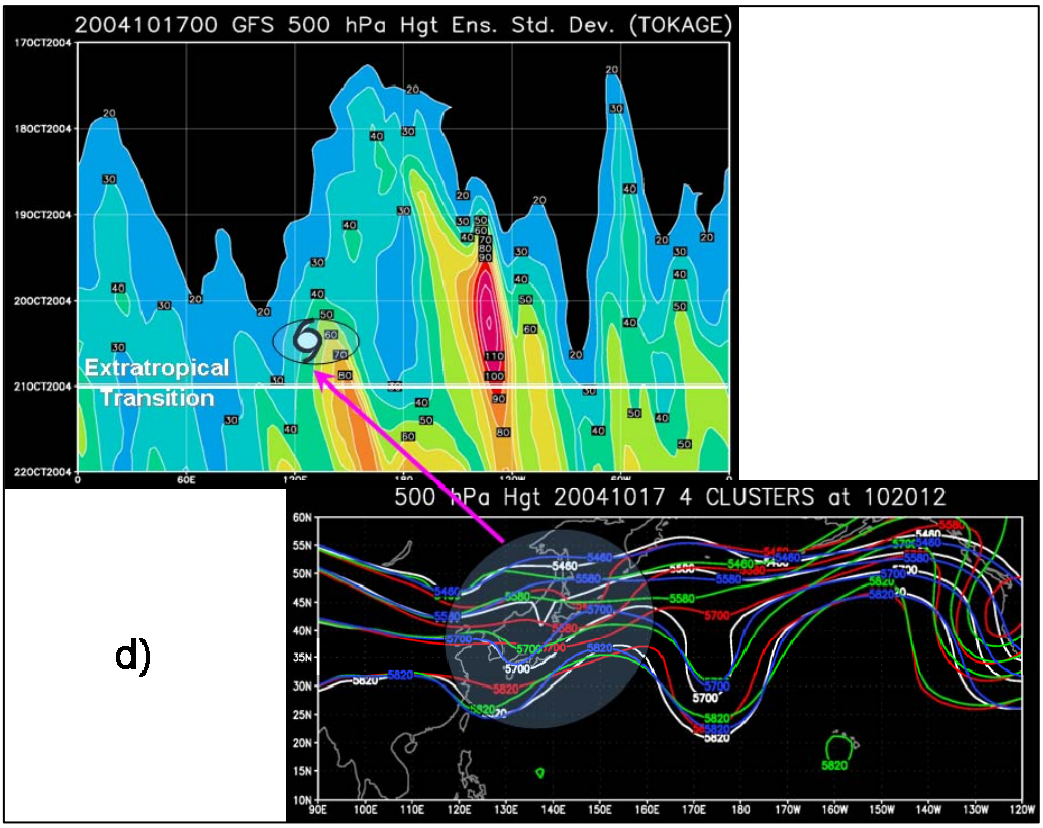

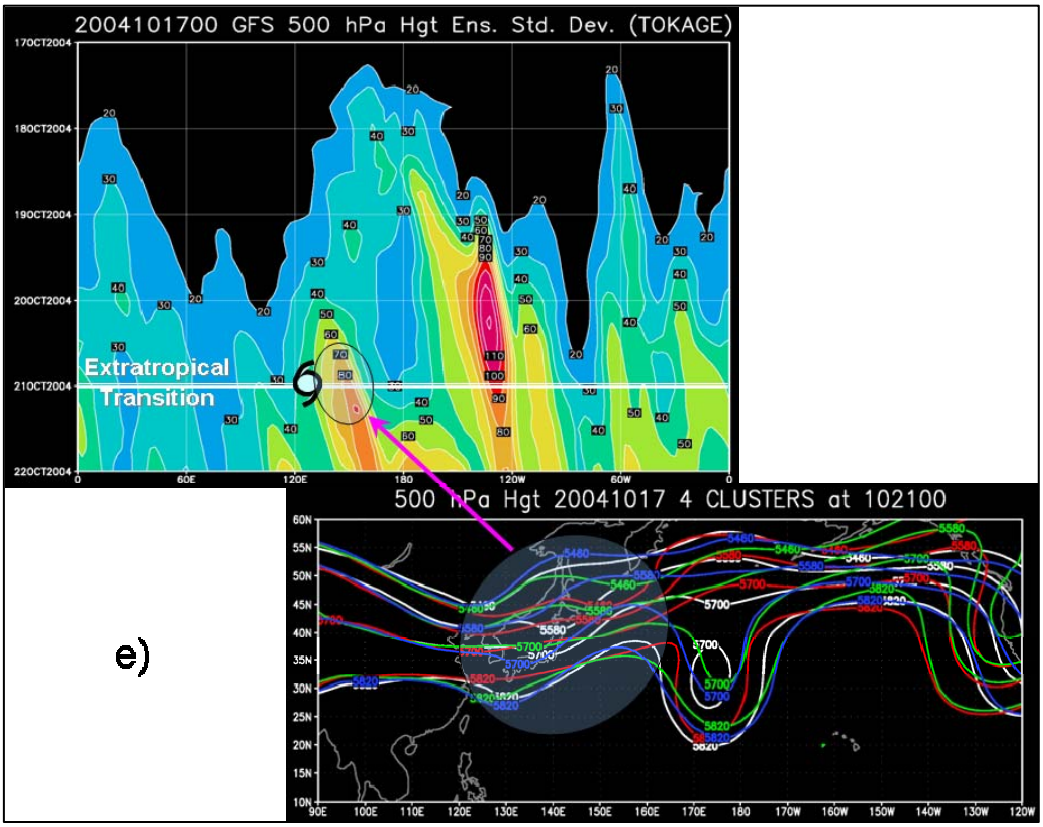

Figure 19. (continued)

In summary, variations in the forecast analysis impact the ensemble spread in the 500 hPa height fields during the ET process. Because the ensemble perturbations altered Tokage's position about the true position, the time when Tokage would interact and become embedded in the midlatitudes was variable. Combined with the uncertainty/variability associated with the analyzed midlatitude circulations, simple spatial perturbations of Tokage in the tropics contributed to a large spread in the ensemble members/clusters and introduce a large variability in the 500 hPa height fields even before Tokage was classified as extratropical. As depicted in Fig. 19, the spread in the midlatitudes starts in the vicinity of the ET event, but then rapidly propagates downstream. The influence of Tokage on the midlatitude long-wave pattern appears to be limited solely to the downstream structure. This large degree of uncertainty only downstream (and not upstream) of the ET event suggests a strong consistency among all four ensemble clusters upstream of the ET event.

By compiling 44 members from the four daily operational EPS runs on 17 October, four recurring synoptic patterns within the ensemble forecast have been identified via EOF/cluster analysis. The 44 meteorological solutions were reduced to four synoptic patterns. However, the long-range ensemble forecast indicated that multiple ET re-intensification scenarios were possible, all of which appear to be sensitive to the phasing of TY Tokage into the midlatitudes.

2. 18 October (78-h to 96-h forecast)

a. Cluster Analysis

The 78 – 96 hour forecasts derived from the four daily ensemble runs produced on 18 October were combined for the next set of cluster analysis. The EPS runs for 18 October still indicated a high degree of uncertainty associated with the ET of TY Tokage (Figs. 4e and 4f). Therefore, it was assumed that the 44 member ensemble forecast would describe three or more ET scenarios. Similar to the previous cluster analysis, the PC1 versus PC2 plot was subdivided into three cluster groups as a first guess (Fig. 20a).

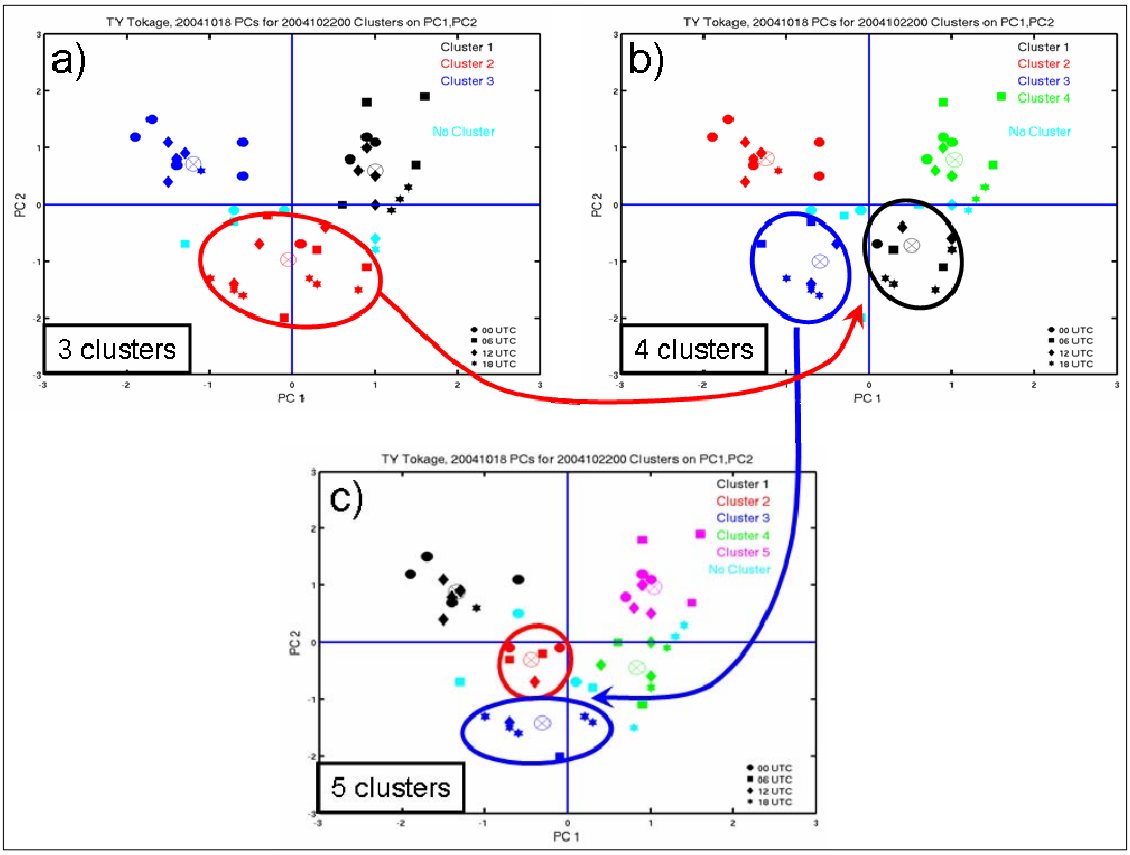

Figure 20. Same as Fig. 11a-c, except for the 18 October EPS runs. a) The red circle highlights cluster (3-2) that was subdivided into clusters (4-1) and (4-3) (black and blue circles in Fig. 20b). b) The blue arrow depicts the subdivision of cluster (4-3) in to clusters (5-2) and (5-3) (red and blue circles in Fig. 20c). c) The five cluster solution.

Examination of the first three cluster solutions (Fig. 20a) quickly identified that cluster (3-2) straddled the zero line of PC1, although all of its members have negative PC2 values. By contrast clusters (3-1) and (3-3) identify a stratification about PC1 with only positive PC2 contributions. Re-clustering the PC plot into four groups (Fig. 20b) split cluster (3-2) into two new clusters, (4-1) and (4-3) respectively. Finally, a five clustering was computed to check for a possible fifth ET mode (Fig. 20c).

Inspection of the averaged MSLP charts for the forecasts in clusters (4-1) and (4-3) suggest that the separation of cluster (3-2) in Fig. 20a did result in valid ET scenarios (Fig. 21a). That is, the cluster (4-1) scenario indicates that TY Tokage will re-intensify in the vicinity of the Kuril Islands, while the cluster

(4-2) scenario predicts that TY Tokage will rapidly move to the east of Kamchatka as a weaker baroclinic cyclone. Higher-order clustering of the PCs does not identify additional ET modes. That is, the division of cluster (4-3) in Fig. 20b into two new clusters (Fig. 20c) is unwarranted as the differences between clusters (5-2) and (5-3) are minimal (Fig. 21b). A comparison of the scenarios from clusters (5-2) and (5-3) reveals a slight position shift of the ET vortex center, but the cyclone intensity for both clusters is the same. Thus, it was concluded that the 44 ensemble members of the 18 October run should be divided into four clusters as in Fig. 20b.

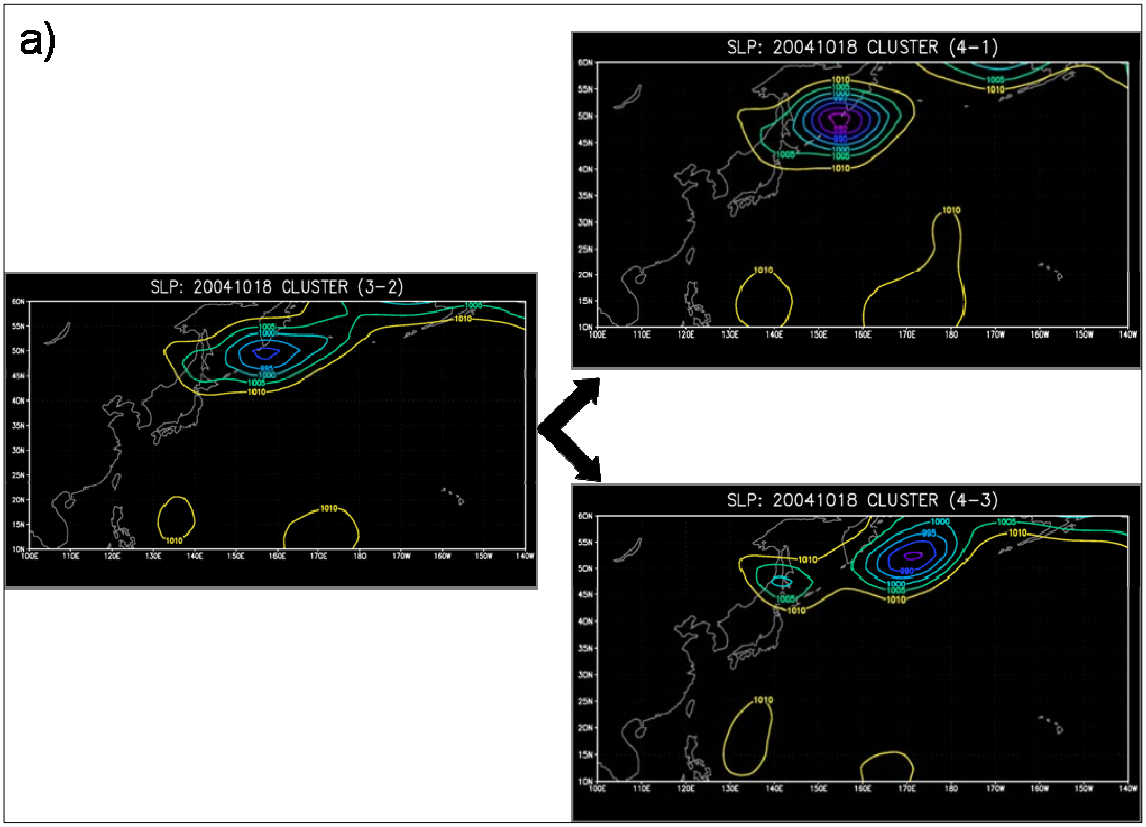

Figure 21. Cluster mean fields of MSLP for the split of (a) cluster (3-2) on the left side into clusters (4-1) and (4-3) on the right side, and (b) cluster (4-3) on the left side into clusters (5-2) and (5-3) on the right side. Contours are in hPa and contours greater than 1010 hPa are not shown.

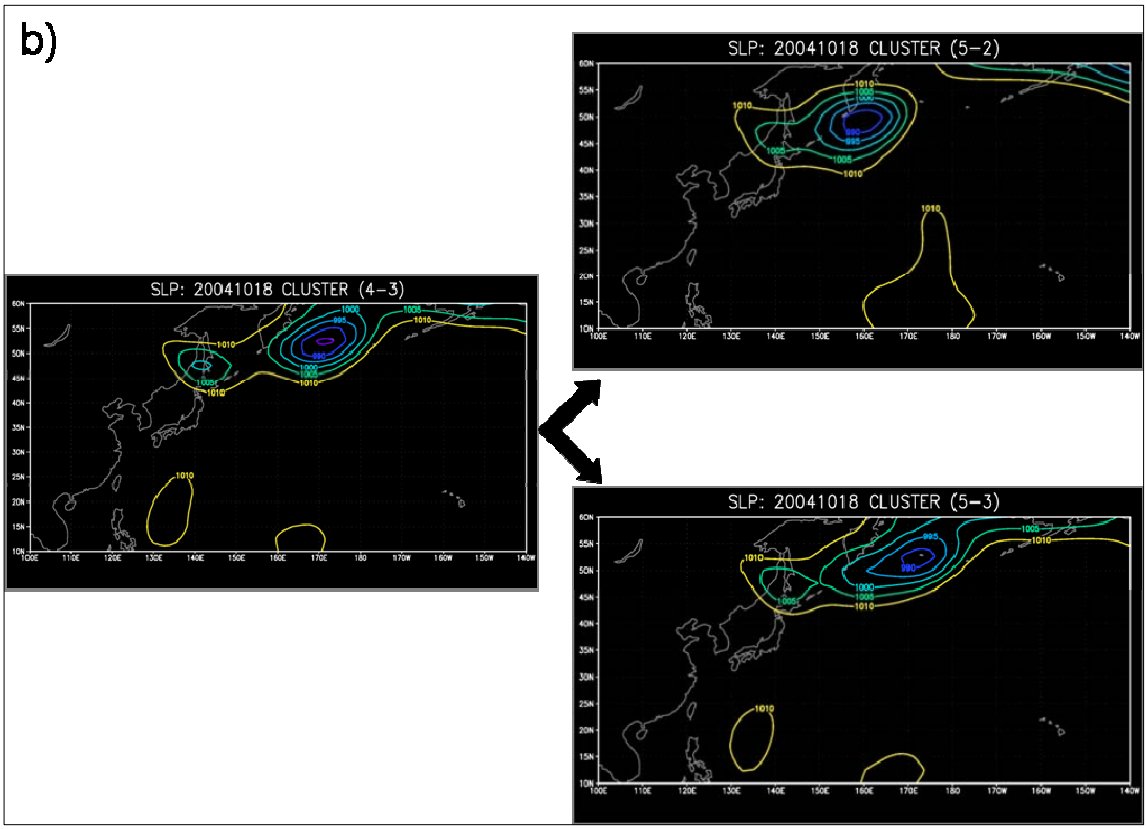

Figure 21. (continued)

As with the cluster analysis for 17 October, four distinct modes were identified in the ensemble forecast:

- Cluster (4-1) represented a strong ET scenario (Fig. 22a and 22e).
- In the opposite sense, Cluster (4-2) represented a weak ET event that moved rapidly across the northwestern Pacific (Fig. 22b and 22f).
- Cluster (4-3) represented a moderate re-intensification stage as the system quickly translates through the midlatitudes (Fig. 22c and 22g)
- Finally, cluster (4-4) revealed a slowly propagating cyclone that would undergo a major re-intensification stage over the Sea of Japan (Fig. 22d and 22h).

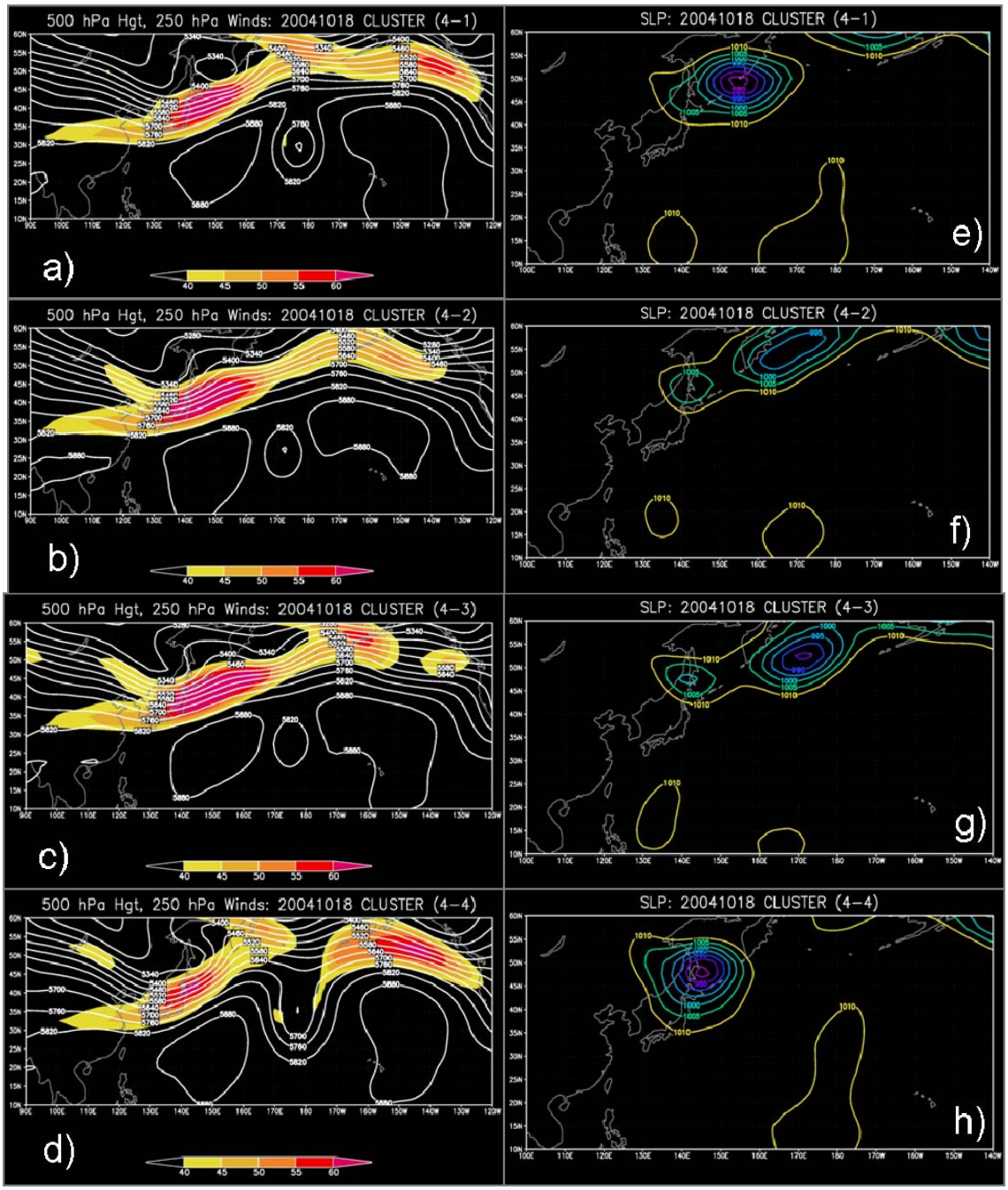

Figure 22. Same as Fig. 14, except for 18 October.

b. Variations in the Analysis for Each Set of Ensemble Cluster Forecasts

A comparison of the cluster-averaged ensemble analyses for the forecast 500 hPa and 250 hPa winds for 18 October was conducted (Fig. 23). In contrast to the anomaly fields from 17 October, the magnitudes of anomaly

perturbations introduced by the observational error appear more consistent with expected values. Contrary to the findings from the 17 October analyses associated with each set of forecasts, examination of the 500 hPa height/250 hPa wind anomalies revealed that the largest variability in the analysis fields of the four clusters was limited to the tropics, as is evident by the weak anomalies over the midlatitudes. Consistent with the results from 17 October is the relationship between the translation of Tokage into the midlatitudes and its placement either ahead or behind the best-track position. In clusters (4-2) and (4-3), Tokage is placed ahead of the best-track position. Both clusters represent rapid movement into the midlatitudes. Conversely, clusters (4-1) and (4-4), which are both behind the best-track position, represent a slower propagating midlatitude system.

The re-intensification scenarios of the ET no longer appear related to the intensity anomaly (Fig. 23). Even though clusters (4-1) and (4-2) were analyzed as a slightly more intense tropical cyclone than the 44 member mean, the re-intensification scenarios for the two clusters were significantly different. Cluster (4-1) re-intensified into a strong 980 hPa midlatitude cyclone (Fig. 22), while cluster (4-2) represented a much weaker system (i.e., 990 hPa). Similarly, even though cluster (4-3) was initialized as a more intense system (Fig. 23c), the final extratropical cyclone only moderately re-intensified. The more rapid movement of cluster (4-3) into the midlatitudes may have acted to counter the deeper-than-mean amplitude of the cyclone in the forecast analysis. The ensemble clusters represent a strong re-intensification scenario when the perturbation places Tokage behind its best-track position.

In summary, the phasing of Tokage into the midlatitudes appears to be the critical factor in determining the translation speed during ET, which is consistent with the results from 17 October. Conversely, the re-intensification scenario of the ET process now appears to be coupled with the TC position relative to the best-track rather than the analyzed intensity anomalies, which contradicts the findings from the previous day. That is, based on the 18 October analysis anomalies, ET re-intensification scenarios that were weak (4-2) and

moderate (4-3) were ahead of the best-track position and the ET scenarios that were strong ((4-1) and (4-4)) were analyzed behind the best-track position.

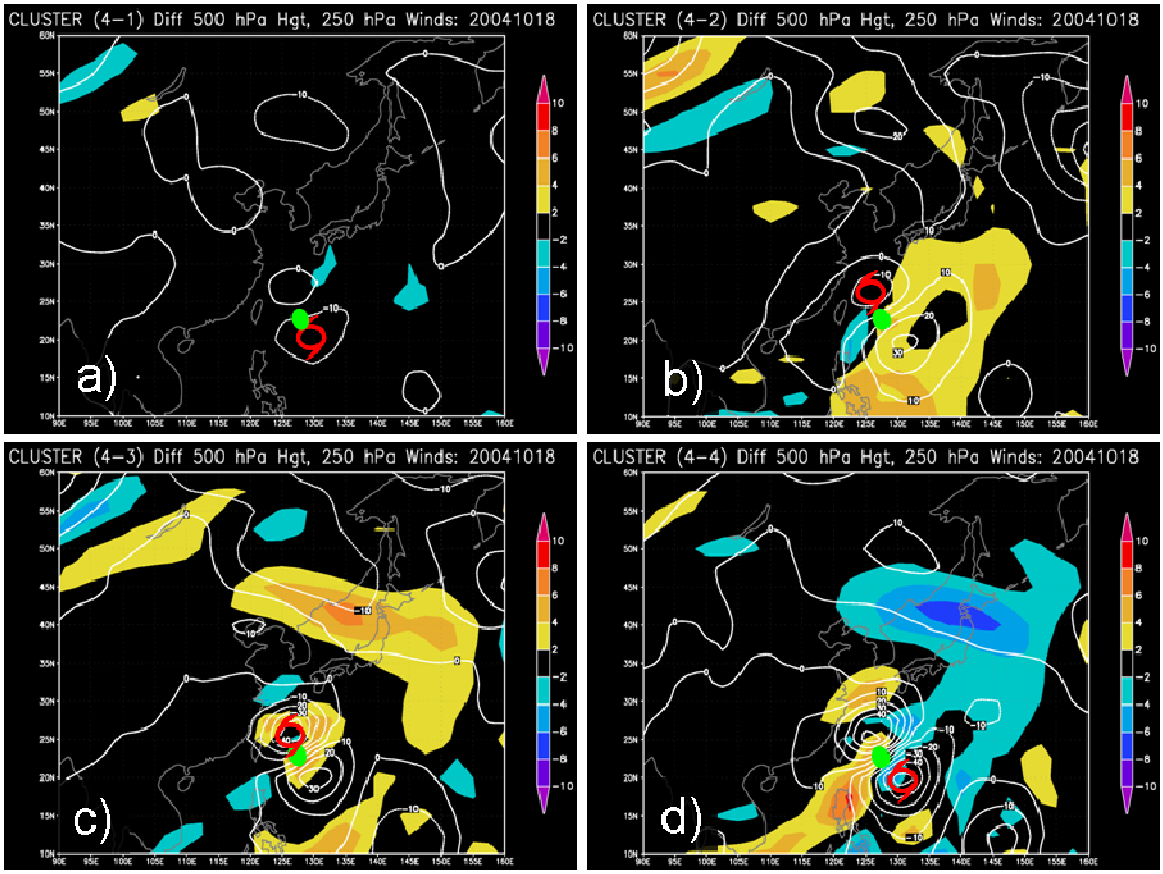

Figure 23. Same as Fig. 15, except for the 18 October analysis. a) Cluster (4-1): Strong re-intensification stage. b) Cluster (4-2): Weak re-intensification as it moves quickly into the midlatitudes. c) Cluster (4-3) Moderate re-intensification but moves quickly into the midlatitudes. d) Cluster (4-4): Strong re-intensification stage, but moves slowly in the westerlies.

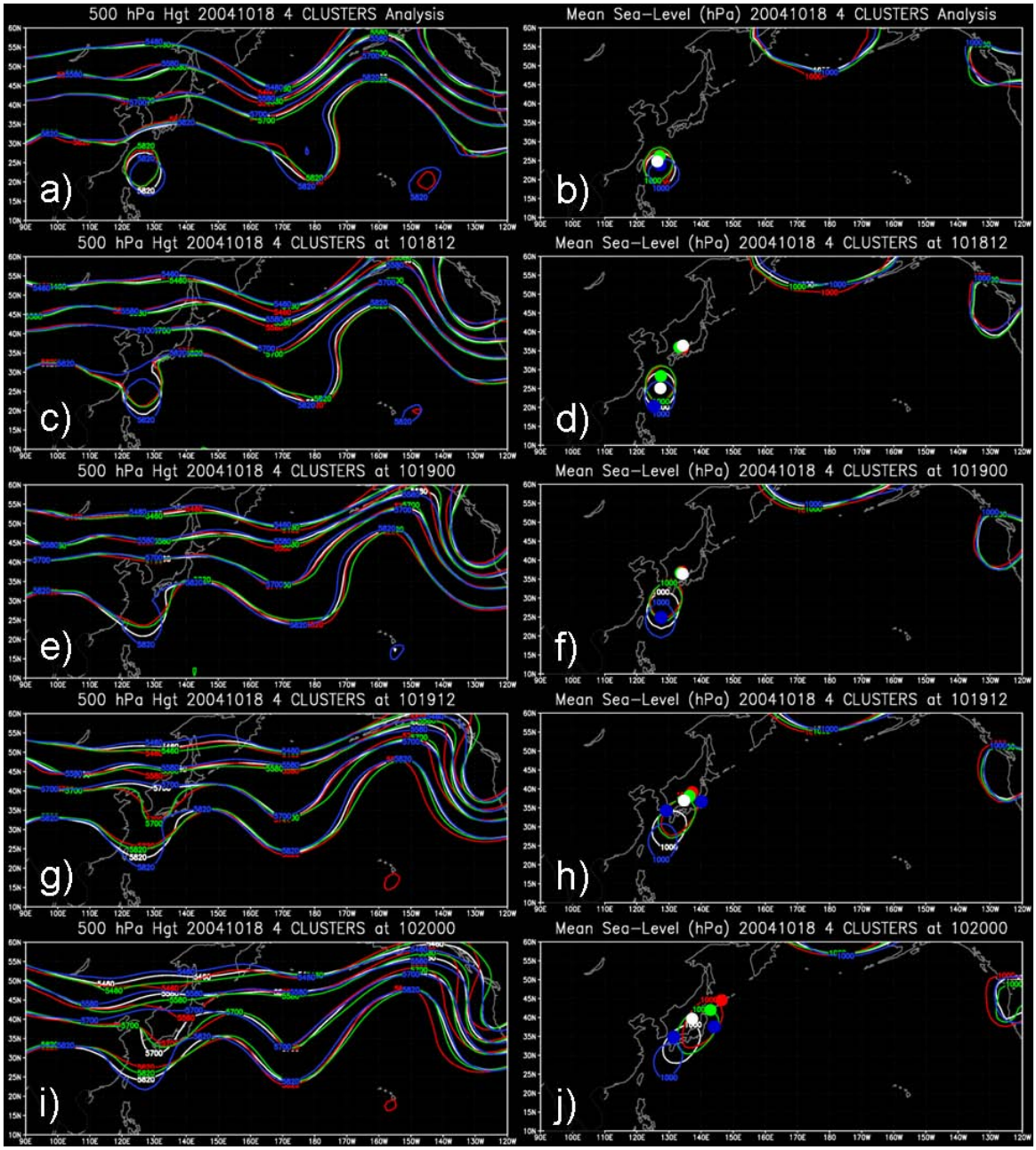

Figure 24. Same as Fig. 18, except for the analysis through 48-h forecast for clusters (4-1) (white), cluster (4-2) (red), cluster (4-3) (green), and cluster (4-4) (blue) starting at 0000 UTC 18 October.

Examination of upper-level divergence maxima relative to the low-level circulation center helps to interpret the overall patterns of motion and intensity forecasts during ET (Fig. 24). Initially, the tropical cyclone in all four clusters is isolated from the midlatitudes (Figs. 24a and 24b). However, within 12

hours (Figs. 24c and 24d) the outflow associated with clusters (4-1), (4-2) and (4-3) appears to be coupled with the midlatitude jet, while cluster (4-4) remains isolated within the tropics. At this point, the divergence maxima are well ahead of clusters (4-1), (4-2), and (4-3) and appear to be ideally situated for a strong re-intensification scenario. However, only cluster (4-1) re-intensifies as a strong extratropical cyclone. Because the decaying tropical cyclone in cluster (4-2) and cluster (4-3) begins to accelerate into the westerlies, which acts to quickly reduce the separation distance from the vortex center and upper-level divergence maximum, the surface vortex does not have time to deepen significantly (Figs. 24e and 24f). Cluster (4-1) does not speed up in the westerlies, but rather propagates slowly and maintains an optimal separation (Klein et al. 2002) between the surface vortex and the upper-level divergence maximum. Even though all the other clusters are connected to the midlatitude flow by the 24-h forecast, cluster (4-4) continues to drift in the tropics, and thus is dynamically removed from the jet. By the 36-h forecast (Figs. 24g and 24h), all four clusters are interacting with the midlatitude flow. Clusters (4-1) and (4-4) are maintaining an optimal separation from the divergence maxima. Clusters (4-2) and (4-3) have continued to move into the midlatitudes more quickly. Finally, by the 48-h forecast (Figs. 24i and 24j) and beyond, the two clusters (4-1) and (4-4) that contain a slow-moving tropical cyclone begin to move into the midlatitudes.

From the analysis of the ensemble forecasts from both 17 and 18 October, a consistent phasing pattern can be inferred. For a tropical cyclone to re-intensify in the midlatitudes, there apparently exists an optimal horizontal separation between the surface vortex and the upper-level divergence maximum that will maximize the deepening of the surface low. This is in agreement with Klein et al. (2002). The longer this separation distance is maintained, the stronger the re-intensification stage will be in the midlatitudes. Based on the cluster analysis obtained over the two days analyzed, the three clusters that represent a strong re-intensification scenario in the midlatitudes (cluster (4-2) from the 17 October analysis and clusters (4-1) and (4-4) from the 18 October analysis) appeared to sustain this optimum horizontal separation between the

surface vortex and the upper-level divergence maximum. Thus, the proper phasing of Tokage into the midlatitudes would be critical to the proper identification of the ET mode by the ensemble forecast.

Similar to the previous results, a large ensemble spread was observed by perturbing the intensity in the vicinity of the ET event and phasing of Tokage into the midlatitudes (Fig. 25a). As the Hovmoller plot indicates, a variability maximum was just downstream of Tokage (circled area in Hovmoller plot in Fig. 25a). Examining the corresponding 500 hPa height fields for the four clusters (lower right Fig. 25a) reveals the largest spread among the ensemble members is isolated to the region slightly downstream of where Tokage will enter the midlatitudes (shaded region lower right side of Fig. 25a). Both the upstream wave pattern and far downstream pattern (far left and far right, Fig. 25a) appear to initially be unaffected by the entrance of Tokage into the midlatitudes, as the four ensemble predictions are tightly clustered in these regions. Over the next 12 hours (Hovmoller chart, Fig. 25b), the standard deviation maximum between the ensemble members has propagated slightly to the east. The 500 hPa cluster analysis (lower right, Fig. 25b) depicts varying midlatitude responses to the entrance of Tokage. For example, cluster (4-4) has a strong ridge building over the Sea of Okhotsk, while clusters (4-2) and (4-3) depict a weaker response (shaded region, Fig. 25b, lower right figure). These observations are consistent with the patterns identified via the cluster analysis. It is expected that cluster (4-4), which was identified as a slowly propagating, rapidly re-intensifying cyclone over the Sea of Japan, would have a large amplitude response in the midlatitudes. Conversely, clusters (4-2) and (4-3), which were both identified as weaker systems than cluster (4-4), are expected to have a smaller amplitude response in the midlatitudes. Note that the standard deviation maxima are confined to the downstream wave pattern. By 0000 UTC 22 October (Fig. 25c), all four clusters have comparable 500 hPa heights upstream of the ET event (i.e., west of Japan) and by the 120-h forecast (Fig. 25e), the tightly clustered height fields have extended east of Japan. That is, the spread among the ensemble 500 hPa heights tightens upstream of the ET event (Fig. 25e) as the standard

deviation maximum propagates eastward. In successive 12-h forecasts (Figs. 25c-e), the ensemble spread introduced by the ET event (shaded regions) quickly propagates to the east, which introduces progressively higher uncertainty to the downstream wave pattern. However, it appears that the upstream pattern is not perturbed by the ET event. In summary, it is the phasing uncertainty of the ET event that produced large standard deviations among the 500 hPa heights previously indicated in the Hovmoller plots (compare Fig. 4 and Fig. 25).

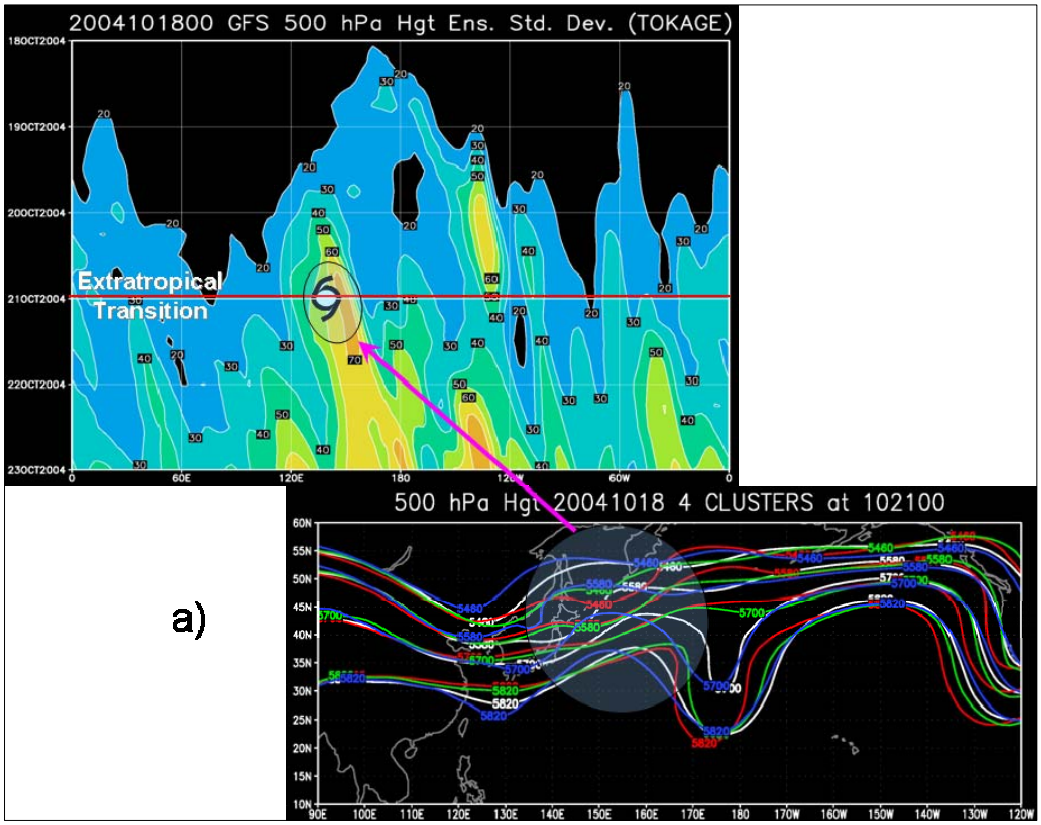

Figure 25. a) - e): Same as Fig. 19, except for 18 October. The tropical cyclone symbol indicates the appropriate longitude when Tokage was classified ET. The red line corresponds with the appropriate 500 hPa height forecast. The shaded areas indicate corresponding spatial regions between the two plots. In the 500 hPa height charts, clusters (4-1), (4-2), (4-3), and (4-4) are represented by the white, red, green, and blue lines, respectively. a) 72-h forecast when Tokage was classified as ET. Largest ensemble spread has been shaded. b) – e) Phasing differences of Tokage into the midlatitudes lead to a large ensemble spread that propagates to the east.

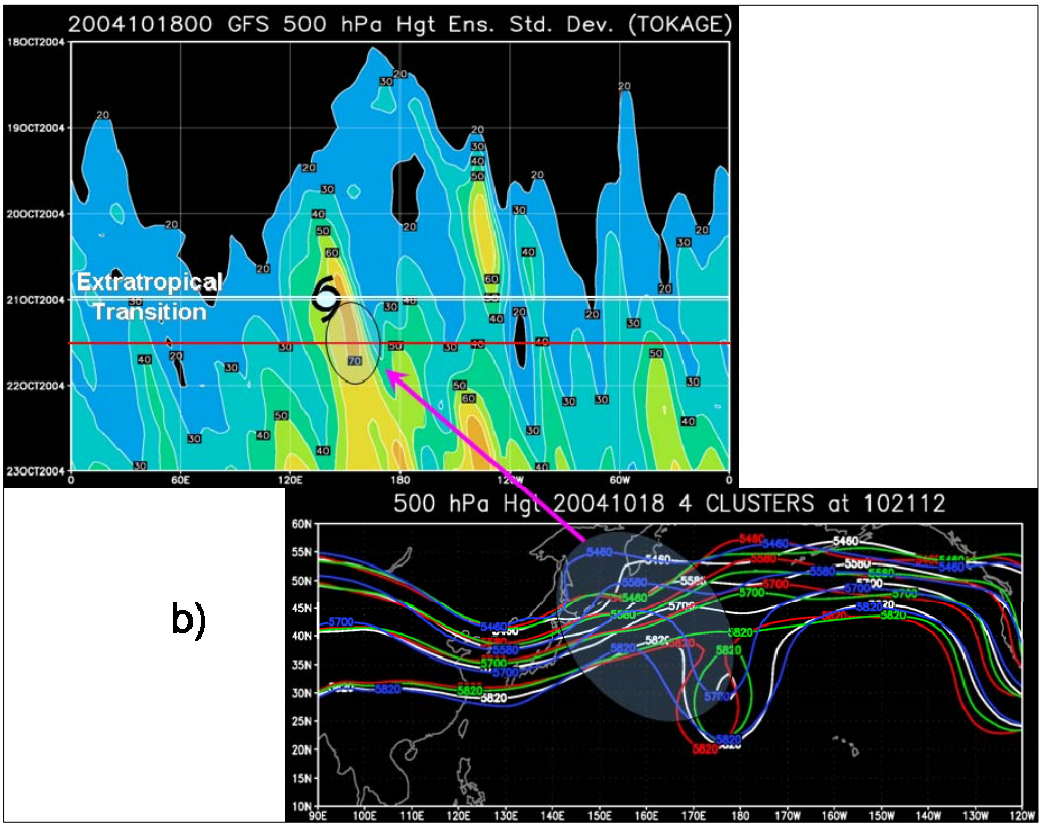

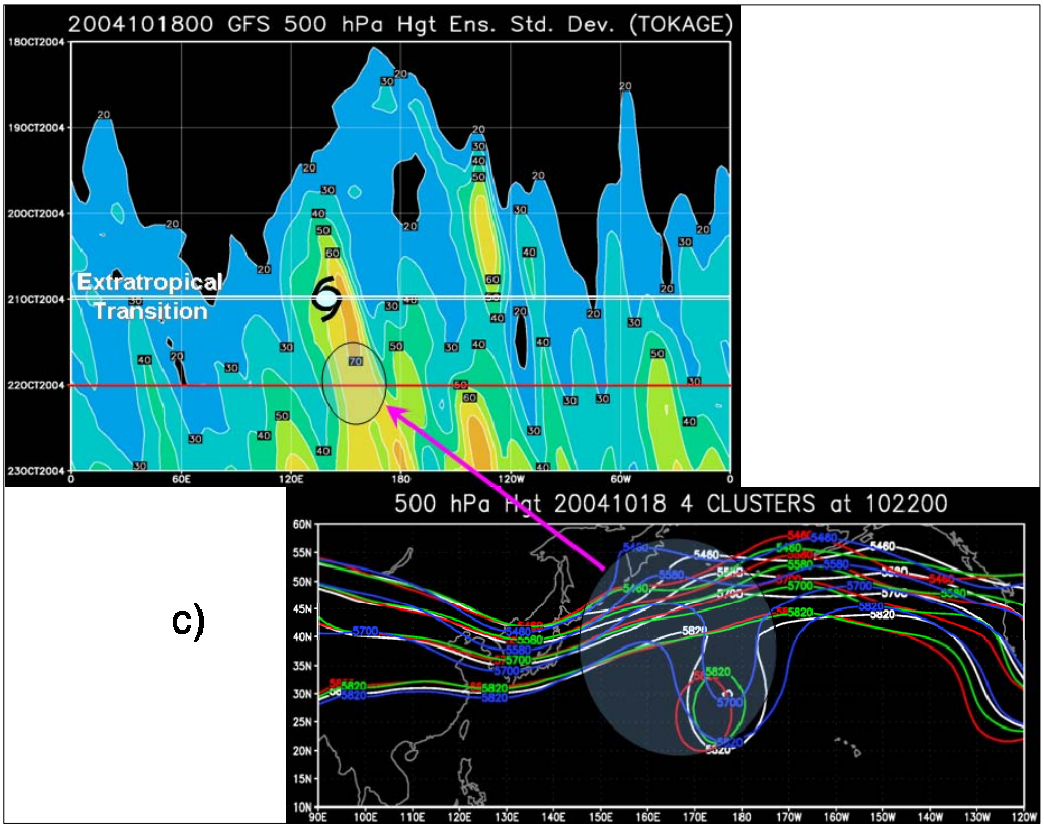

Figure 25. (continued)

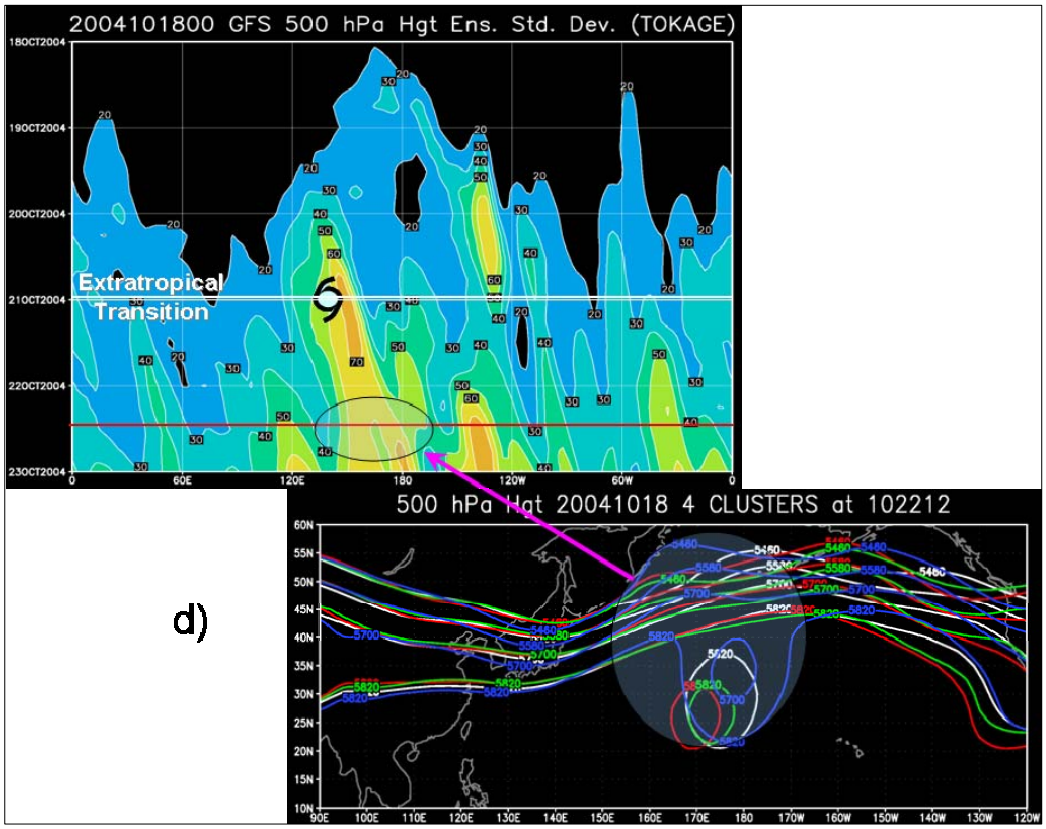

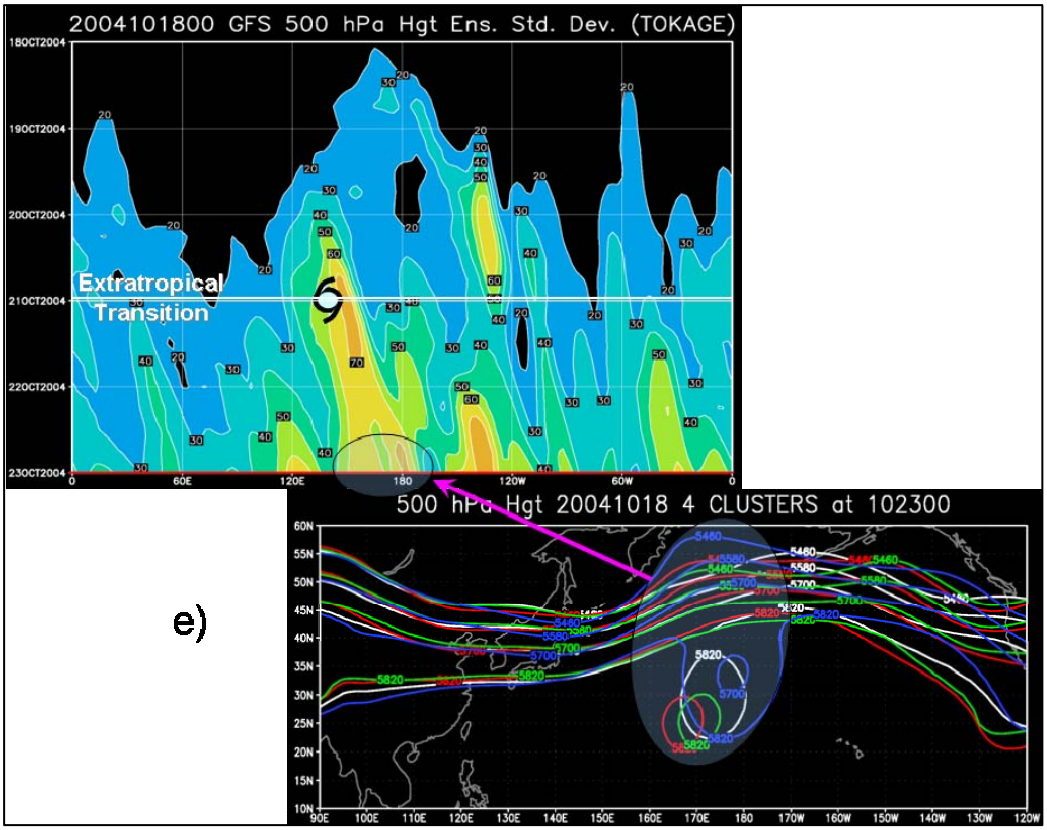

Figure 25. (continued)

The four-day ensemble forecasts from 18 October continue to indicate that multiple extratropical transition modes are present in the 44-member ensemble. Two of the four ensemble clusters represent a strong re-intensification scenario following Tokage's transformation stage. The other two clusters represent a weak or moderate transition. A strong sensitivity of the ensemble forecast was observed with respect to the midlatitude phasing of the ET event and re-intensification scenarios. Finally, the number of possible synoptic outcomes was not reduced between 17 October (102-h to 120-h forecasts) and 18 October (78-h to 96-h forecasts).

3. 19 October (54-h to 72-h forecast)

a. Cluster Analysis

Based on the cluster analyses for 17-18 October, three cluster groupings were initially examined for the PC values generated from the 19 October ensemble forecast (Fig. 26). Initially, the three-cluster solution appeared to be an adequate distribution. However, higher-order cluster solutions were evaluated.

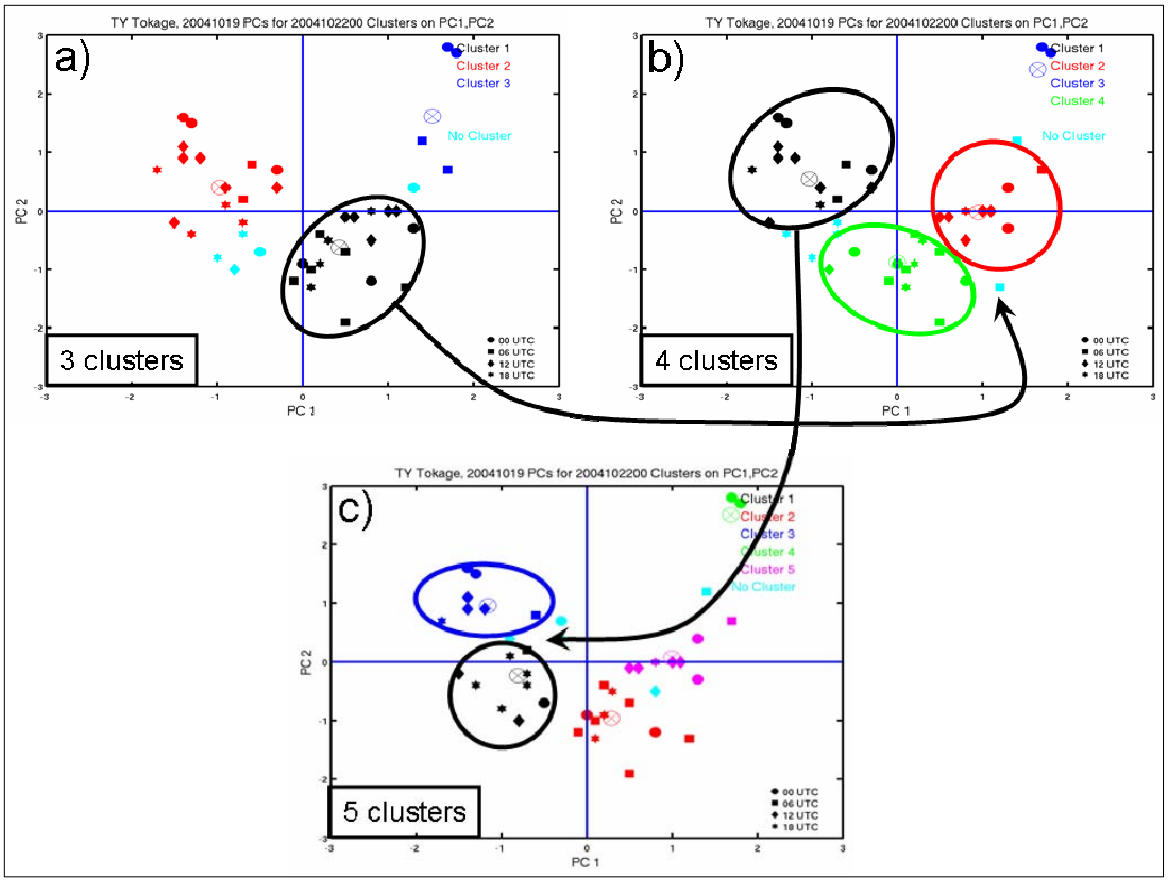

Figure 26. Same as Fig. 11a-c, except for 19 October EPS run. a) The black circle highlights cluster (3-1) that was subdivided into clusters (4-2) and (4-4) (red and green circles in Fig. 26b). b) The four-cluster solution with the black arrow depicts the subdivision of cluster (4-1) into clusters (5-1) and (5-3) (black and blue circles in Fig. 26c). c) The five-cluster solution.

In the four-cluster solution, cluster (3-1) was divided into clusters (4-2) and (4-4), which then forced a re-distribution of group centers. Centers of clusters (4-2) and (4-4) were aligned along both of the PC1 and PC2 axes, respectively. Comparison of the mean MSLP patterns corresponding to the two clusters reveals that these two modes of differing intensity were initially grouped together (Fig. 27a). Cluster (4-2) represents a strong re-intensification stage northeast of Hokkaido and cluster (4-4) indicates that the former tropical cyclone will re-intensify into a weak midlatitude cyclone once it completes its transformation. Because two of the group centers (i.e., clusters (4-2 and (4-4)) lie along the PC1 and PC2 axes, which indicates the possibility that the two distinct ET modes may have been inadvertently grouped together into one cluster, the

PC clustering algorithm was allowed to have five clusters. The fuzzy cluster process separated cluster (4-1) into clusters (5-1) and (5-3). A comparison of the height fields for these two clusters (Fig. 27b) suggests very little spatial separation exists between the locations of the vortex centers, and both clusters are also pointing toward a strong re-intensification of Tokage east of Kamchatka, with only a 5 hPa intensity difference between the two groupings. Since the difference between these two clusters was minimal, it was deemed appropriate that the PCs should be partitioned into four clusters.

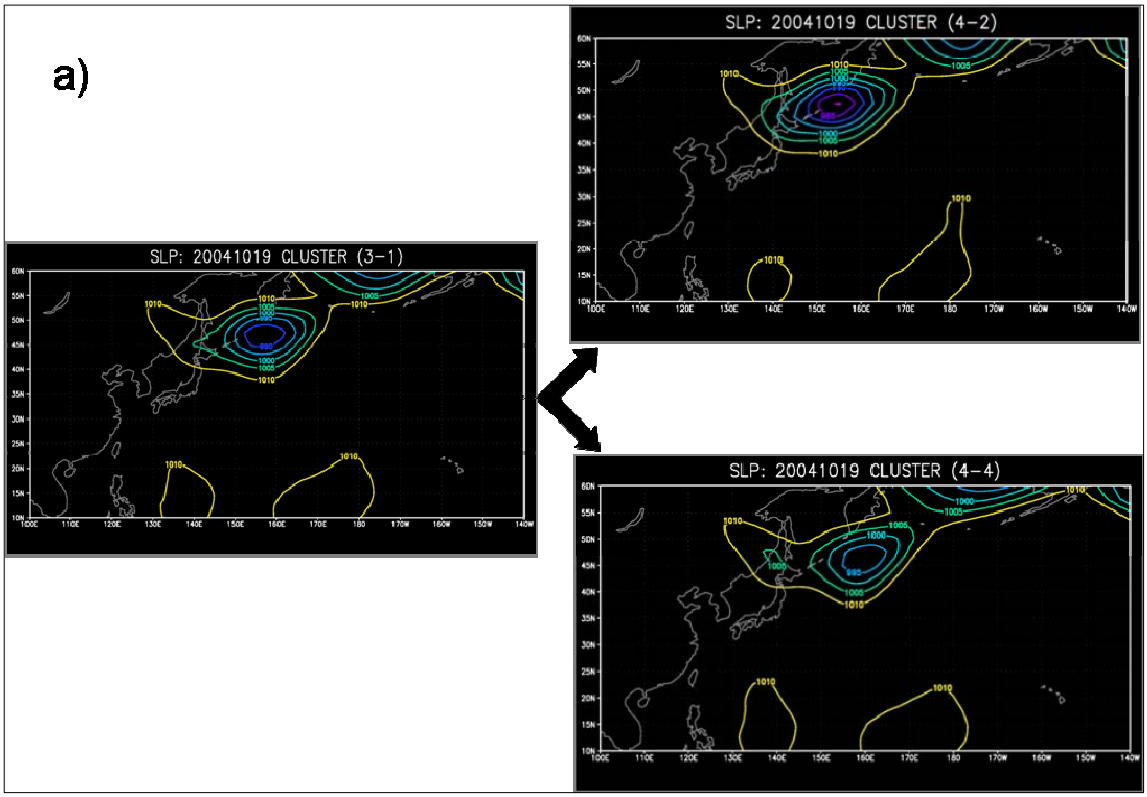

Figure 27. Cluster Analysis for 19 October: a) Separation of cluster (3-1) on the left side into clusters (4-2) and (4-4) on the right side; b) Separation of cluster (4-1) on the left side into clusters (5-1) and (5-3) on the right side.

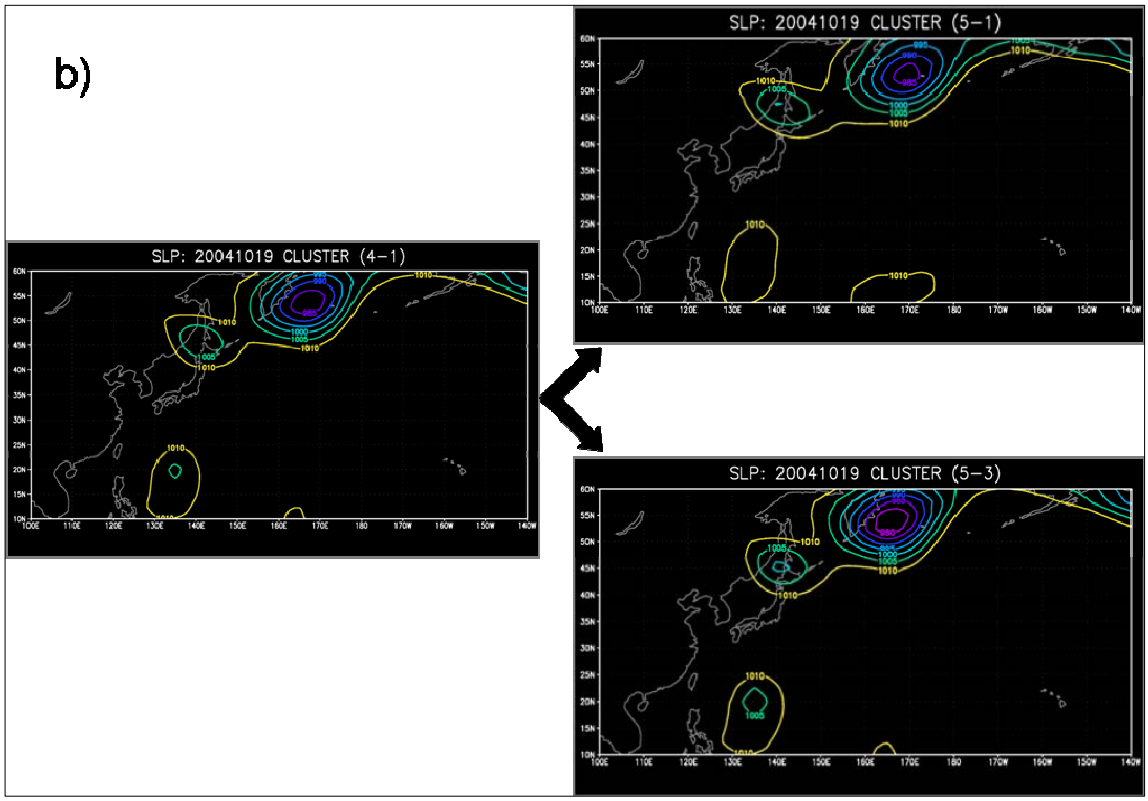

Figure 27. (continued)

It should also be noted that two members of cluster (3-3) (upper right corner Fig. 26a), which originally contained only four ensemble members (~9%), moved to another cluster (upper right corner Fig. 26b). Therefore, cluster (4-3) contained only the two remaining ensemble members and accounted for less than 5% of the total ensemble members. These two ensemble members continued to be evaluated as a valid cluster during further clustering steps, e.g., cluster (5-4) is identical to cluster (4-3). Because the clusters (4-3) and (5-4) membership was less than 5% of the ensemble members, it was determined that these clusters were outlier solutions of the ensemble forecast and may be eliminated as a statistically improbable solution. Although this would reduce the number of cluster solutions from four groups to three groups, the forecaster would be ignoring a major re-intensification scenario by eliminating cluster (4-3). This cluster represents a cyclone that could seriously impact military operations along its path and elimination of this cluster based solely on statistical reasoning may not be prudent. However, if the elimination of cluster (4-3) can be justified,

this provides the first indication that the numerical solutions for the ET mode are beginning to converge. Since cluster (4-3) represents the strongest re-intensification scenario, it will have the strongest influence on the 500 hPa height pattern. Therefore, it is useful to include cluster (4-3) in the subsequent analysis to assess its impact on the total variability as well as to identify common trends among the cluster groups as to how the environment was analyzed and the resulting ET re-intensification scenario.

In summary, four distinct modes were identified in the 19 October ensemble forecast, but one might be eliminated based on statistical considerations:

- Cluster (4-1) represents a moderate ET scenario that propagated rapidly across the northwestern Pacific (Fig. 28a and 28e).
- Cluster (4-2) defines a strong ET event (Fig. 28b and 28f).
- Similar to cluster (4-4) from the 18 October ensemble analysis, cluster (4-3) continued to identify a slowly propagating cyclone that would undergo a major re-intensification stage over the Sea of Japan (Fig. 28c and 28g). This cluster was identified as an outlier.
- Cluster (4-4) also represents a scenario in which the system quickly moves across the North Pacific with a moderate re-intensification (Fig. 28d and 28h).

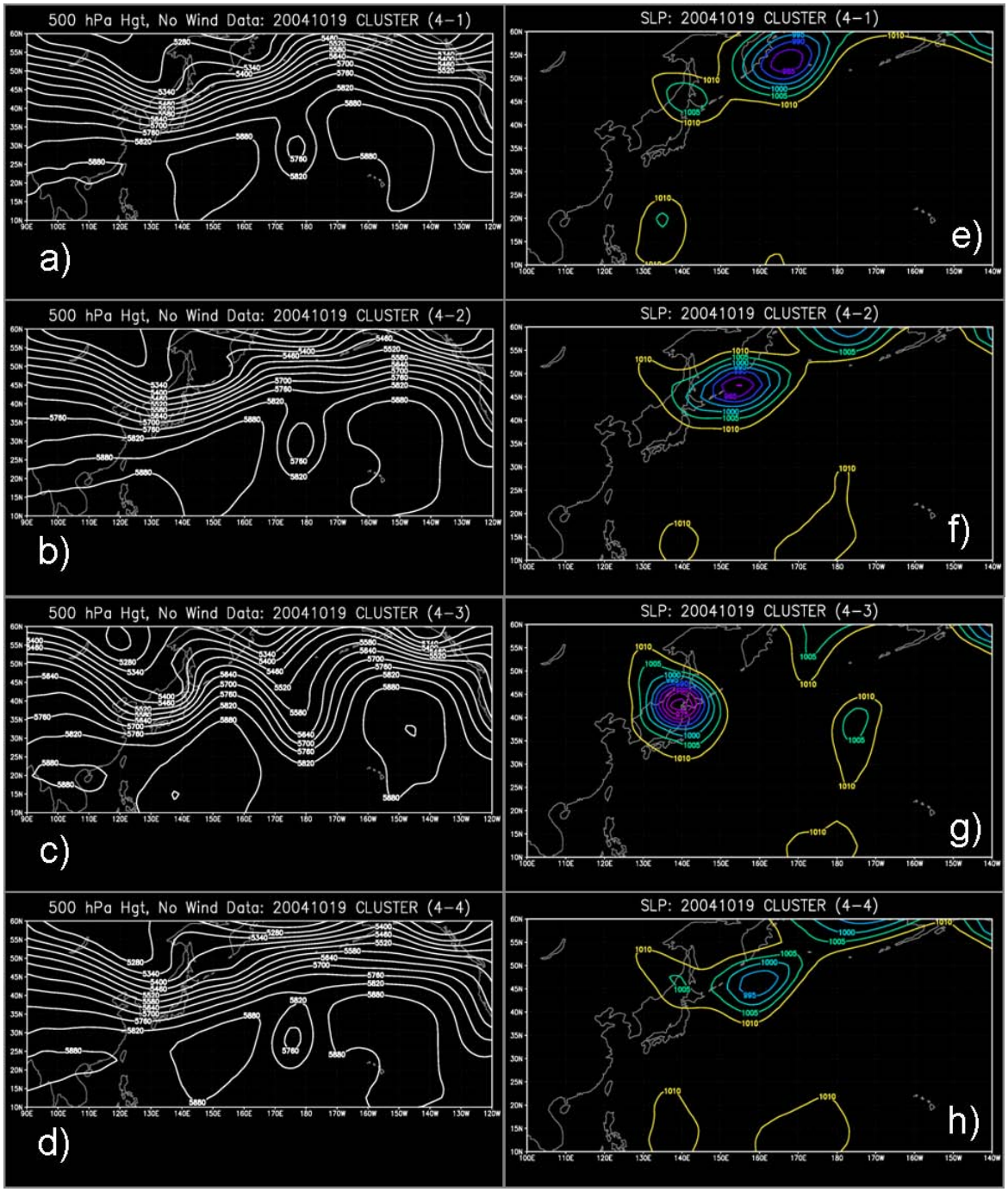

Figure 28. Same as Fig. 14, except for 19 October.

b. Variations in the Analysis for Each Set of Ensemble Cluster Forecasts

Unfortunately, the 250 hPa wind fields were not available for the 19 October ensemble. Therefore, inspection of the variability in the analyses associated with ensemble cluster forecast must be limited to the 500 hPa height anomalies (Fig. 29). Similar to the examination of 18 October, most of the variability in the analysis fields is confined to the region surrounding Tokage. Because minimal height variations are observed in the midlatitudes, it appears Tokage's mid-latitude re-intensification scenario was primarily influenced by the spatial perturbations with respect to the best-track position. Again, although cluster (4-3) could be eliminated as an outlier, it is insightful to include cluster (4-3) in the further analysis to identify trends in the four-cluster solution between the forecast analysis and the ET mode corresponding to each cluster.

Consistent with the results from both 17 October and 18 October is the relationship between the translation of Tokage into the midlatitudes and its placement either ahead or behind the best-track position. Clusters (4-1) and (4-3) (Figs. 29a and 29c) have the largest spatial separation between the analyzed Tokage position and the best-track position. Cluster (4-1) was analyzed the farthest ahead, while cluster (4-3) was analyzed the farthest behind. As identified in previous results, when Tokage was analyzed ahead of the best-track position (i.e., cluster (4-1)), the ET event would quickly move into the midlatitudes (Fig. 28e). Conversely, when Tokage was analyzed behind the best-track position (i.e., cluster (4-3)), the translation speed of the former TC into the midlatitudes during the ET event was significantly reduced (Fig. 28g). That is, clusters (4-1) and (4-4), which were analyzed ahead of the best-track position, represent rapid movement of the transforming TC into the midlatitudes. Conversely, clusters (4-2) and (4-3), which were both behind the best-track position, represent a slower propagating midlatitude system. The phasing of Tokage into the midlatitudes appears to be the dominant influence in determining the translation speed during ET, which is consistent with the previous findings in this study.

The analyzed intensity anomalies are once again compared with the ET re-intensification scenario. Clusters (4-1) and (4-3) were both analyzed as a much stronger storm than clusters (4-2) and (4-4), but were divided on their midlatitude response. While the outlier ensemble cluster (4-3) represented a strong re-intensification scenario, cluster (4-1) re-intensified into a much weaker system. As before, the re-intensification scenarios of the ET do not appear to be related to the intensity anomaly (Fig. 29). Rather, the re-intensification scenario of the ET appears to be more related to the TC position relative to the best-track. Similar to the results of 18 October, the two clusters that predicted a strong midlatitude response had Tokage behind the best-track position in the analysis (Fig. 29b and 29c). The two clusters that had a weak midlatitude cyclone had Tokage ahead of the best-track position in the analysis (Fig. 29a and 29d).

In summary, as before, it appears that the phasing of Tokage into the midlatitudes is the dominant factor in determining the translation speed during ET, but does not influence the re-intensification scenario. Rather, the re-intensification scenario of the ET process appears to be coupled with the TC position relative to the best-track position.

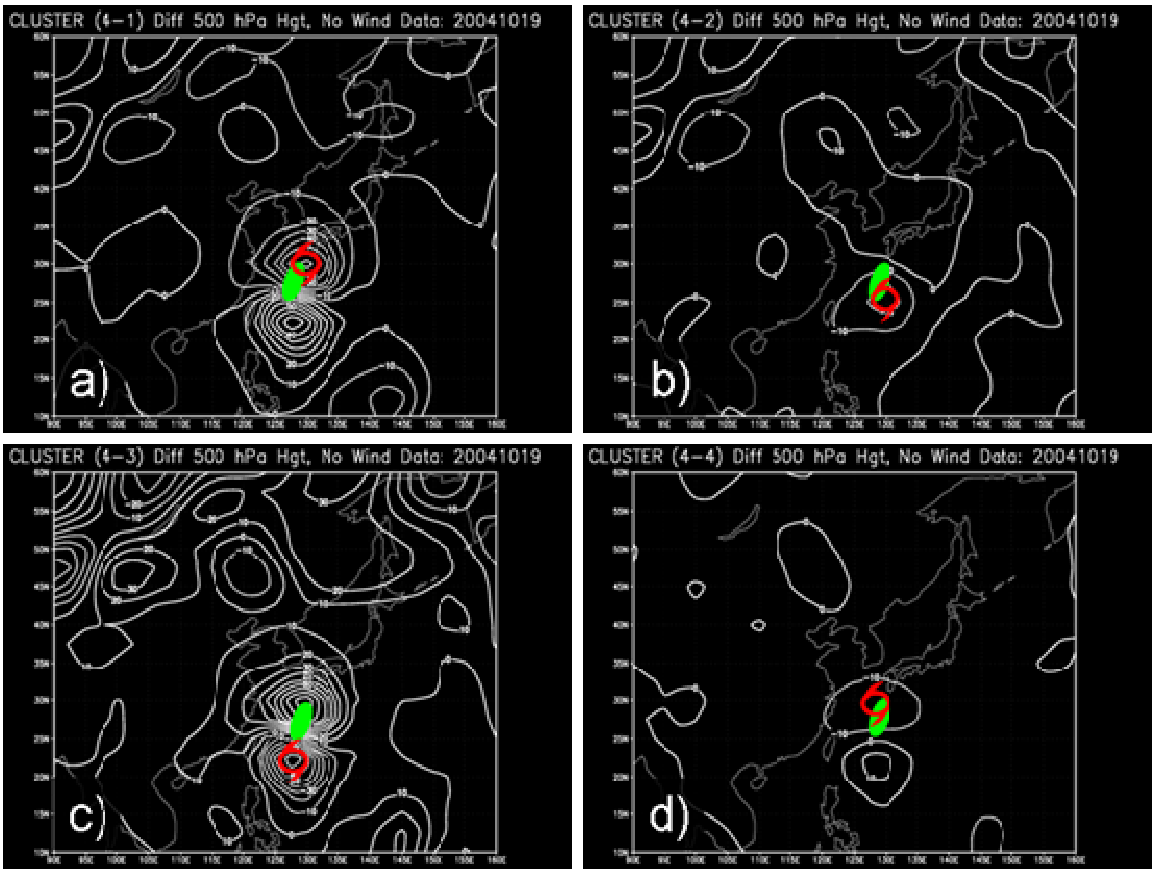

Figure 29. Same as Fig. 15, except for 19 October. a) Cluster (4-1): Moderate re-development as a baroclinic system as it propagates quickly across the northwestern Pacific. b) Cluster (4-2): Strong re-intensification. c) Cluster (4-3) Very strong re-intensification but propagates slowly in the midlatitudes. d) Weak re-intensification stage.

Tokage influenced the long-wave pattern prior to it being classified as an extratropical system (Fig. 30a). The four ensemble clusters had Tokage either ahead or behind the best-track position in the initial conditions. Of note is how the midlatitude phasing of Tokage began to influence the ensemble spread as early as 20 October (Fig. 30a). These phasing differences have introduced a large uncertainty in the 500 hPa height fields 24 hours prior to Tokage being classified as an extratropical system. Not only did the phase difference influence the 500 hPa height variability, but also the analyzed intensity of TY Tokage.

The TC position in clusters (4-2) and (4-3) was analyzed behind the best-track position, and both represented a strong re-intensification scenario.

Inspection of the 19 October MSLP (Fig. 28) for clusters (4-2) and (4-3) indicates that the cyclone in cluster (4-3) is predicted to be a stronger, more intense system. That is, the outlier cluster (4-3) indicated a re-intensification to a 970 hPa midlatitude cyclone, whereas the cyclone in cluster (4-2) deepened to 980 hPa. The 500 hPa height anomaly plot indicates that cluster (4-3) was a much stronger storm than cluster (4-2) in the initial conditions, which suggests that the analyzed storm intensity may also affect the re-intensification scenario and the midlatitude response. Because cluster (4-3) was predicted to develop into a much stronger system than the cyclones in the other three clusters, the modification to the longwave pattern by the ET event would be expected to be stronger. For example, cluster (4-3) builds a much stronger downstream ridge than the other three clusters. Accordingly, the larger downstream ridge will help to amplify a much deeper upstream trough (Figs. 30a-d). As the cluster (4-3) forecast moves Tokage into the midlatitudes, a much larger downstream response is also evident (Fig. 30a) when compared with the other three ensemble clusters. The midlatitude trough associated with cluster (4-3) ET event is significantly deeper than the troughs associated with other three clusters. These ensemble forecasts from 19 October again suggest how the phasing and intensity differences among the four clusters directly influence the midlatitude response. Accordingly, the varying midlatitude responses among the four clusters introduce a strong degree of uncertainty that emanates from the ET event and quickly propagates downstream and influences the downstream synoptic patterns.

Similar to the ensemble forecast from 18 October, the 72-h ensemble forecasts from 19 October continue to indicate that multiple extratropical transition modes are present. Two of the four ensemble clusters continue to represent a strong re-intensification of Tokage in the midlatitudes. However, the other two cluster solutions represent a weak or moderate transition. As observed in the 17-18 October cluster analyses, the Tokage re-intensification scenario in the midlatitudes is apparently sensitive to the phasing of the tropical cyclone into the westerlies. Although the number of ensemble clusters was not

reduced from 18 October, one of the clusters might be eliminated as being statistically improbable considering this cluster was comprised of only two out of the 44 ensemble members. By eliminating cluster (4-3), the number of solutions would be reduced to three and provide a first indication that the ET process is becoming better defined in the ensemble forecast.

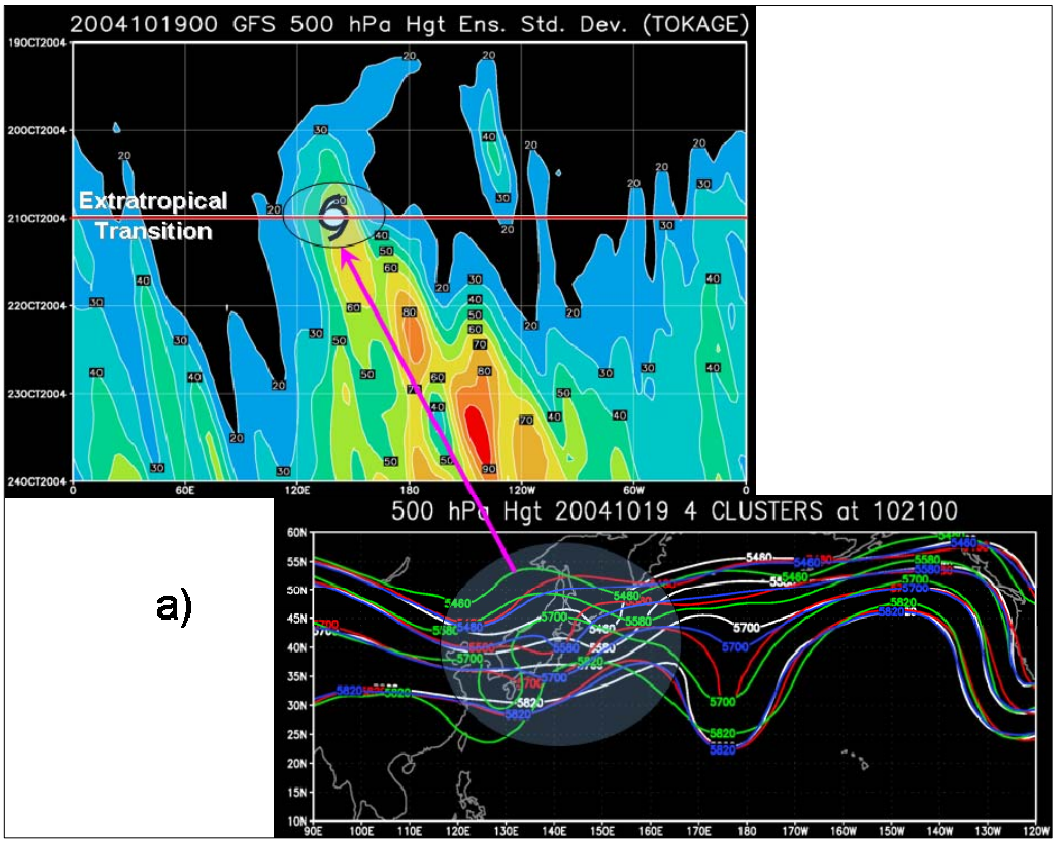

Figure 30. a) - d): Same as Fig. 25, except for 19 October. On the 500 hPa height charts, clusters are defined by color as white (4-1), red (4-2), green (4-3), and blue (4-4). a) 48-h forecast when Tokage was classified as ET. Largest ensemble spread has been shaded. b) – d) Phasing differences of Tokage into the midlatitudes lead to a large ensemble spread that propagates to the east.

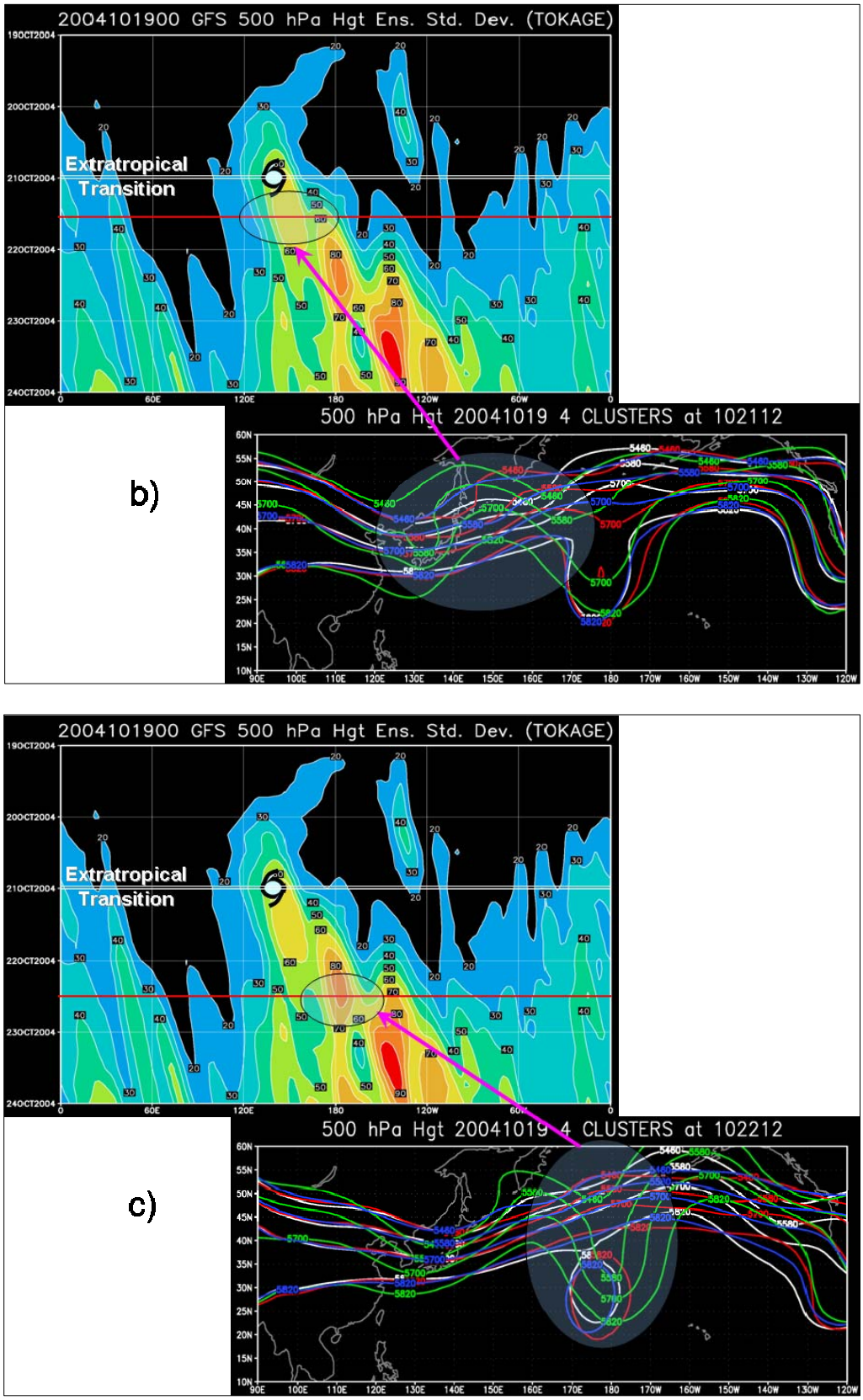

Figure 30. (continued)

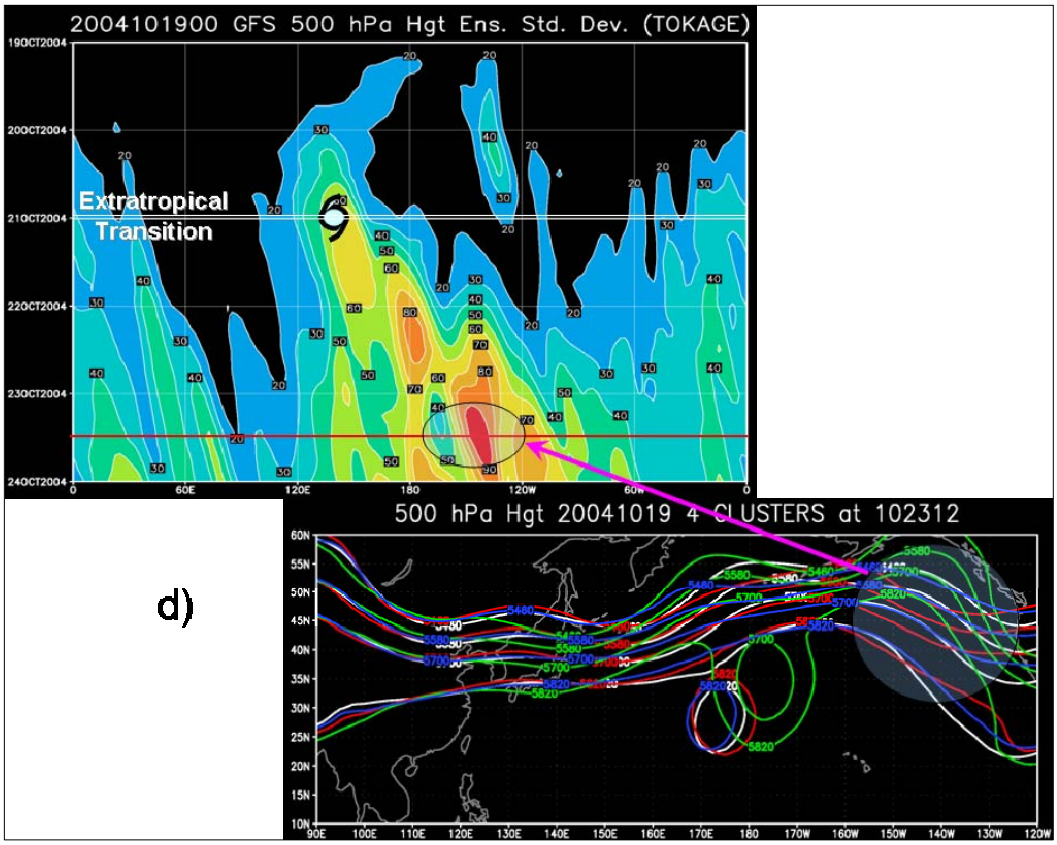

Figure 30. (continued)

4. 20 October (30-h to 48-h forecast)

a. Cluster Analysis

Given the hypothesis that the number of clusters (i.e., the possible meteorological solutions) should decrease at decreasing forecast intervals, only two clusters were initially specified for the clustering of the synoptic patterns (PC1 and PC2). Once the first two clusters were identified, the PC plots were further sub-divided into three- and four-cluster solutions (Fig. 31). As before, cluster-mean synoptic charts were examined for the division of cluster (2-2) in Fig. 31a into clusters (3-1) and (3-2) in Fig. 31b. This comparison (Fig. 32a) did not indicate any significant difference between the three-cluster solution and the two-cluster solution. All three clusters depict a decaying extratropical cyclone that propagates quickly across the western North Pacific with a trailing weak disturbance over the northern Sea of Japan (Fig. 32a). Since the central pressure difference between clusters (3-1) and (3-2) is only 5 hPa, it was determined that

this separation did not identify an independent synoptic pattern. Likewise, the subdivision of cluster (3-2) in Fig. 31b into clusters (4-2) and (4-3) in Fig. 31c was deemed unwarranted as this subdivision revealed similar synoptic forecasts (Fig. 32b).

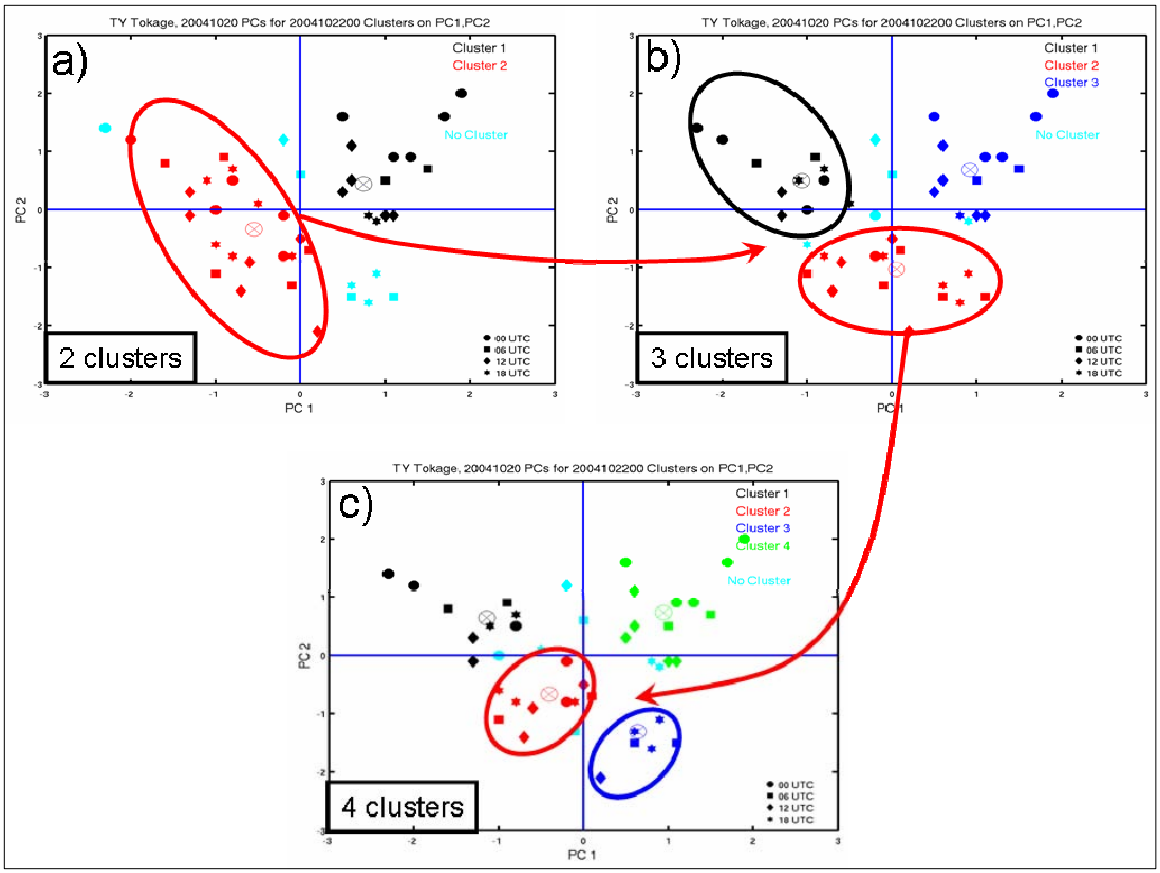

Figure 31. Same as Fig. 11a-c, except for 20 October. a) The red circle highlights cluster (2-2) that was subdivided into clusters (3-1) and (3-2) (black and red circles in Fig. 31b). b) The red arrow depicts the subdivision of cluster (3-2) in to clusters (4-2) and (4-3) (red and blue circles in Fig. 31c). c) The four-cluster solution.

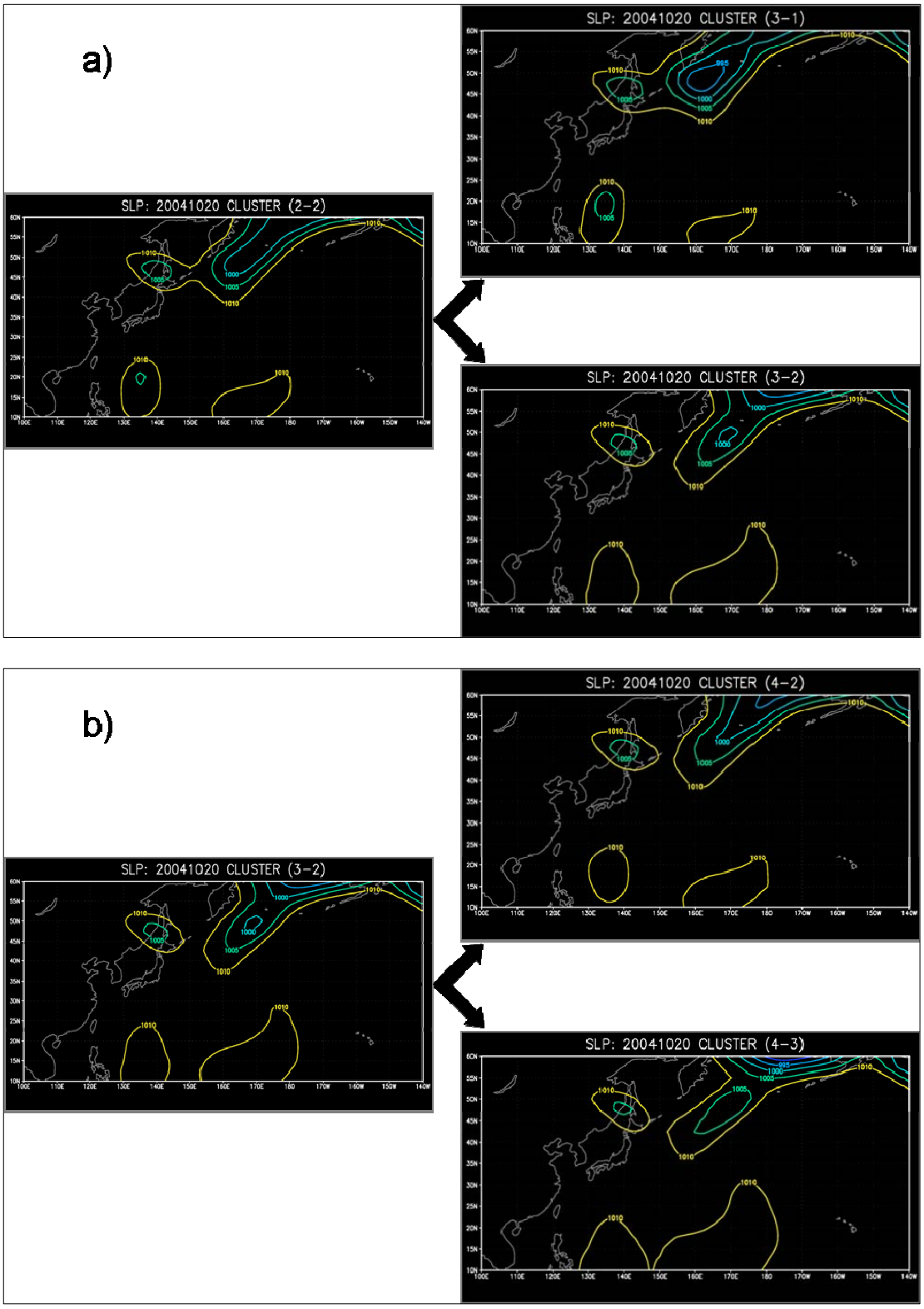

Figure 32. Cluster Analysis for 20 October: a) Separation of cluster (2-2) on the left side into clusters (3-1) and (3-2) on the right side; b) Separation of cluster (3-2) on the left side into clusters (4-2) and (4-3) on the right side.

This 20 October analysis suggests a continuing reduction in the variability among the cluster groupings. From the two-cluster groupings, it appears that the ensemble members have properly identified two similar ET modes:

- Cluster (2-1) represented a weak ET scenario (Fig. 33a and 33c).
- Cluster (2-2) also represents a weak ET event; however, the system is forecast to propagate slightly farther east in the 48-h forecast (Fig. 33b and 33d).

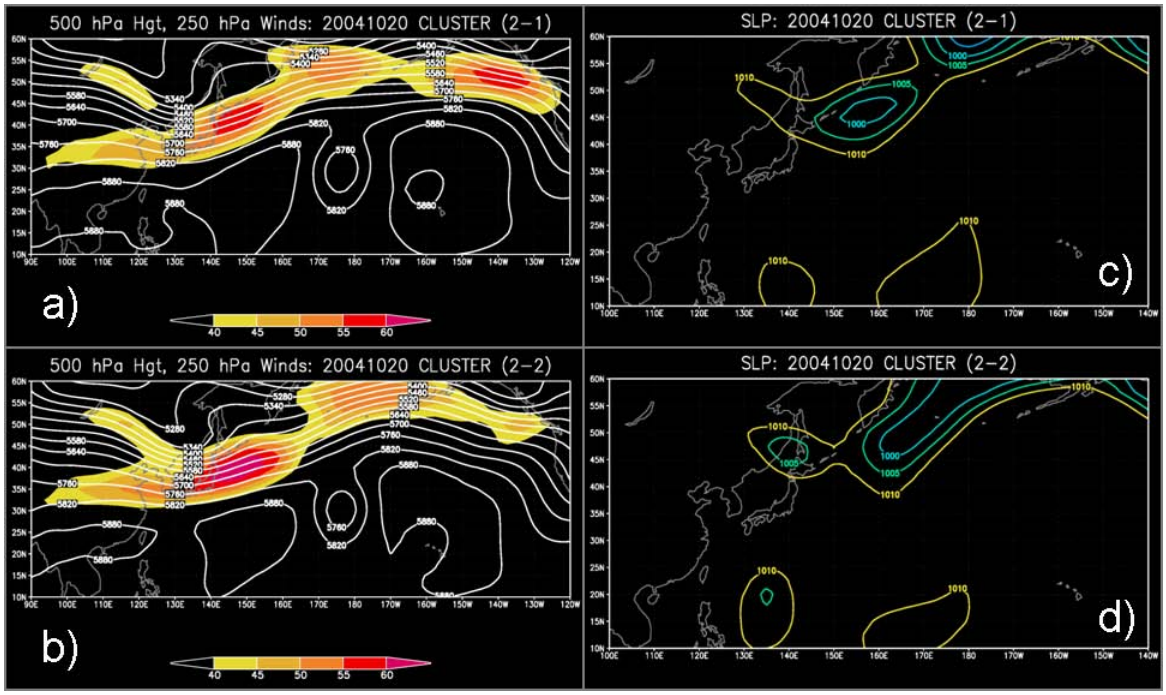

Figure 33. Same as Fig. 14, except for 20 October.

b. Variations in the Analysis for Each Set of Ensemble Cluster Forecasts

The primary difference between the two clusters (2-1) and (2-2) in the ensemble forecast from 20 October is a shift in location of the low-level vortex (Fig. 33c and d). Analysis of the initial-condition perturbations helps clarify this spatial separation. The initial TC position in cluster (2-2) was farther downstream than in cluster (2-1) (Fig. 34). Little sensitivity to the initial placement

of the tropical cyclone with respect to the best-track position and the re-intensification mode is evident, as both clusters represent a weak midlatitude system.

The Hovmoller plot for 0000 UTC 20 October (shaded regions, Figs. 35a) indicate that the maximum uncertainty in the 500 hPa height forecast heights remains associated with the ET event. In comparison to the Hovmoller plot for 19 October (Fig. 30), the magnitude of the deviation maxima has decreased during the 24-h period, which can be explained by considering a couple of key issues. First, as the ET event continues to evolve and becomes better defined in the EPS, decreasing uncertainty is expected in the forecast fields. As the spread of the ensemble members decreases, so should the 500 hPa height deviations. Secondly, both clusters favored weak re-intensification scenarios. The ET process should result in small amplitude disturbances propagating in the 500 hPa height fields, and possibly lead to small height deviations. Rather than observing significantly smaller height deviations, the Hovmoller plot for 20 October indicated only a slight decrease. Examination of the 500 hPa heights fields for the two-cluster solution helps explain this discrepancy (Figs. 35a-d). By 0000 UTC 21 October, Tokage was classified as extratropical, and similar to previous analyses, a variability maximum was present east (downstream) of Tokage (shaded region, Fig. 35a). As was previously identified in Fig. 34, in cluster (2-2) Tokage moved into the midlatitudes ahead of cluster (2-1). Both clusters have identified a short-wave trough west of the Korean Peninsula and have placed the former TC ahead of this short-wave (shaded region, Fig. 35a). The ET of Tokage in the midlatitudes is represented as the low amplitude troughs along the southern coast of Japan (cluster (2-1)) and to the east of Japan (cluster (2-2)). Since these weak perturbations seem to be approximately the same magnitude, it appears that the relatively large variability found in the 500 hPa height fields is primarily influenced by the spatial separation between the two troughs (i.e., phase difference). By 1200 UTC 21 October, the variability maximum has shifted eastward (shaded region, Fig. 35b). Note that the short-wave that was previously west of the

Korean Peninsula has propagated eastward and is now over the western Japan Sea. This short-wave is a separate feature from the perturbation troughs associated with the ET event. Cluster (2-1) has moved Tokage slightly east of Japan while cluster (2-2) has moved Tokage south of the Kamchatka Peninsula (shaded region, Fig. 35.b). In the following 12-h forecast, the variability perturbations generated by the ET event into the 500 hPa fields continue to move rapidly to the east (shaded regions, Figs. 35c and 35d). Although the trough associated with cluster (2-1) in Figs. 35c and 35d weakens and becomes increasingly difficult to identify in the 500 hPa height field, an eastward propagating deviation maximum can be identified in the Hovmoller plot. A comparison between the Hovmoller plot and the 500 hPa height field identifies the height uncertainty that originally emanated from the ET process. Also note how the short wave that originated near the Korean Peninsula continues to move slowly to the east, but the perturbation troughs associated with the ET event appear to propagate more rapidly to the east. These “variability perturbations” in Figures 35a-35d generated during the ET process can propagate across two-thirds of the ocean basin in approximately 48 hours. An estimation of the group speed for these “variability perturbations” can be found in Section III, Part C.

In summary, slight phasing differences of Tokage moving into the midlatitudes did not alter the ET mode (Fig. 35). Within 48 hours of the common forecast valid time (0000 UTC 22 October), the ensemble forecast has properly identified the ET mode. Slight phasing differences between the two ensemble clusters are still producing downstream maxima in the height standard deviations, but these downstream uncertainty values are much smaller than those calculated from the 19 October ensemble fields (Fig. 35 and 30, respectively). Finally, these maxima in the height standard deviations appear to propagate downstream more rapidly than synoptic systems (i.e., short waves).

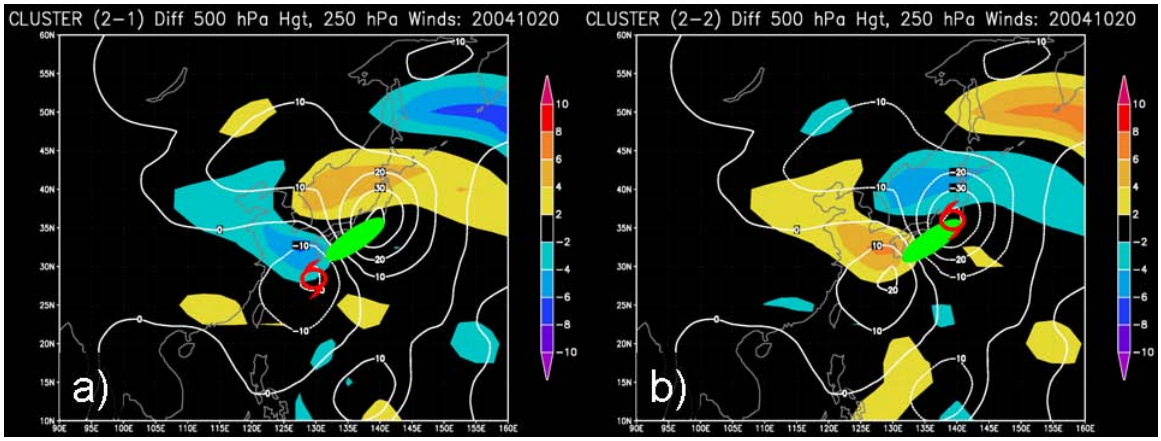

Figure 34. Same as Fig. 15, except for 20 October. a) Cluster (2-1): Weak re-development as a baroclinic system. b) Cluster (2-2): Also weak re-intensification as it propagates quickly across the western North Pacific.

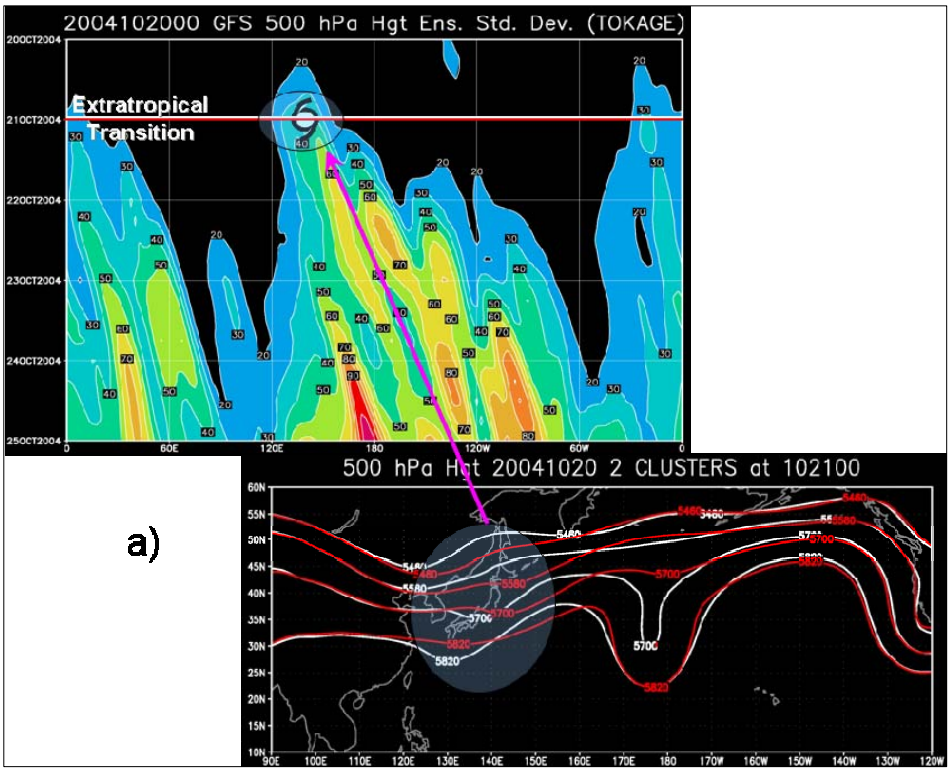

Figure 35. a) - d): Same as Fig. 25, except for 20 October. On the 500 hPa height charts, clusters are defined by color as white (2-1) and red (2-2). a) 24-h forecast when Tokage was classified as an ET system. Largest ensemble spread has been shaded. b) – d) Although the ET process was better defined in the ensemble model, phasing differences of Tokage into the midlatitudes still lead to a small amplitude ensemble spread far downstream.

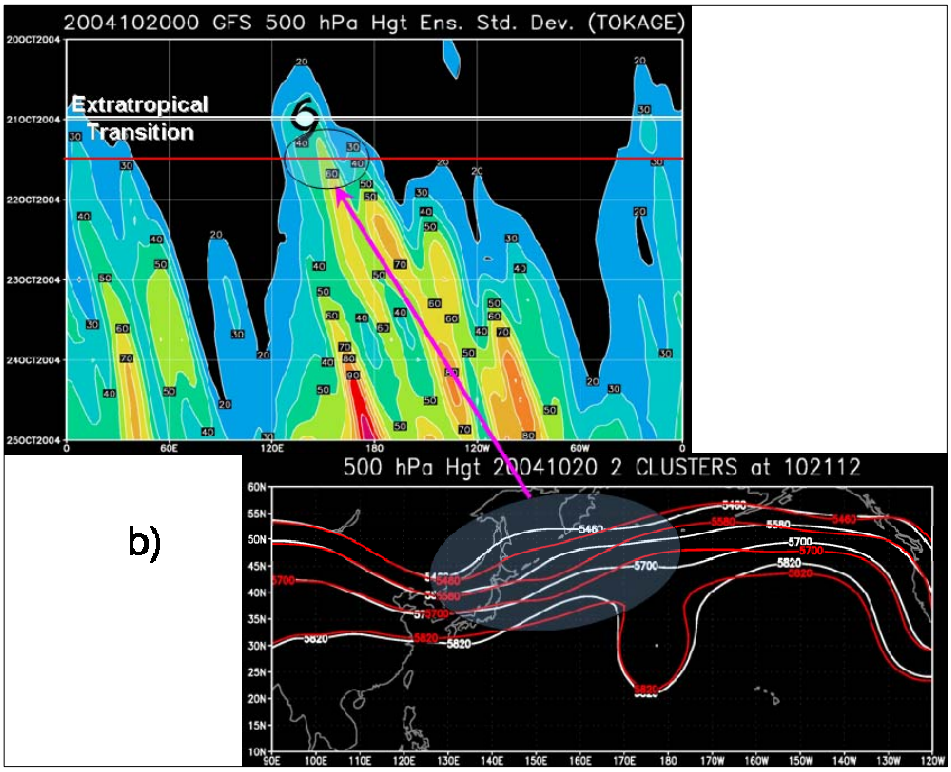

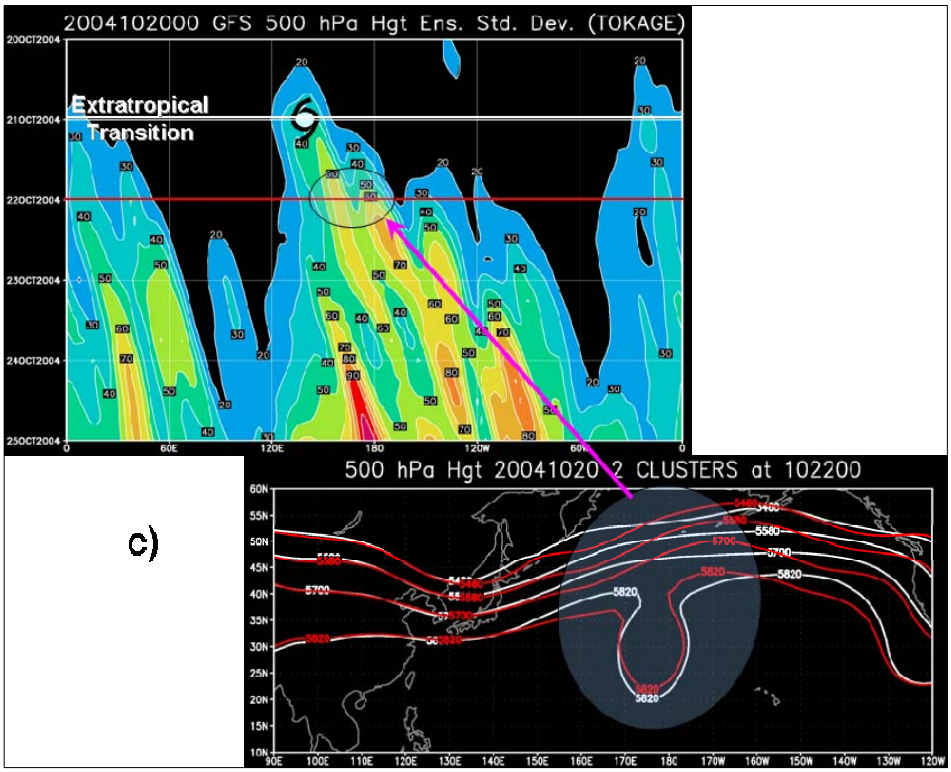

Figure 35. (continued)

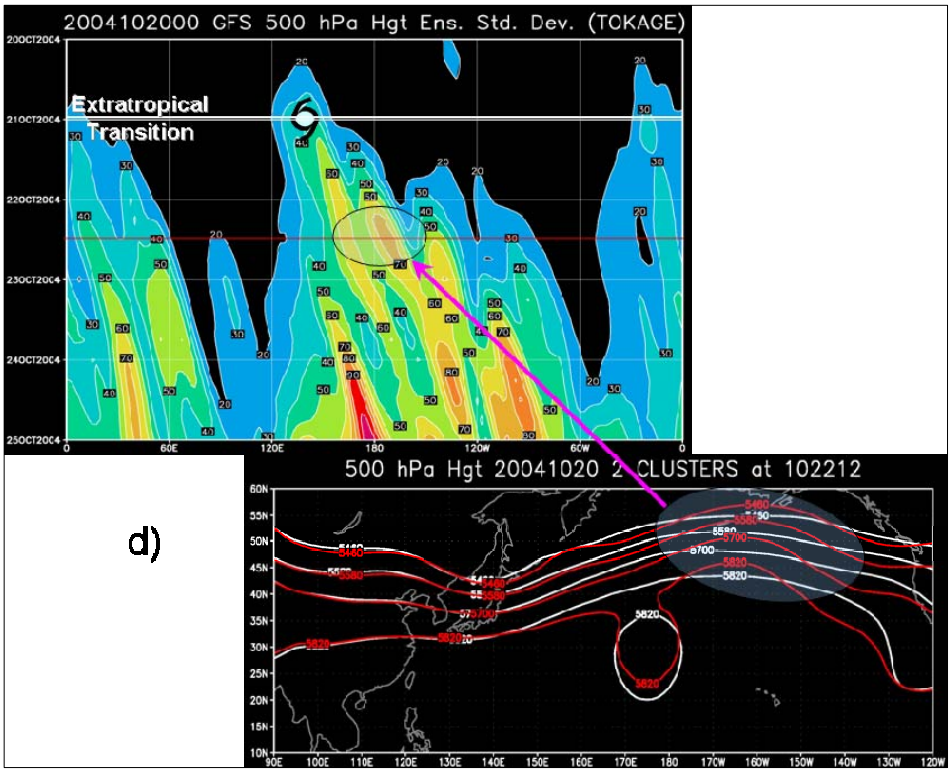

Figure 35. (continued)

5. 21 October (06-h to 24-h forecast)

a. Cluster Analysis

The results for the final cluster analysis of the 21 October (06-h to 24-h forecast) were almost identical to the results associated with the 30-h to 48-h forecast. Only two synoptic patterns were initially specified for the 44 member ensemble (Fig. 36a). The progressive separation of the PCs into higher order clusters (Figs. 36b and c) did not help identify any additional ET modes. When cluster (2-1) was separated into clusters (3-1) and (3-2), the mean MSLP charts for these two clusters both indicated a weak ET mode with a broad region of low pressure extending over the northwestern Pacific (Fig. 37a). Additionally, no significant difference was observed in the synoptic solutions (Fig. 37b) when cluster (3-3) was subdivided into clusters (4-1) and (4-3). Consequently, it was determined that no more than two ET modes were common to all 44 ensemble members.

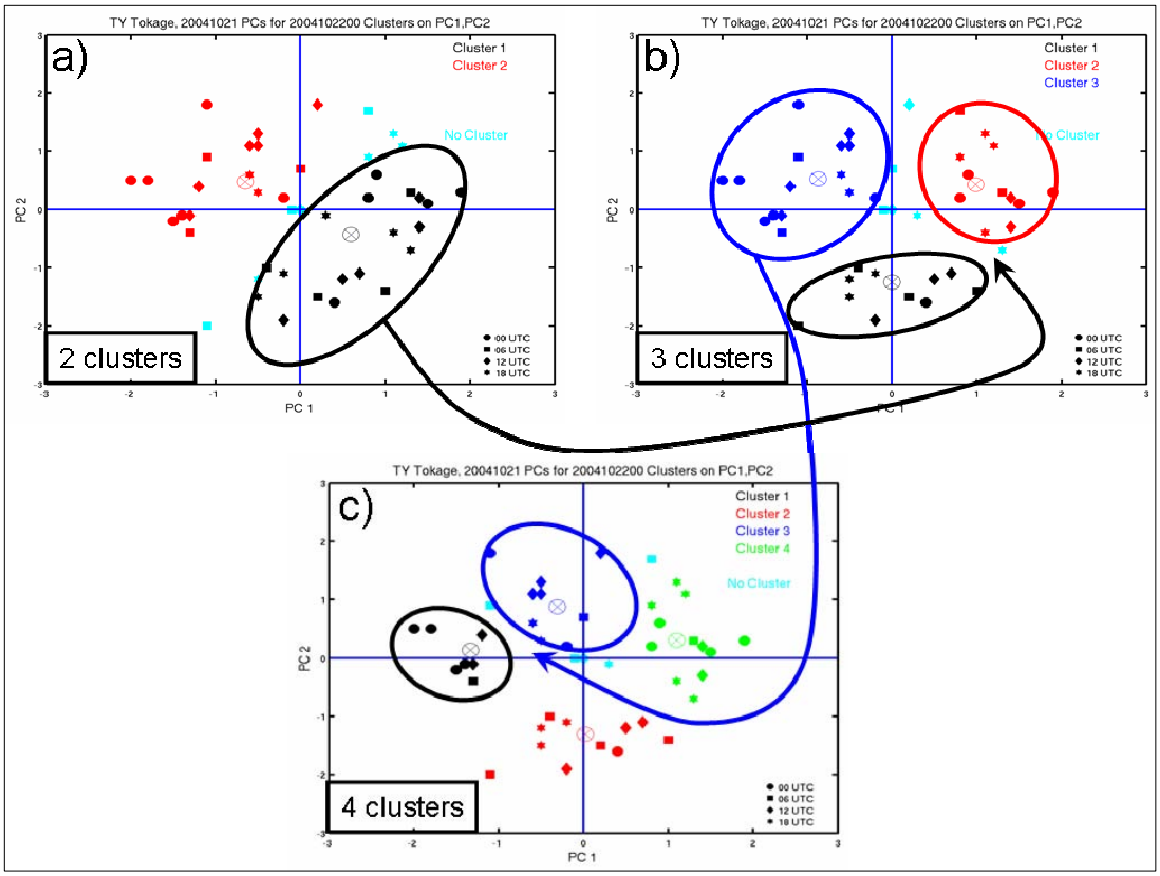

Figure 36. Same as Fig. 11a-c, except for 21 October. a) The black circle highlights cluster (2-1) that was subdivided into clusters (3-1) and (3-2) (black circle and red circle in Fig. 36b). b) The blue arrow depicts the subdivision of cluster (3-3) in to clusters (4-1) and (4-3) (black and blue circles in Fig. 36c). c) The four-cluster solution.

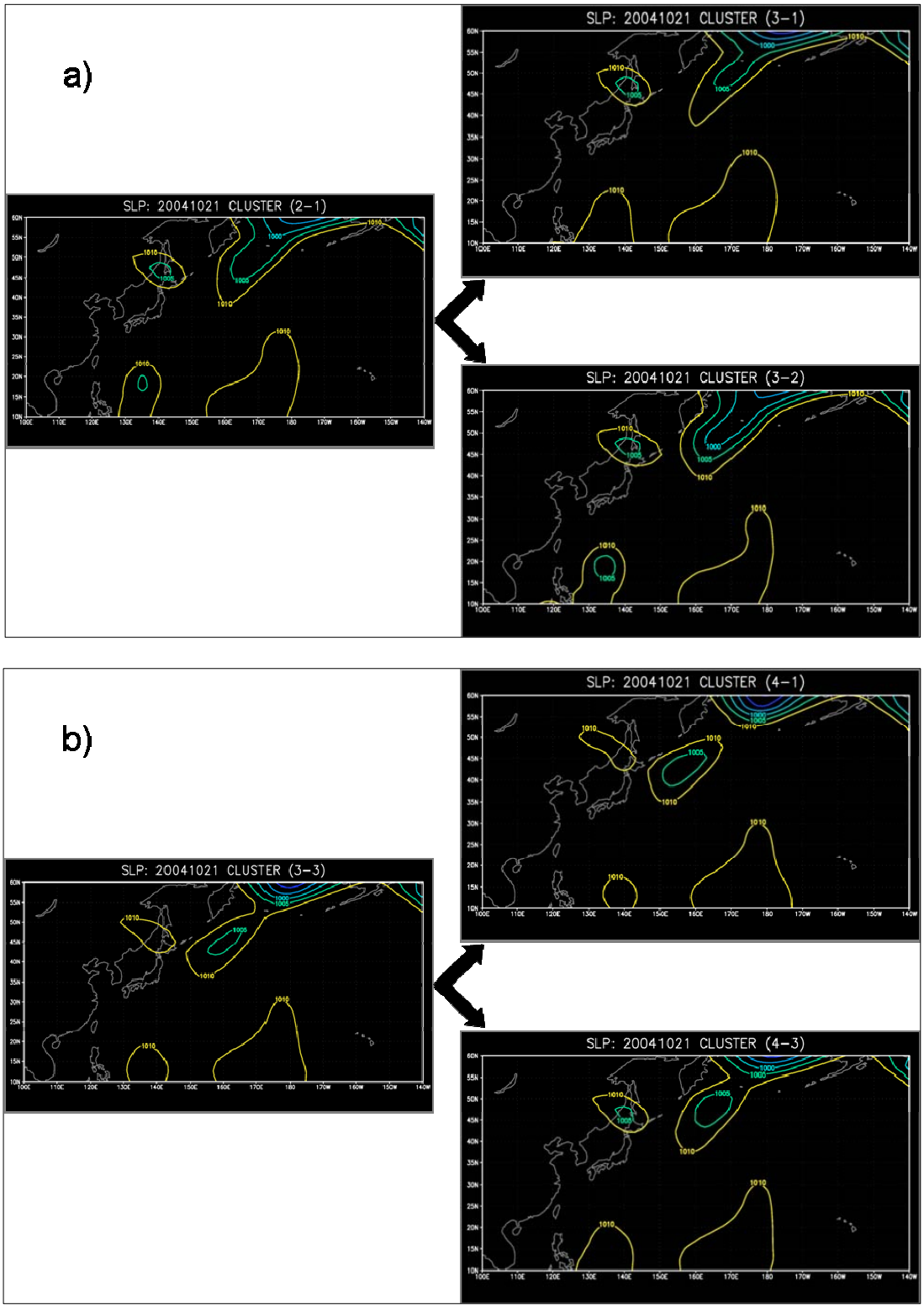

Figure 37. Cluster Analysis for 21 October: a) Separation of cluster (2-1) on the left side into clusters (3-1) and (3-2) on the right side; b) Separation of cluster (3-3) on the left side into clusters (4-1) and (4-3) on the right side.

The synoptic pattern in the two clusters from the 06-h to 24-h ensemble forecast was consistent with the synoptic pattern from the 30-h to 48-h ensemble cluster solutions. Both clusters appear to have properly identified the ET mode:

- Cluster (2-1) represented a weak ET scenario (Fig. 38a and 38c).
- Cluster (2-2) also represents a weak ET event (Fig. 38b and 38d).

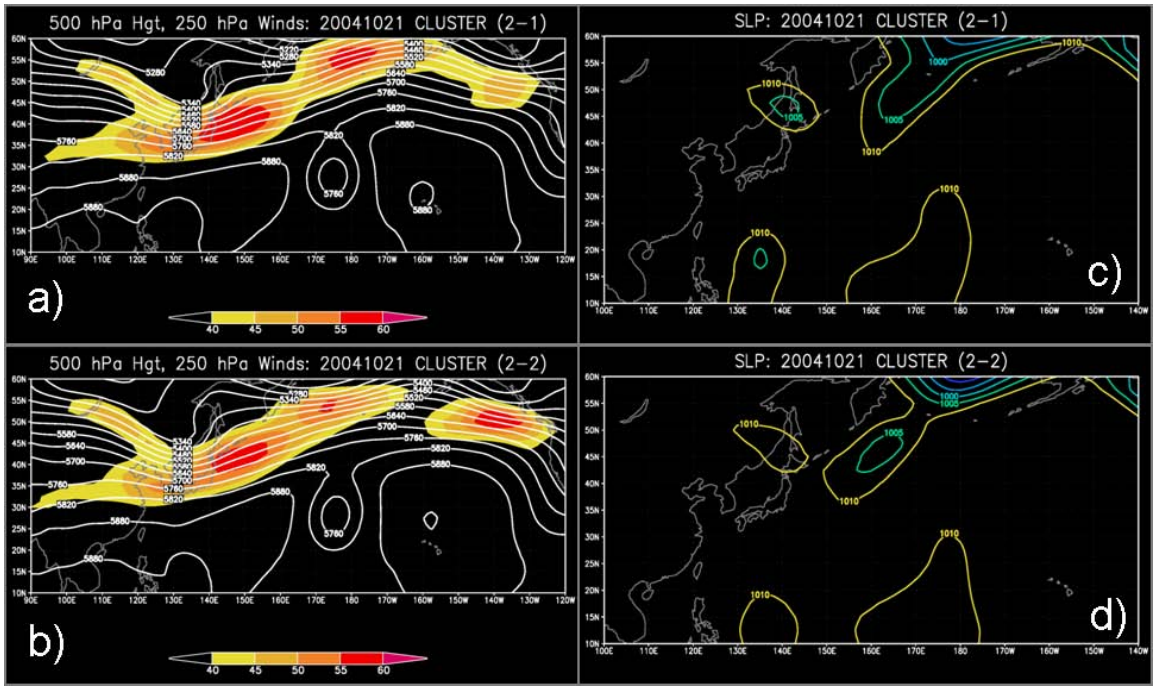

Figure 38. Same as Fig. 14, except for 21 October.

b. Variations in the Analysis for Each Set of Ensemble Cluster Forecasts

As with the previous ensemble from 20 October, the perturbations in the initial conditions for the 21 October ensemble were confined to be around Tokage (Fig. 39). The phasing of Tokage moving into the midlatitude circulation did not appear to be a significant influence to the re-intensification scenario, as both clusters continued to forecast a decaying midlatitude system. The differences in the phasing of Tokage into the midlatitudes are the leading contributor to the downstream uncertainty. However, a comparison of the 21

October Hovmoller plot with the Hovmoller plot from 20 October indicates that the downstream variability of the 500 hPa height fields continues to decrease in the ensemble forecasts (Fig. 40 and 35, respectively).

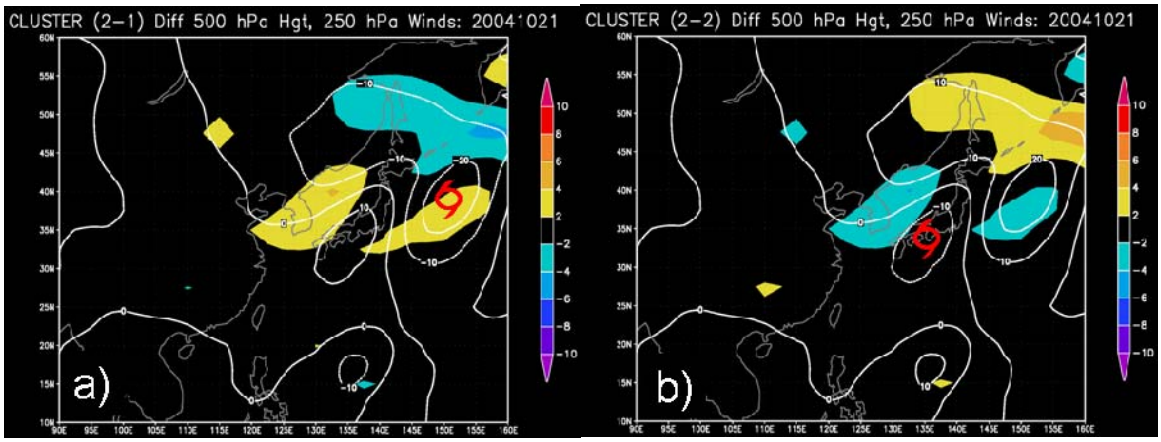

Figure 39. Same as Fig. 15, except for 21 October. a) Cluster (2-1): Weak re-development as a baroclinic system. b) Cluster (2-2): Also weak re-intensification scenario.

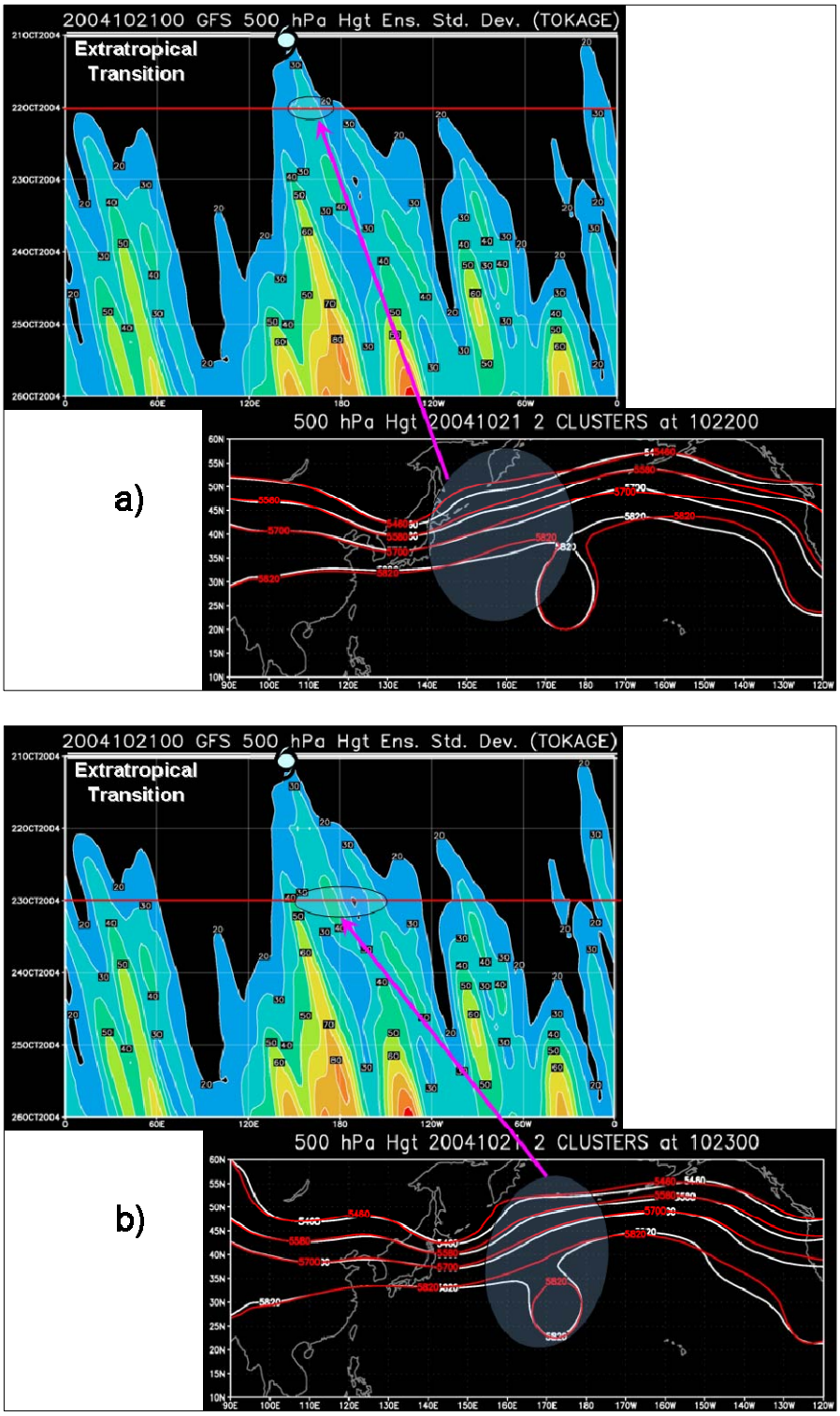

Figure 40. a) - d): Same as Fig. 25, except for 21 October. On the 500 hPa height charts, clusters are defined by color as white (2-1) and red (2-2). a) Tokage has been classified as an ET system. Largest ensemble spread has been shaded. b) – c) Although the ET process was better defined in the ensemble model, phasing differences of Tokage into the midlatitudes continue to introduce a small amplitude ensemble spread downstream.

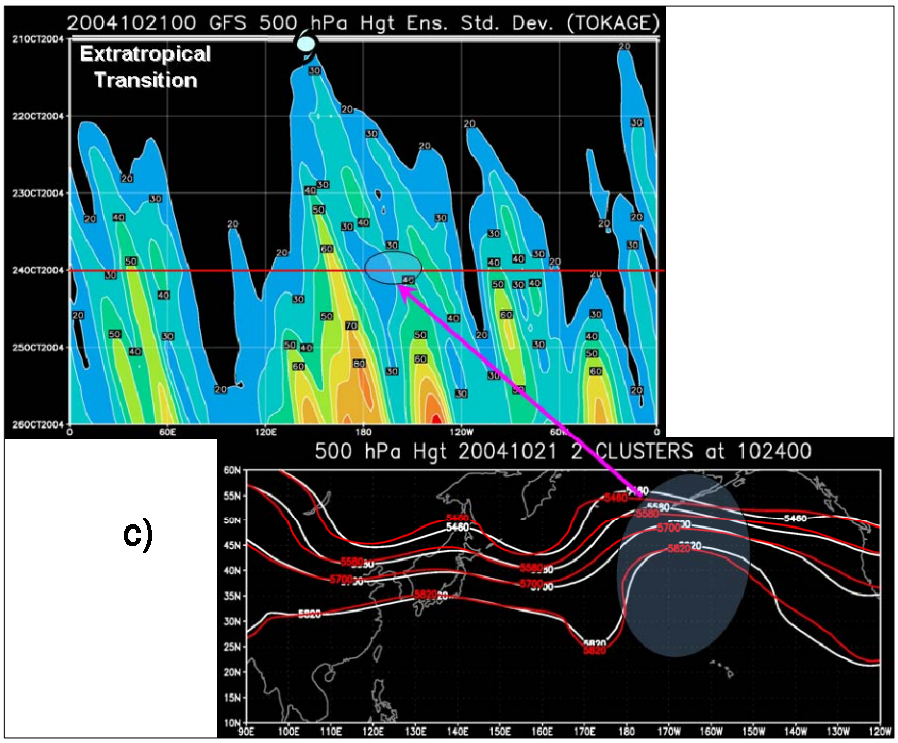

Figure 40. (continued)

C. PROPAGATION OF THE VARIABILITY DOWNSTREAM

In this section, the downstream propagation of the ET-related variability is examined. The translation speed of the decaying tropical cyclone and eventual extratropical cyclone are compared with the propagation of the downstream variability defined from the Hovmoller plots. The movement of Tokage into the midlatitudes initiated a variability maximum near the ET event. This variability maximum propagates downstream at a speed that is detectable on the Hovmoller plots (Fig. 41a). That is, the slope of the maximum variability will determine the phase speed of individual variability "packets."

Starting with the 1200 UTC ensemble forecast from 16 October, the axis of maximum variability was plotted every 12 hours on consecutive Hovmoller diagrams (Figs. 41a-i). The phase speed appears to be consistent at the extended forecast time intervals (Figs. 41a–d). However, a change in phase speed appears starting with the 60-h forecast (Figs. 41e-i). A compilation of the group speeds is given in Fig. 42. At the extended forecast intervals (108 h to

72 h) (labeled as “Group Speed 1” in Fig. 42), a fairly consistent speed of approximately 23 m/s was calculated. Starting with the 1200 UTC 18 October forecast, the speed increased to approximately 46 m/s (labeled as “Group Speed 2” in Fig. 42). These wave-like features appear to propagate similar to Rossby waves and are faster than the movement of the synoptic-scale systems. Variation in the background flow may account for some of the differences in speeds. Stronger background flow (westerlies) would advect the ensemble spread more quickly downstream, while a weaker background flow would allow for a more gradual propagation downstream. Unfortunately, the 500 hPa wind fields were not available for comparison. This could be an area of future study.

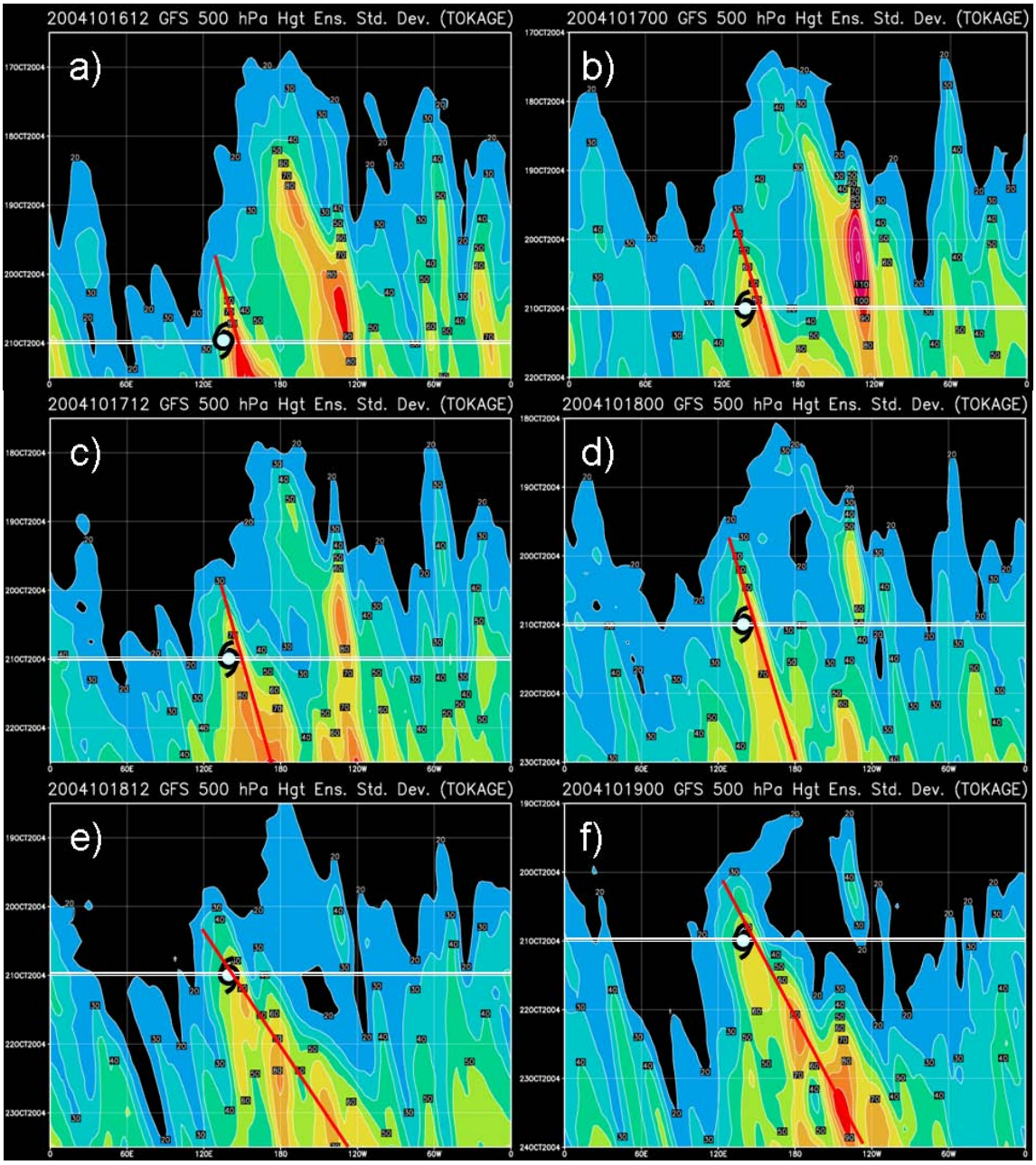

Figure 41. Same as Fig. 4, except red line has been drawn along the axis of maximum height deviations. These lines correspond to the group speed of the ensemble spread (uncertainty).

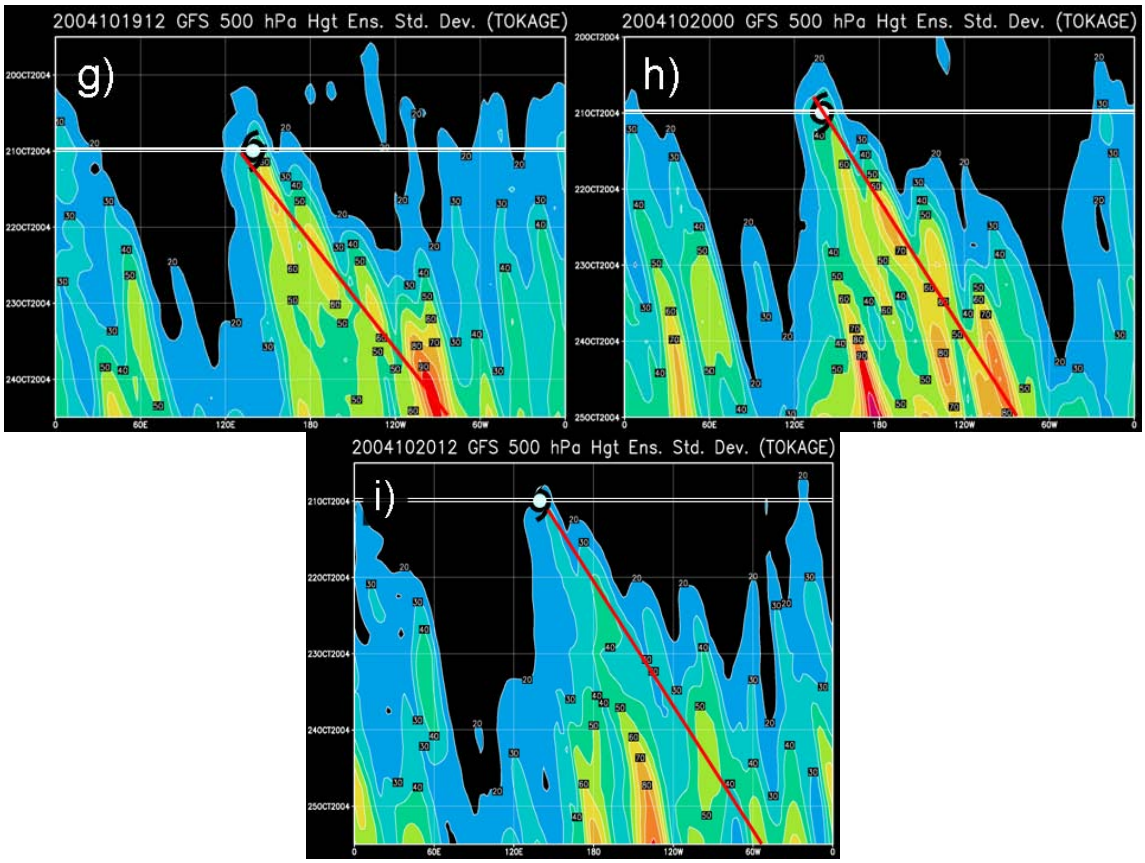

Figure 41. (continued)

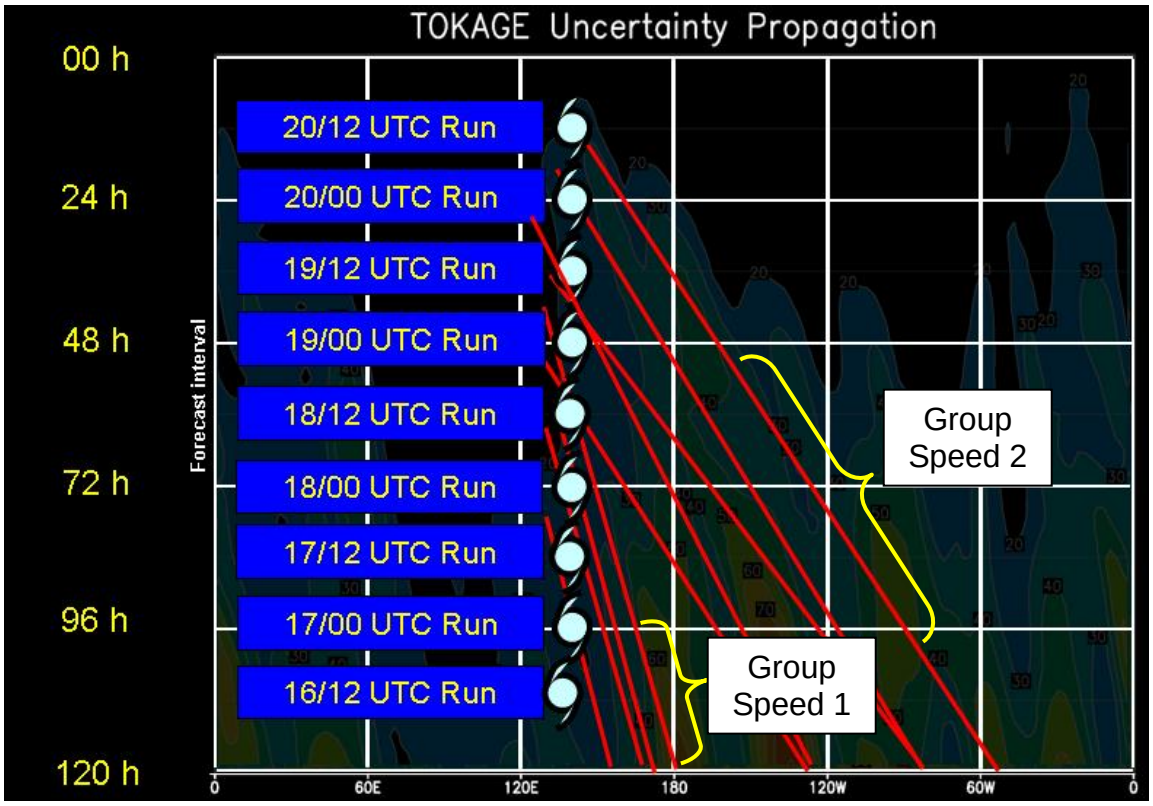

Figure 42. The red lines indicate the zonal movement of individual "packets" of uncertainty as determined from Figs. 41a – i. Similar to those Hovmoller diagrams, the longitude is plotted along horizontal axis. The vertical axis represents the forecast interval (i.e., 00 h, 12 h, 24 h, etc.), with the top horizontal line corresponding to the analysis (00 h) for each model run. The tropical cyclone symbol is plotted at the corresponding forecast interval when it was classified as extratropical (0000 UTC 21 October). The box next to the tropical cyclone symbol indicates the forecast run. For example, based on the 0000 UTC 17 October ensemble run, Tokage would be classified as an extratropical system by the 96-h forecast. Likewise, based on the 1200 UTC 20 October ensemble, Tokage will be classified as an extratropical system within 12 hours of the analysis (i.e., the 12-h forecast)

IV. CONCLUSION

A. SUMMARY

For the five 24-h periods prior to the ET of TY Tokage, the four-daily integrations of the NCEP ensemble forecast system with 11 members were combined to define sets of 44 ensemble members. An EOF analysis of the 500 hPa heights was calculated to identify modes of variability in the sets of 44 ensemble groups. The EOF patterns identify ensemble variability within 102 h to 120 h, 78 h to 96 h, 52 h to 72 h, 30 h to 48 h, and 06 h to 24 h periods prior to the ET event. A fuzzy cluster analysis of the principal components associated with each of the five ensemble sets was used to determine recurring synoptic patterns within each set of 44 ensemble members. Analysis of successive ensemble forecasts suggests the number of forecast ET modes decreases as the ET process becomes better defined in the ensemble forecasts.

1. Ensemble Spread during ET Events

Ensemble spread was related to variations in the initial analyses generated by the ensemble prediction system. This uncertainty first appears near the point where the tropical cyclone moves into the midlatitudes, and then the variability propagates downstream. This downstream ensemble spread impacts the distribution of the synoptic-scale systems and reduces the confidence in the model predictions. In this case study, the movement of Tokage into the midlatitudes did not appear to influence the variability upstream, which contrasts with some previous results that identified modifications to the upstream wave patterns during ET events. Additional case studies are necessary to determine what role the recurving tropical cyclone may have on the upstream distribution of the long-wave pattern.

2. Decreasing Number of Modes as the ET Progresses

As the recurving tropical cyclone first enters the midlatitudes at extended forecast intervals, a large spread exists in the ensemble forecasts. Long-range forecast accuracy is hampered by the growth of uncertainties introduced in the initial conditions. These uncertainties attempt to capture observational and

analysis errors. These perturbations alone can produce a wide spread in the ensemble forecast. Because the ET event is a gradual process that involves numerous processes on varying spatial and temporal scales, numerical model forecasts of many ET events have shown a high degree of uncertainty in their forecasts. Adding to the long-range forecast uncertainty are the nonlinear processes associated with the ET process, which contribute to an even larger spread among the ensemble members. Even with these limitations, a few recurring synoptic patterns within the 44 ensemble members were identified via EOF/cluster analysis. Thus, the degrees of freedom were reduced from 44 meteorological solutions to four in both the 102-h to 120-h ensemble forecasts and 78-h to 96-h ensemble forecasts (Fig. 43). As the ET process evolved and became better defined, the numbers of clusters decreased from four to two as the ensemble spread decreased (Fig. 43). Finally, within 48 hours of the common forecast valid time, the ensemble model appears to have properly identified the ET mode.

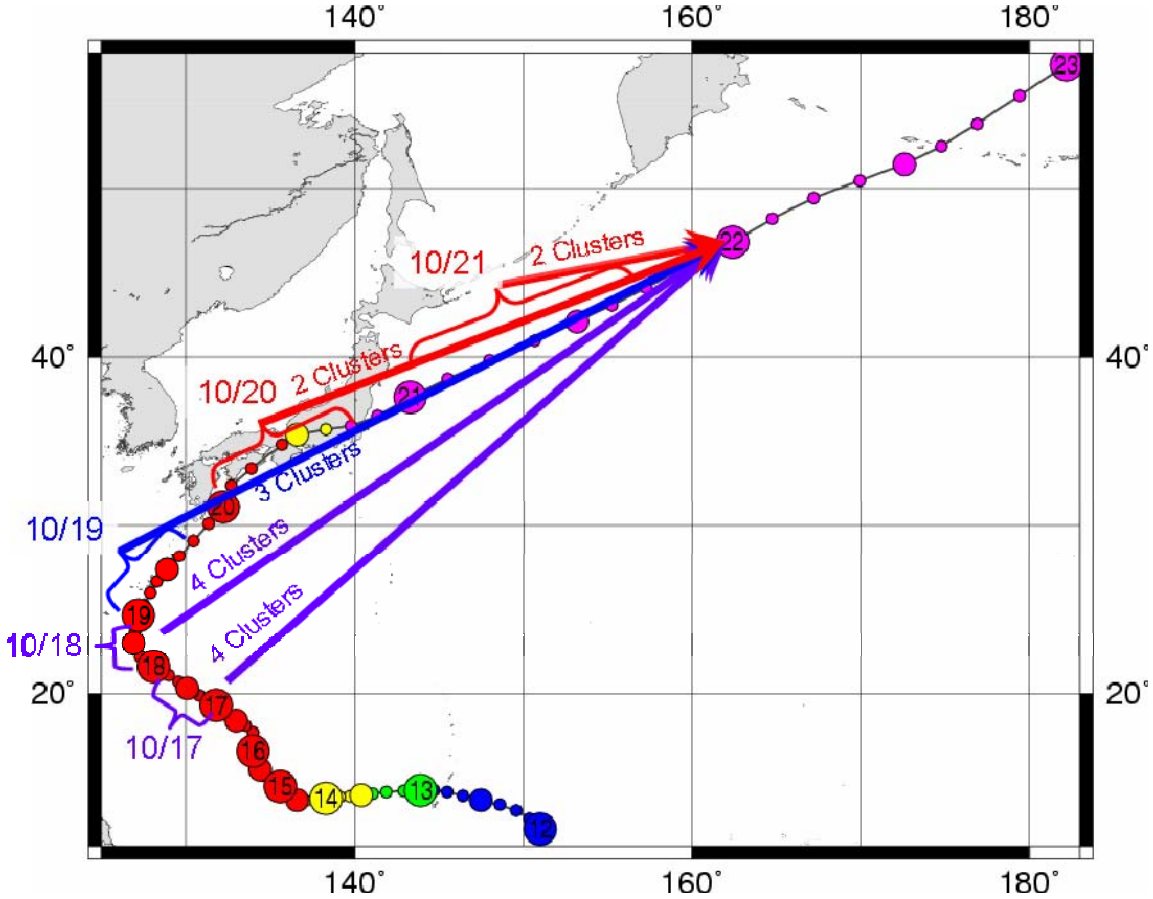

Figure 43. Summary of the cluster analysis for the extratropical transition of TY Tokage in which 22 October was established as the common forecast valid time. Best-track graphic is from Digital Typhoon website.

3. ET Modes Related to the Initial Conditions

The re-intensification scenarios specific to each cluster were consistent with respect to perturbations of the initial conditions used to generate the ensemble forecast. The ensemble clusters that predicted a slow movement of Tokage into the midlatitudes, and maintained a dynamic coupling between the outflow from the tropical cyclone and the midlatitude jet maximum, tended to favor the strongest re-development as a mature baroclinic cyclone. The ensemble clusters that predicted an accelerated movement of Tokage into the midlatitude flow minimized the dynamic coupling and favored a weak, decaying ET pattern. These findings are consistent with model results of Klein et al. (2002) who demonstrated the sensitivity of the re-intensification pattern to the analyzed initial conditions.

4. Propagation of Uncertainty Maxima in the Downstream Flow

The uncertainty maxima found in the ensemble forecast originate as part of the ET process. These maxima emanate from the vicinity of the tropical cyclone entrance into the midlatitude flow, and rapidly propagate downstream. Two propagation speeds were identified using Hovmoller diagrams of ensemble 500 hPa height standard deviations. These calculated speeds suggest that maxima in the uncertainty propagate much faster downstream than the storm center. These maxima correspond to the largest spread in the ensemble forecast and severely impact the downstream wave pattern.

5. Effective Reduction of the Degrees of Freedom

The combination of 44 ensemble members produced in the four daily EPS forecasts allowed for a statistically robust analysis of wave patterns common to all members. Cluster analysis of the principal components effectively reduced the number of forecast solutions from 44 to four or less, which can significantly aid the forecaster by minimizing "information overload." The clusters identify possible numerical solutions common to all 44 members. Further gains may be possible if the forecaster is able to identify the cluster that best represents the real-world synoptic situation.

B. FUTURE STUDY

This study was limited to one case study in which a tropical cyclone underwent ET in a weak northwest pattern (Harr and Elsberry 2000). Future studies should examine both ET patterns (northeast and northwest) as well as differing baroclinic re-intensification modes.

The ensemble properly identified the ET pattern by about the 48-h forecast. Future studies should verify the temporal cluster convergence to a solution as in this study as well as the optimal forecast interval when the ET event has been correctly identified in the ensemble model.

LIST OF REFERENCES

Digital Typhoon, March 2005, http://agora.ex.nii.ac.jp/digital-typhoon/

Evans, J. L., and C. Velden, 2000: Improved data assimilation in the study of Hurricane Floyd (1999). Preprints, *24th Conf. Hurricanes and Tropical Meteorology*, Ft. Lauderdale, FL, Amer. Meteor. Soc., 126-127.

Harr, P. A., and R. Elsberry, 1995: Large-scale circulation variability over the tropical western North Pacific. Part I: Spatial patterns and tropical cyclone characteristics. *Mon. Wea. Rev.*, **123**, 1225- 1246.

Harr, P. A., and R. Elsberry, 2000: Extratropical transition of tropical cyclones over the western North Pacific. Part I: Evolution of structural characteristics during the transition process. *Mon. Wea. Rev.*, **128**, 2613- 2633.

Hello, G., F. Lalaurette, and J.-N. Thépaut, 2000: Combined use of sensitivity information and observations to improve meteorological forecasts: A feasibility study applied to the 'Christmas storm' case. *Quart. J. Roy. Meteor. Soc*., **126**, 621-647.

Jones, S. C., P. Harr, J. Abraham, L. Bosart, P. Bowyer, J. Evans, D. Hanley, B. Hanstrum, R. Hart, F. Lalaurette, M. Sinclair, R. Smith, and C. Thorncroft, 2003: The extratropical transition of tropical cyclones: Forecast challenges, current understanding, and future directions. *Wea. Forecasting*, **18**, 1052-1092.

Klein, P. M., P. Harr, and R. Elsberry, 2000: Extratropical transition of western North Pacific tropical cyclones: An overview and conceptual model of the transformation stage. *Wea. Forecasting*, **15**, 373-395.

Klein, P. M., P. Harr, and R. Elsberry, 2002: Extratropical transition of western North Pacific tropical cyclones: Midlatitude and tropical cyclone contributions to reintensification. *Mon. Wea. Rev.*, **130**, 2240-2259.

MacAfee, A. W., and P. Bowyer, 2000a: Trapped-fetch wave in a transitioning tropical cyclone (Part I – The need and theory). Preprints, *24th Conf. Hurricanes and Tropical Meteorology*, Ft. Lauderdale, FL, Amer. Meteor. Soc., 292-293.

MacAfee, A. W., and P. Bowyer, 2000b: Trapped-fetch wave in a transitioning tropical cyclone (Part II – Analytical and predictive model). Preprints, *24th Conf. Hurricanes and Tropical Meteorology*, Ft. Lauderdale, FL, Amer. Meteor. Soc., 165-166.

McTaggart-Cowan, R., J. Gyakum, and M. Yau, 2003: The influence of the downstream state on extratropical transition: Hurricane Earl (1998) case study. *Mon. Wea. Rev.*, **131**, 1910-1929.

National Centers for Environmental Prediction (NCEP) Ensemble Background, April 2005, http://wwwt.emc.ncep.noaa.gov/gmb/ens/info/ens_detbak.html

Rabier, F., E. Klinker, P. Courtier, and A. Hollingsworth, 1996: Sensitivity of forecast errors to initial conditions. *Quart. J. Roy. Meteor. Soc*., **122**, 121-150.

Richman, M. B., 1986: Rotation of principal components. *J. Climatology*, **6**, 293-335.

Scott, A. J., and M. J. Symons, 1971: Clustering methods based on likelihood ratio criteria. *Biometrika*, **27**, 387-397.

Sinclair, M. R., 2004: Extratropical transition of southwest Pacific tropical cyclones. Part II: Midlatitude circulation characteristics. *Mon. Wea. Rev.*, **132**, 2145-2168.

Thorncroft, C. D., and S. Jones, 2000: The extratropical transitions of Hurricanes Felix and Iris in 1995. *Mon. Wea. Rev.*, **128**, 947- 972.

Toth, Z., and E. Kalnay, 1997: Ensemble forecasting at NCEP and the breeding method. *Mon. Wea. Rev.*, **125**, 3297-3319.

U.S. Department of Transportation – Marine Transportation System Fact Sheet, March 2005, http://www.dot.gov/mts/fact_sheet.htm

INITIAL DISTRIBUTION LIST

1. Defense Technical Information Center
   Ft. Belvoir, Virginia

2. Dudley Knox Library
   Naval Postgraduate School
   Monterey, California

3. Dr. M. Steven Tracton
   Office of Naval Research
   Arlington, Virginia

4. Professor Philip Durkee
   Naval Postgraduate School
   Monterey, California

5. Professor Russell Elsberry
   Naval Postgraduate School
   Monterey, California

6. Professor Patrick Harr
   Naval Postgraduate School
   Monterey, California

7. Director, Joint Typhoon Warning Center
   Naval Pacific Meteorology and Oceanography Center
   Pearl Harbor, Hawaii

8. Lieutenant Commander Justin Reeves
   Naval Postgraduate School
   Monterey, California